Defence Research and Development Canada
Recherche et développement pour la défense Canada

Electrical impedance imaging study

Final report

G. Bouchette
Neptec Design Group

CSA: J.E. McFee, DRDC Suffield, 403-544-4739

Defence R&D Canada – Suffield

Contract Report

DRDC Suffield CR 2012-122

March 2012

Canada

Electrical impedance imaging study

Final report

G. Bouchette

Neptec Design Group
320 Legget Drive
Kanata, ON K2K 1Y5

Contractor's Document Number: NDG011406

Contract Project Manager: P. Church
PWGSC Contract Number: W7702-09-R241
CSA: J.E. McFee, DRDC Suffield, 403-544-4739

Defence R&D Canada – Suffield

Contract Report
DRDC Suffield CR 2012-122
March 2012

NDG011406 Rev 1
March, 2012

ELECTRICAL IMPEDANCE IMAGING STUDY

FINAL REPORT

CONTRACT NO.: W7702-094241/001/EDM

Prepared for:

Dr. John McFee
DRDC Suffield

Abstract

This final report summarizes the findings obtained during the electrical impedance tomography study carried out during the period of July 2010 to March 2012 (Contract No: W7702-09 R241/001/EDM). The project was intended to evaluate the capability of detecting underground tunnels using EIT as well as to pursue various means of improving signal-to-error ratio through examination of random noise, modeling error and hardware imperfections. Phenomenology studies were conducted and the applications of tunnel detection and detection of munitions in culverts were examined.

Recommendations are made for a potential new instrument to be used for research and development purposes. Investigation into detection of ammunition rounds led to the conclusion that EIT is not an effective technology for this application

Résumé

Le présent rapport final résume les résultats obtenus au cours de l'étude de la tomographie par impédance électrique (TIE) réalisée de juillet 2010 à mars 2012 (n^{o} de contrat : W7702-09R241/001/EDM). Le projet visait à évaluer la capacité de détecter des tunnels souterrains au moyen de la TIE ainsi qu'à chercher divers moyens pour améliorer le rapport signal sur erreur, grâce à l'examen d'un bruit aléatoire, d'une erreur de modélisation et des imperfections du matériel. Des études phénoménologiques ont été réalisées, et des applications relatives à la détection de tunnels et de munitions dans les ponceaux ont été examinées.

Le rapport présente des recommandations relativement à un nouvel instrument potentiel à utiliser aux fins de recherche et développement. Les études sur la détection des munitions ont permis de conclure que la TIE n'est pas une technologie efficace pour cette application.

This page intentionally left blank.

Executive summary

Electrical impedance imaging study: Final report

Gail Bouchette; DRDC Suffield CR 2012-122; Defence R&D Canada – Suffield; March 2012.

This final report summarizes the findings obtained during the EIT Study carried out during the period of July 2010 to March 2012 (Contract No: W7702-09R241/001/EDM). The project was intended to evaluate the capability of detecting underground tunnels using EIT as well as to pursue various means of improving signal-to-error ratio. Error is generated from random noise and from non-random error associated with the system (such as modelling error and hardware imperfections). Many of the project tasks addressed various factors affecting signal-error ratio. The main tasks of the project were:

- development of a calibration strategy to quantify and account for hardware imperfections such as electronic bias (reducing non-random systematic error);
- study of electrode polarization to mitigate the effect of polarization on voltage measurements (reducing non-random systematic error);
- development of stimulation patterns to improve sensitivity to trans impedance variations at greater depth (enhancing signal strength);.
- study of EIDORS algorithm variants to improve reconstruction quality;
- evaluation of EIT for detecting underground tunnels and for detecting the presence of explosives packed inside a culvert;
- investigation of electrode contact with a soil medium, including effects of bad contact, methods of achieving good contact, and work-arounds for bad-contact cases (reducing noise and non-random systematic error);
- development of recommendations for any future re-design of the sensing electronics or instrument; and
- continued investigation of EIT capability for detecting ammunition rounds.

Calibration was shown to be of little value, since hardware error is small compared to other sources of error. Polarization was shown to be mitigable by balancing the current input. A newly developed stimulation pattern shows demonstrably increased sensitivity to transimpedance variations at depth. Four algorithm variants were studied, two of which may show some promise. The EIT system was successful at detecting the presence of simulated tunnels and culverts in the lab, although the presence of a simulated explosive packed inside a simulated culvert was not detected.

As part of the tunnel/culvert task a thorough investigation was undertaken into electrode contact with a soil medium, leading to a new understanding of factors contributing to good contact and work-around options for bad-contact cases. The results of this work have suggested that the next major error source limiting EIT performance is inaccurate modeling of the electrode-soil interface, including physical relative position of electrodes and electrical properties of the interface. It is recommended that future development of EIT technology focus on this challenge.

Recommendations are made for a potential new instrument to be used for research and development purposes. Investigation into detection of ammunition rounds led to the conclusion that EIT is not an effective technology for this application.

Sommaire

Electrical impedance imaging study: Final report (étude de l'imagerie par impédance électrique : rapport final)

Gail Bouchette. DRDC Suffield CR 2012-122, R & D pour la défense Canada – Suffield, mars 2012.

Le présent rapport final résume les résultats obtenus au cours de l'étude de la TIE réalisée de juillet 2010 à mars 2012 (n° de contrat : W7702-09R241/001/EDM). Le projet visait à évaluer la capacité de détecter des tunnels souterrains au moyen de la TIE ainsi qu'à chercher divers moyens pour améliorer le rapport signal sur erreur. Une erreur est produite par un bruit aléatoire et une erreur non aléatoire associée au système (comme une erreur de modélisation et des imperfections du matériel). Une bonne partie des tâches du projet portent sur divers facteurs qui influent sur le rapport signal sur erreur. Les principales tâches du projet sont :

- élaboration d'une stratégie d'étalonnage pour calculer et tenir compte des imperfections du matériel, comme une polarisation électronique (qui réduit l'erreur systématique non aléatoire);
- étude de la polarisation des électrodes afin de réduire l'effet de polarisation sur les mesures de la tension (réduction de l'erreur systématique non aléatoire);
- développement de modèles de stimulation pour améliorer la sensibilité aux variations transimpédances à une profondeur plus grande (amélioration de la puissance du signal);
- étude des variantes de l'algorithme d'EIDORS pour améliorer la qualité de la reconstruction;
- évaluation de la TIE pour détecter les tunnels souterrains ainsi que la présence d'explosifs placés dans un ponceau;
- étude du contact des électrodes avec le sol terreux, y compris les effets d'un mauvais contact, les méthodes pour obtenir un bon contact et les solutions de rechange pour les cas de mauvais contact (réduction du bruit et erreur systématique non aléatoire);
- formulation de recommandations pour modifier ultérieurement la conception des capteurs électroniques ou des instruments;
- étude continue de la capacité de la TIE de détecter des munitions.

L'étalonnage s'est avéré peut utile, car l'erreur du matériel est petite par rapport aux autres sources d'erreur. La polarisation peut être réduite en équilibrant l'entrée de courant. Un nouveau modèle de stimulation montre une augmentation considérable de la sensibilité aux variations de transimpédance en profondeur. Quatre variantes d'algorithme ont été étudiées, dont deux suscitent certains espoirs. Le système de la TIE a réussi à détecter la présence de tunnels et de ponceaux simulés en laboratoire, même si la présence d'explosifs simulés placés dans un ponceau simulé n'a pas été détectée.

Dans le cadre du projet sur les tunnels et les ponceaux, une étude approfondie a été réalisée relativement au contact des électrodes avec le sol terreux, et a entraîné une nouvelle compréhension des facteurs qui contribuent à un bon contact et aux solutions de rechange en cas de mauvais contact. Les résultats des

travaux semblent indiquer que la prochaine source d'erreurs importantes qui limite les performances de la TIE est la modélisation inexacte de l'interface électrode-sol, y compris la position relative des électrodes et les propriétés électriques de l'interface. On recommande que le développement futur de la technologie TIE porte sur ce défi.

Le rapport présente des recommandations relativement à un nouvel instrument qui pourrait être utilisé aux fins de recherche et développement. Les études sur la détection des munitions ont permis de conclure que la TIE n'est pas une technologie efficace pour cette application.

TABLE OF CONTENTS

SECTION TITLE **PAGE**

LIST OF FIGURES

LIST OF TABLES

This page intentionally left blank.

1 Executive Summary

This final report summarizes the findings obtained during the EIT Study carried out during the period of July 2010 to March 2012 (Contract No: W7702-09R241/001/EDM). The project was intended to evaluate the capability of detecting underground tunnels using EIT as well as to pursue various means of improving signal-to-error ratio. Error is generated from random noise and from non-random error associated with the system (such as modelling error and hardware imperfections). Many of the project tasks addressed various factors affecting signal-error ratio. The main tasks of the project were:

- Development of a calibration strategy to quantify and account for hardware imperfections such as electronic bias (reducing non-random systematic error).
- Study of electrode polarization to mitigate the effect of polarization on voltage measurements (reducing non-random systematic error).
- Development of stimulation patterns to improve sensitivity to transimpedance variations at greater depth (enhancing signal strength).
- Study of EIDORS algorithm variants to improve reconstruction quality.
- Evaluation of EIT for detecting underground tunnels and for detecting the presence of explosives packed inside a culvert.
- Investigation of electrode contact with a soil medium, including effects of bad contact, methods of achieving good contact, and work-arounds for bad-contact cases (reducing noise and non-random systematic error).
- Development of recommendations for any future re-design of the sensing electronics or instrument.
- Continued investigation of EIT capability for detecting ammunition rounds.

Calibration was shown to be of little value, since hardware error is small compared to other sources of error. Polarization was shown to be mitigable by balancing the current input. A newly developed stimulation pattern shows demonstrably increased sensitivity to transimpedance variations at depth. Four algorithm variants were studied, two of which may show some promise. The EIT system was successful at detecting the presence of simulated tunnels and culverts in the lab, although the presence of a simulated explosive packed inside a simulated culvert was not detected.

As part of the tunnel/culvert task a thorough investigation was undertaken into electrode contact with a soil medium, leading to a new understanding of factors contributing to good contact and work-around options for bad-contact cases. The results of this work have suggested that the next major error source limiting EIT performance is inaccurate modelling of the electrode-soil interface, including physical relative position of electrodes and electrical properties of the interface. It is recommended that future development of EIT technology focus on this challenge.

Recommendations are made for a potential new instrument to be used for research and development purposes. Investigation into detection of ammunition rounds led to the conclusion that EIT is not an effective technology for this application.

2 Introduction

Background:

The work performed under the current contract is a follow-on to a previous contract (W7702-07-R159), which was aimed at developing several aspects of EIT technology. Project objectives included evaluation of the EIDORS algorithm suite, experimentation with a finer-resolution array, evaluation of performance in various water conditions (salinity, turbidity, rustiness of target), and comparison of EIT to traditional EMI detection in salt water. The research led to further recommendations for more detailed research, which formed the technical objectives of the current project.

Project Objectives:

This project has the following technical objectives:

- Develop a calibration strategy to reduce or compensate for hardware errors.
- Investigate further algorithm variations in the EIDORS framework.
- Study the polarization phenomenon that occurs in a water medium and investigate ways to reduce or mitigate its effects.
- Conduct further ammunition round experiments to determine how the presence of paint, including spotty paint coverage, affects the detectability of a round using EIT.
- Evaluate the feasibility of EIT to detect underground tunnels and to detect the presence of materials hidden in culverts, using lab mock-ups of these operational scenarios.
- Make recommendations for desired features of a next-generation hardware design, including the data collection instrument and electronics.

This report provides a brief description of the EIT technology and presents the results obtained from the aforementioned work.

3 Applicable Documents & References

3.1 Applicable Documents

Final report, contract W7702-07-R159.

3.2 References

[1] H Gagnon, AE Hartinger, M Cousineau, A Adler, R Guardo. A resistive mesh phantom for assessing the performance of EIT systems. IEEE T Biomed. Eng., 57:2257-2266, 2010.

[2] A Adler. Accounting for erroneous electrode data in electrical impedance tomography. Physiol. Meas., 25:227-238, 2004.

[3] A Adler, G Elke, S Pulletz, J Scholz, N Weiler, I Frerichs. Assessment of regional lung ventilation and aeration by electrical impedance tomography – effects of different image reconstruction procedures. (submitted 2012).

[4] A Adler, PO Gaggero, Y Maimaitijiang. Adjacent Stimulation and Measurement Patterns Considered Harmful. Physiol. Meas., 32:731-744, 2011.

4 EIT System

4.1 Architecture

The functional architecture of the EIT system is shown in Figure 1 below. The data acquisition software resides on a stand-alone computer, either desktop or laptop, and controls the data acquisition electronics residing in a separate enclosure. The data acquisition software reads the set of configurations defining the stimulation and recording patterns and directs the data acquisition electronics to activate the proper electrode configurations on the electrode array. The measured data is in turn transferred to the data acquisition computer that can also run a Matlab application doing a volumetric reconstruction and detection.

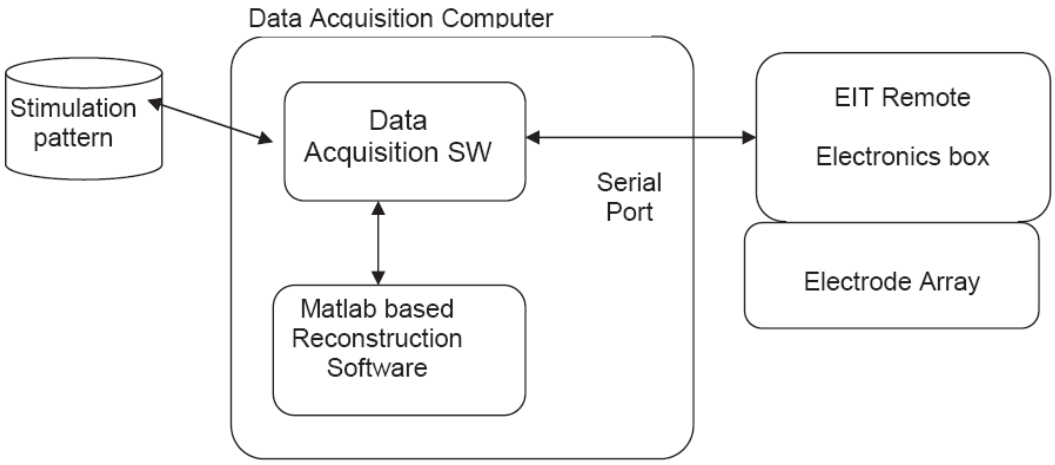

Figure 1. EIT functional system architecture

4.2 Electrode Array Construction

An electrode array has been designed and built so that it can be used underwater or on soil (as described below, the electrode shape was found to be ill-suited for good electrode contact in soil, but the system can safely operate in this environment and can produce good data under certain circumstances). The support is made of a sheet of Plexiglas with a pitch of 4cm between each electrode in both directions. The size of the array is 36x36cm; however, the electrodes span a size of 28x28cm.

The Plexiglas plate has a 2.2cm thickness. It is machined with a 1cm indentation over a surface of 31x31cm. The electrodes (one-inch stainless steel bolts) are threaded through the holes with a ring lug connector on each electrode. The indentation is then filled with an epoxy compound that solidifies in place and ensures that the top side of the electrode array is electrically insulated. This arrangement forces the current lines to move below the array, in the medium of interest.

Figure 2 shows a picture of the electrode array, with 4 harnesses connecting 16 electrodes each. The electrode array is held by four large nylon bolts attached to a structure on top of the water tank that can move on rollers along the *x* direction. Figure 3 shows the set-up. The electrode array can be lowered in the water tank by adjusting the position of the nylon nuts

holding the Plexiglas structure on the large nylon bolts. Nylon was used as a non-conductive support material in order to prevent the disruption of the current lines.

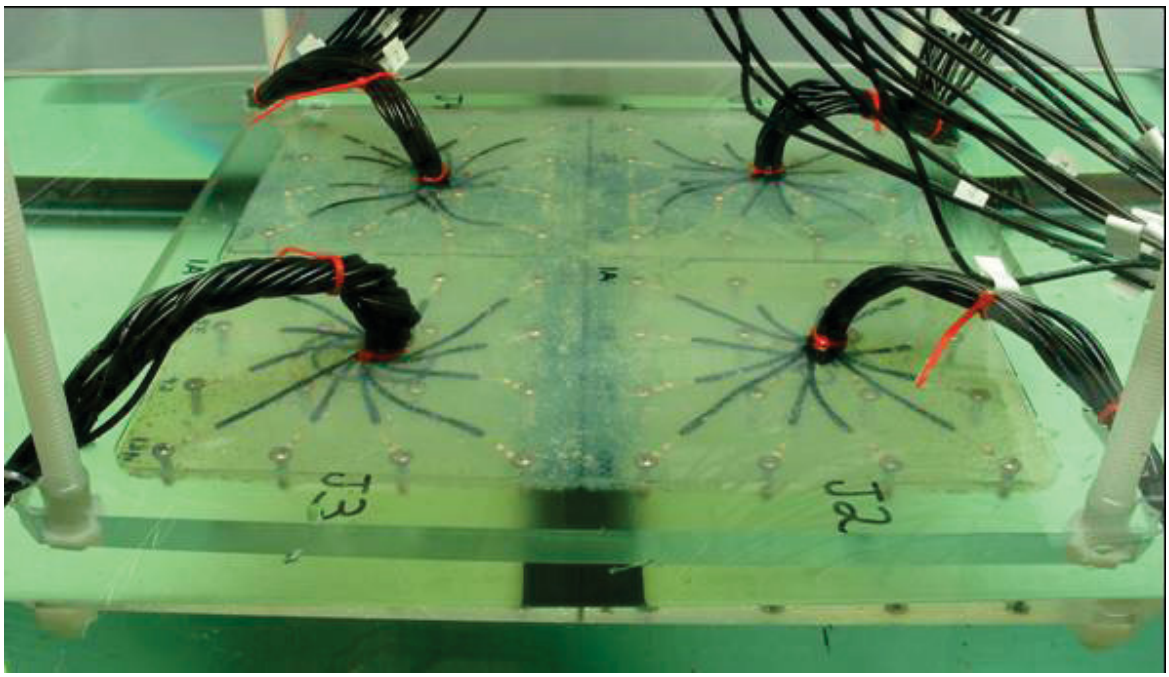

Figure 2. The electrode array

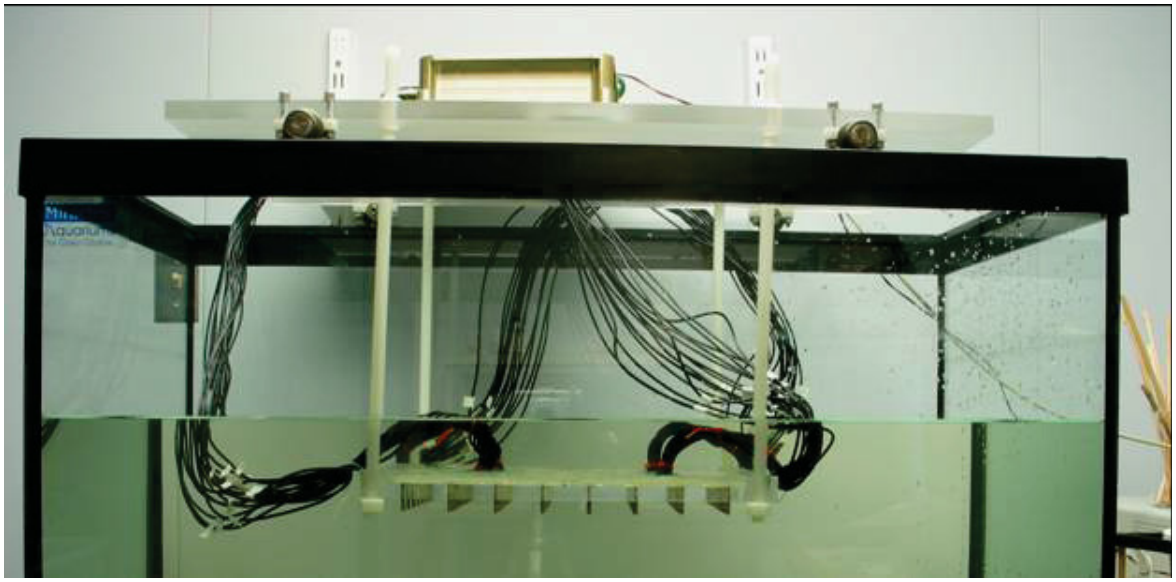

Figure 3. The moving structure holding the electrode array

Figure 4 shows the electrode numbering convention on the array. The coordinate system origin is set at the center of the array, with the positive *y* axis pointing upward and the positive *x* axis pointing to the right.

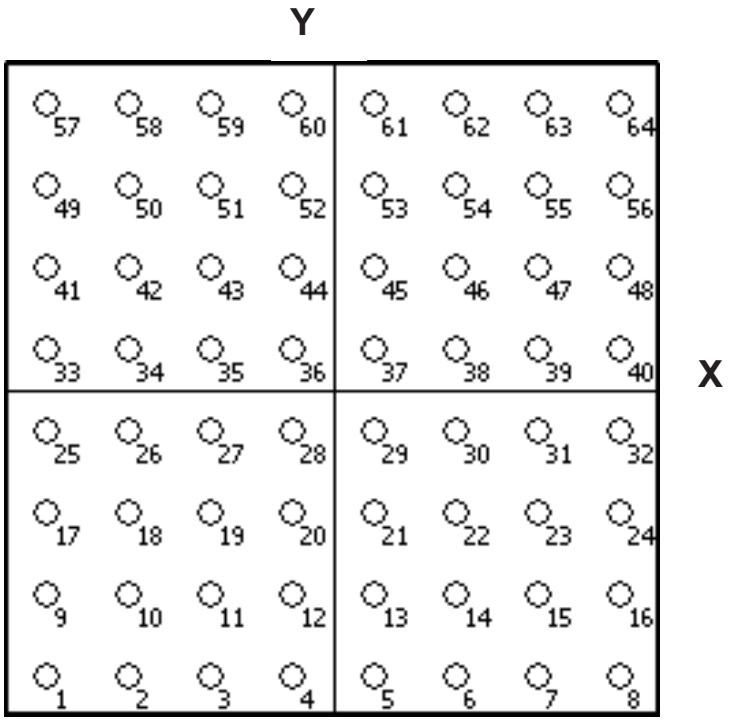

Figure 4. Electrode array numbering and coordinate system

5 Results

5.1 Calibration task

The goal in developing a calibration procedure was to quantify and compensate for unmodelled error sources in the system hardware. Error sources include imperfect common mode rejection in differential amplifiers, error in resistance values of circuit components, and contact impedance at electrode-medium interfaces. It was believed that these hardware error sources were a dominant factor limiting the quality of reconstruction results.

The development of a calibration procedure was to be broken down into three stages, beginning with determining whether system errors can be measured by acquisitions of a known medium. The second and third stages would comprise determining whether these measurements could be used to improve image quality and then developing a strategy appropriate for field use.

During the first stage of the calibration task hardware system errors were measured and were found to be much lower than expected. Hardware error is not a dominant factor limiting reconstruction results as previously believed. Other aspects of the technology such as electrode stimulation pattern and system modelling are likely more influential on image quality.

The error measurement strategy and results are described in the subsequent sections. Two instrument configurations were used to take hardware error measurements. First a preliminary test was performed using a network of resistors connected to a subset of electrodes in the array. Second the array was put in the tank with a water-and-sand medium and measurements on one set of electrodes were taken periodically over several days to measure hardware drift.

5.1.1 Resistor network experiments

The first experiment to assess hardware error levels used a network of resistors connected to a subset of electrodes in the array. Precision resistors were used, manufactured with a 1% tolerance and measured to approximately 0.1% tolerance. A simple circuit was connected to nodes in the array as shown in Figure 5.

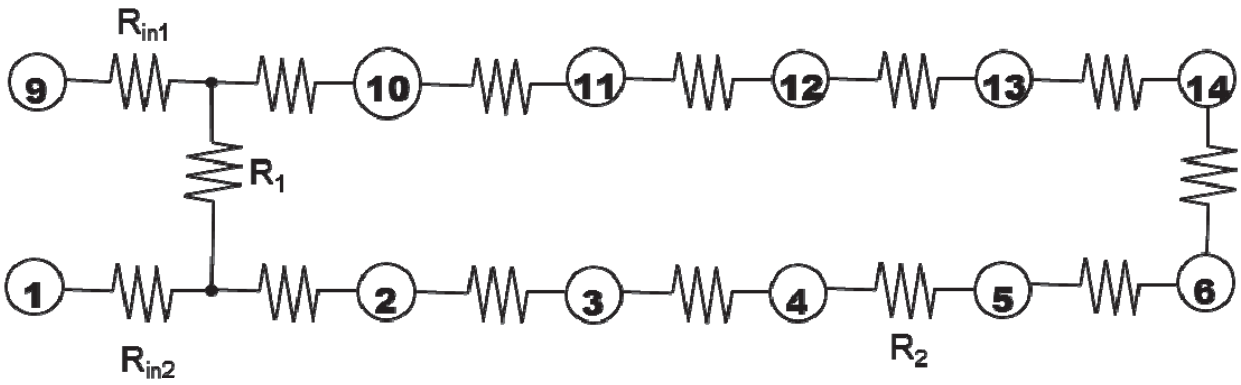

Figure 5. Resistor network for calibration. All unlabelled resistances are 1kΩ.

Transimpedances of this set-up were measured by stimulating an adjacent pair of electrodes with the current and recording the voltage on each other adjacent pair of electrodes, then moving the stimulating current to another adjacent pair. For example, electrodes 9 and 1 were stimulated while voltage recordings were made on pairs 2-3, 3-4, …, 11-10. Then pair 1-2 was stimulated while recordings were made on pairs 3-4, 4-5, …, 10-9.

The theoretical and actual transimpedance values associated with the stimulation pattern are related as follows

$$A = T + n_o + n_i,$$

where

A is the actual measured transimpedances
T is the theoretical transimpedances
n_o is random noise
n_i is the contribution of the non-ideal properties of the system to the measurements.

The theoretical transimpedances were computed and the actual values were measured using the EIT instrument. The difference $n = n_o + n_i$ cannot be separated into its two components to explicitly compute the non-ideal behaviour of the system, but the noise n_o may be estimated and in this case was estimated to be on the order of 0.1% based on the measurements taken of the precision resistors.

Several different resistor network configurations were used to gather information about different aspects of non-ideal behaviour. Table 1 lists the resistor configurations used and the resulting error values.

	R_1	R_{in1}	R_{in2}	R_2	**Test goal**	**Error (%)**
1	1kΩ	0	0	1kΩ	Evaluate linearity of measurements (compare to configurations 2 and 3).	0.078
2	2kΩ	0	0	1kΩ	Evaluate linearity of measurements (compare to configurations 1 and 3).	0.081
3	3kΩ	0	0	1kΩ	Evaluate linearity of measurements (compare to configurations 1 and 2).	0.072
4	1kΩ	1kΩ	0	1kΩ	Evaluate effects of current source imperfections.	0.085
5	1kΩ	1kΩ	1kΩ	1kΩ	Evaluate effects of current source imperfections.	0.098
6	1kΩ	0	0	1kΩ	Repeat linearity evaluation on a different electrode pair.	-
7	1kΩ	0	0	2kΩ	Repeat linearity evaluation on a different electrode pair.	-

Table 1 - Circuit configurations for resistor network experiment.

Percentage error was calculated as the rms difference between predicted and measured transimpedance values divided by the rms measured value. In all configurations the theoretical and actual transimpedances differed on the order of 0.1%; that is to say the non-ideal behaviour of the system was not discernible above the noise. For this reason it was not possible to identify specific sources of non-ideal behaviour.

This result indicates that, contrary to the initial hypothesis, hardware error sources are not a dominant limiter on reconstruction quality. One error source that does not appear in this configuration but may occur in the operational setting is polarization of electrodes in the water medium. This topic is discussed in Section 5.3.

5.1.2 Drift experiments

Drift of the electronics was measured with the array in the aquarium using a sand-and-water medium; the array was suspended near the top of the water layer, approximately 20 cm from the sediment (see Figure 6). A simple pattern was used, stimulating on just one pair of electrodes and recording on one neighbouring pair. This configuration was repeated nine times to create a ten-configuration stimulation pattern. A data acquisition using this pattern was performed every ten minutes for 116 hours, with the results shown in Figure 7.

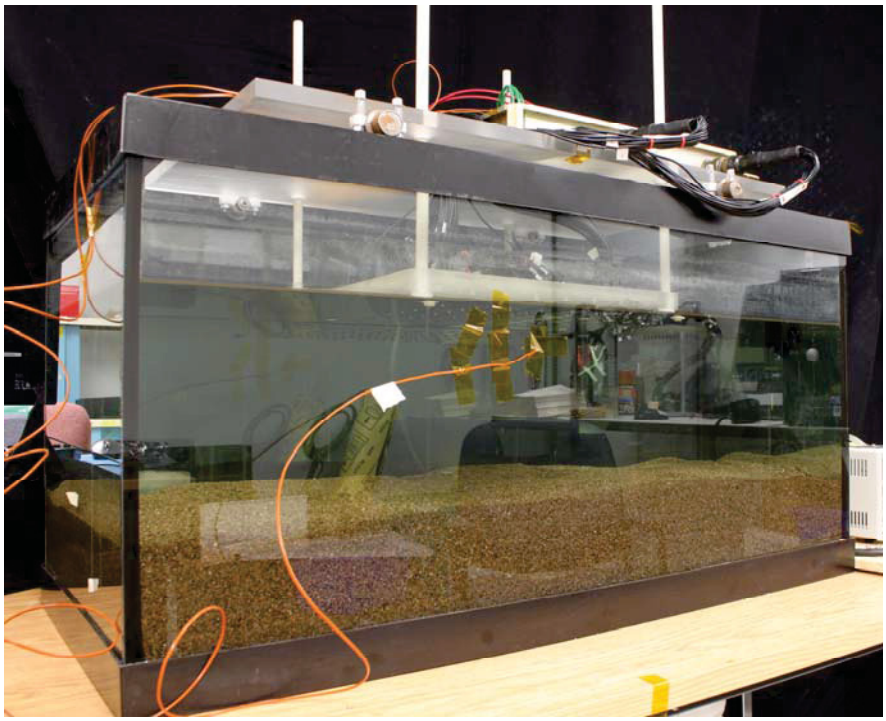

Figure 6. Drift test set-up.

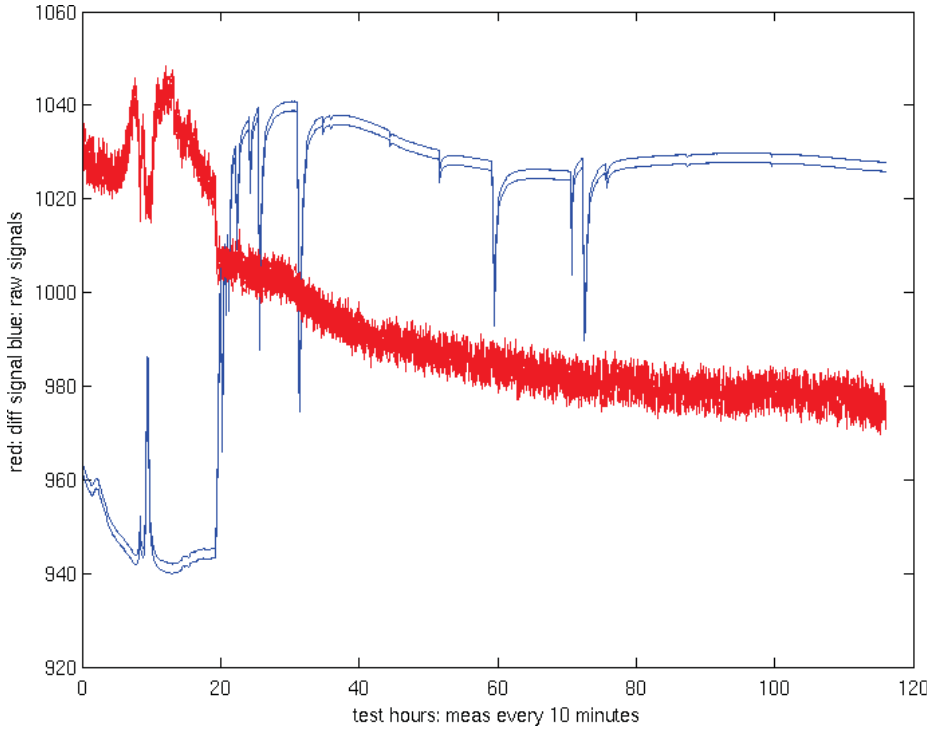

Figure 7. Voltage measurements from drift test. The two blue lines show voltage measurements from the respective recording electrodes. The red plot shows the difference between the two measurements, representing the transimpedance. The vertical axis measures the voltage difference in counts.

The voltage difference, shown in red, has an unusual fluctuation in the first twenty hours, which has not been explained. It is possible that temperature fluctuations in the laboratory caused this behaviour. After hour twenty the drift is slow – under 2% over the ensuing 96 hours – indicating that hardware drift is not a problem under stable data acquisition conditions.

It is concluded that hardware calibration is not a dominant source of system error. Other areas of performance improvement may be more fruitful to pursue, such as contact impedance reduction/compensation and stimulation pattern design.

5.2 EIDORS investigation

Two investigations were undertaken in this task. First the development of stimulation patterns that are more sensitive to transimpedance variations was explored. Second, using the original stimulation pattern and one developed during this study, several reconstruction algorithm variations were investigated with the goal of improving reconstructed image quality.

5.2.1 Stimulation patterns

The accurate measurement of transimpedance is the first requirement in generating reliable EIT images. Effective algorithms for processing the measurements to reconstruct conductivity profiles can also enhance image quality greatly. Another important factor is the choice of

measurements to be made, that is the pattern of stimulation (and recording) on electrodes within the array.

It is not practicable to stimulate on every combination of electrodes (for an array of 64 electrodes there are nearly four million possible electrode quadruples). A shorter stimulation pattern must therefore be chosen to extract enough information from the medium to generate an image with the desired accuracy. The choice of stimulation pattern can have a great effect on the reconstructed results and has not yet been studied in detail on this program. In this project a study was undertaken to find stimulation patterns that maximize the sensitivity of the measurements to conductivity variations within the desired region. A theoretical development of sensitivity analysis is presented in Appendix D.

Sensitivity of a measurement is essentially the signal-noise ratio corresponding to small changes in transimpedance [4]. Using this SNR definition of sensitivity the goal is to maximize sensitivity at different layer depths. Randomly selected stimulation patterns were generated and tested, and found to have good sensitivity. Additional goals for improving on this starting point include:

- using the same stimulating pair for many configurations, so that 'warm-up' times can be inserted into the stimulation pattern (see Section 5.5.3.1).

- segregating stimulation and measurement electrodes, that is designating each electrode for stimulation or recording but never both, to

    - facilitate not measuring on stimulation electrodes.

    - afford a potential future design with electrodes specifically designed for either stimulation or measurement.

- using fewer stimulating than measuring electrodes. Medium contact is particularly important for stimulating electrodes, so fewer electrodes having this requirement make a more robust instrument.

- symmetry in the pattern to facilitate visual inspection to observe trends. Symmetry will also allow special tests to measure sensitivity in carefully designed cases.

- good sensitivity at greater depths, which may be achieved by measuring across electrodes that are far apart.

A stimulation pattern was developed based on these goals, as shown in Figure 8; the pattern has come to be known as the May 19th stimulation pattern, after the date on which it was created. Stimulating pairs were selected from among the twenty-eight electrodes around the outer ring of the array, Each of these electrodes was paired with the electrode eleven steps away from it, counting counter-clockwise around the periphery (top left). This approach creates stimulating pairs that are far apart to improve depth penetration.

Measurement pairs are selected in several stages (all measurement pairs are then put into a list to generate the final stimulation pattern). In the first stage the next ring of the electrode is used, that is the set of electrodes that are adjacent to an outer ring electrode (Figure 8, top right).

Each electrode is paired with the one seven steps away from it; this approach creates recorded pairs that are far apart, which also improves depth penetration.

The second stage of measurement pair selection (Figure 8, bottom right), uses a 4 x 4 ring in the bottom right quadrant of the electrode array, with pairs separated by four steps. The bottom-left quadrant of the array is measured likewise (Figure 8, bottom left), as are the top left and top right quadrants (not shown). These quadrants of closer measurements improve sensitivity in their respective regions.

The full stimulation pattern was generated by using the full set of measurement pairs with each stimulating pair.

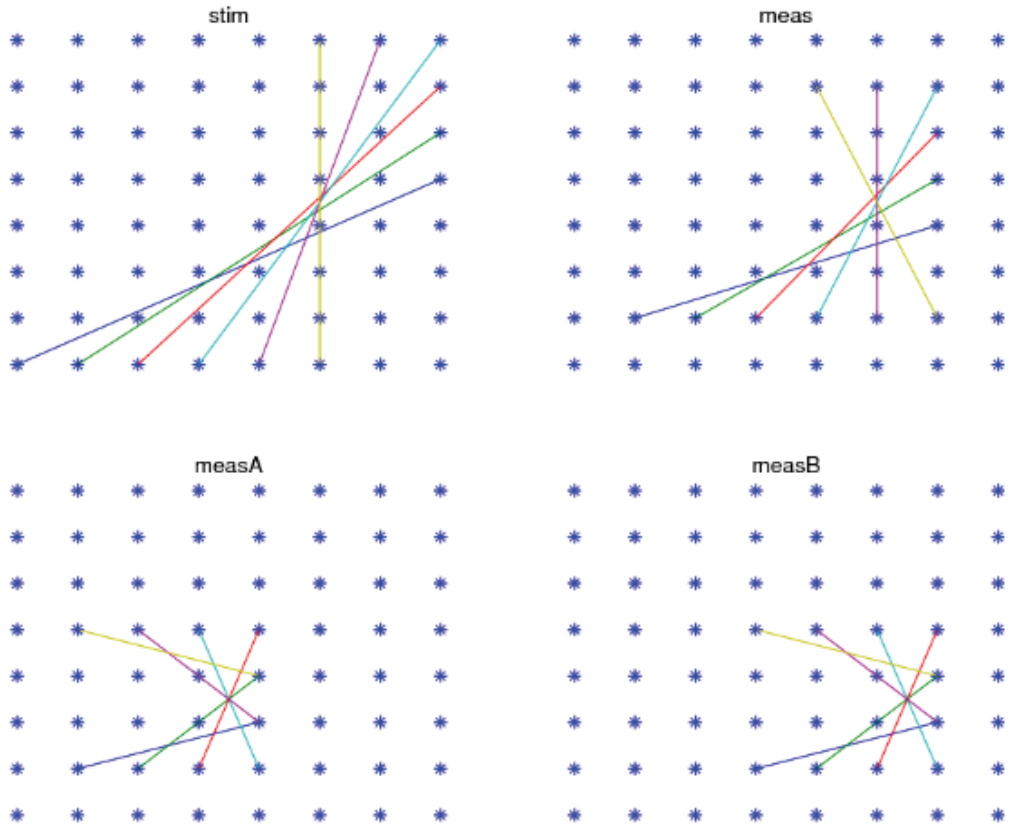

Figure 8. Stimulation pattern designed for sensitivity at depth. Coloured lines connect (stimulating or recording) electrode pairs.

Figure 9 shows the sensitivity of the new stimulation pattern and the original Augbb pattern at three different depths. In both cases the sensitivity is very high near the surface and drops off as depth increases. The May 19th pattern drops off much less than the Augbb pattern, however.

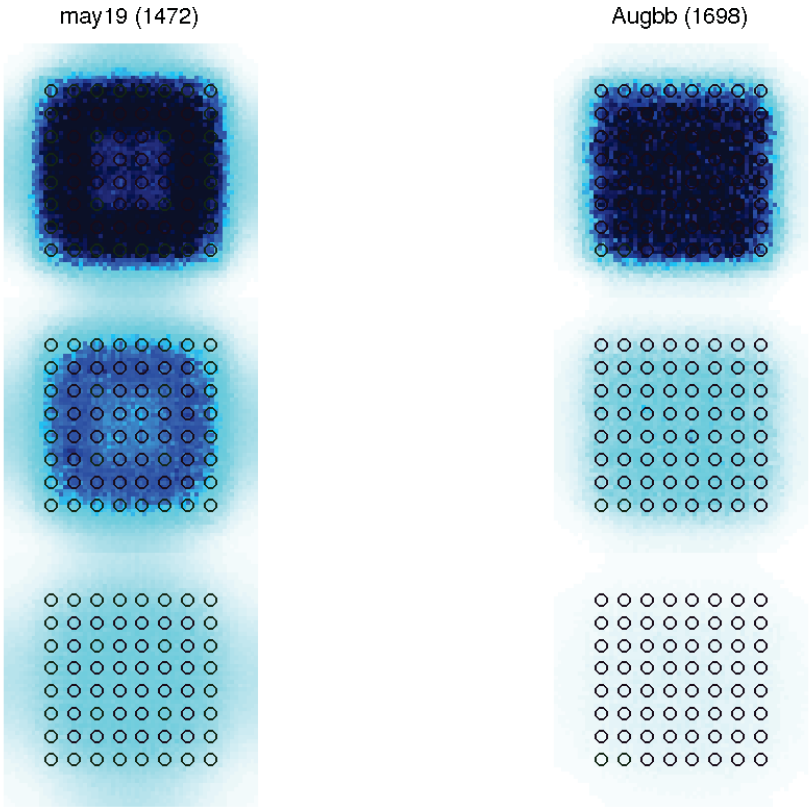

Figure 9. Sensitivity of May 19th stim pattern (left) and original Augbb stim pattern (right) at depths of 3cm, 5cm, and 8cm (top to bottom). Darker blue corresponds to greater sensitivity.

Figure 10 shows cross-sections of the sensitivity distributions shown in Figure 9. The sensitivity levels decrease with depth, as expected, and do so more severely in the Augbb pattern. The May 19th pattern exhibits a dip in conductivity near the centre of the array, especially at shallower depths.

This dip can likely be corrected with minor modifications to the stimulation pattern. The May 19th pattern is an early attempt to improve sensitivity using the aforementioned design criteria, but it has not undergone a rigorous optimization process.

Figure 11 shows the sensitivity as a function of depth, for various points under the array. Again, the May 19th stimulation pattern loses sensitivity much more gradually than the Augbb pattern.

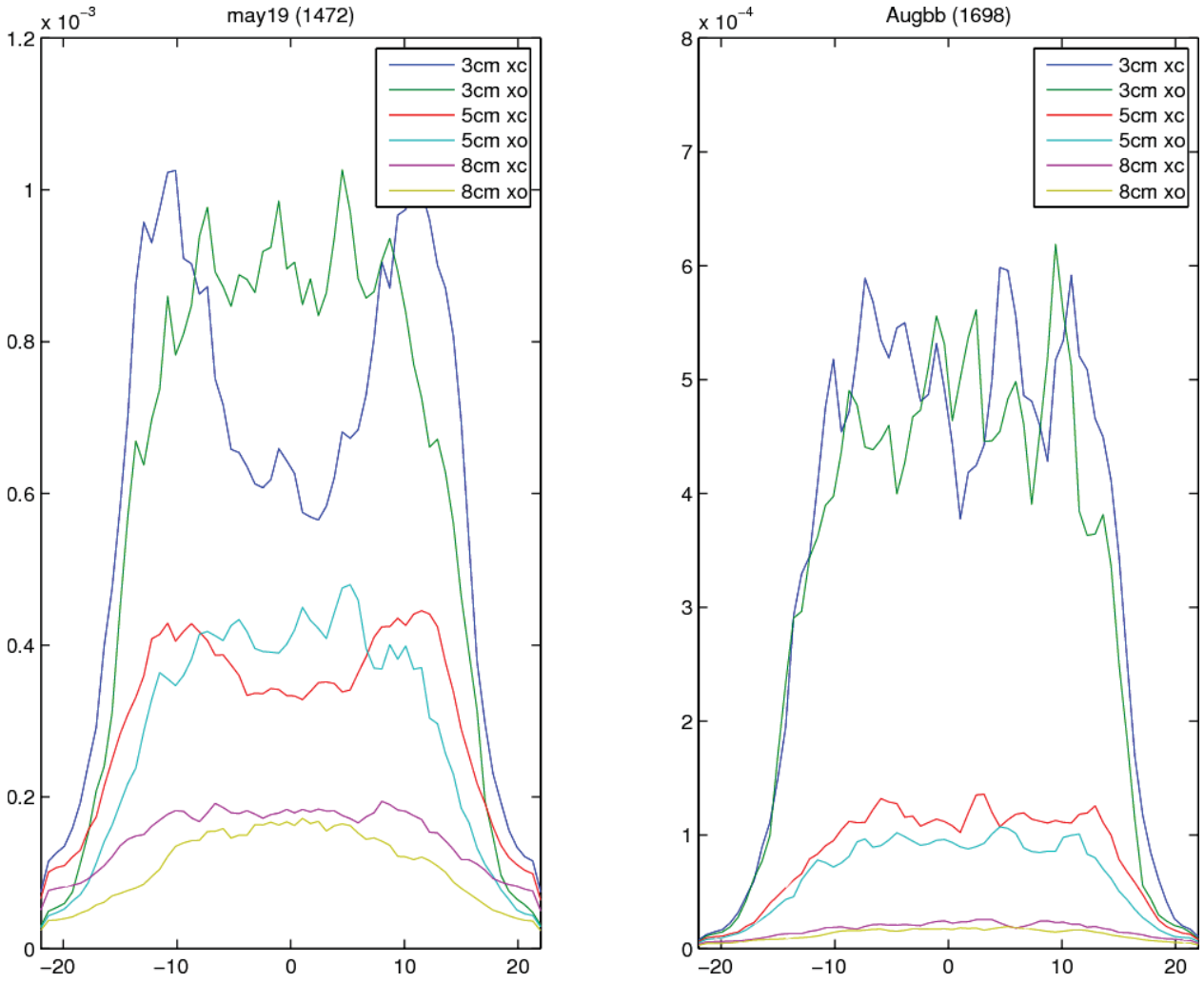

Figure 10. Cross-sections of sensitivity images from Figure 9. Distance from left to right across the array is plotted on the *x* axis, and sensitivity is on the *y* axis. Plots labelled 'xc' are sections taken across the centre of the array, between the fourth and fifth electrode rows; those labelled 'xo' are taken between the second and third rows.

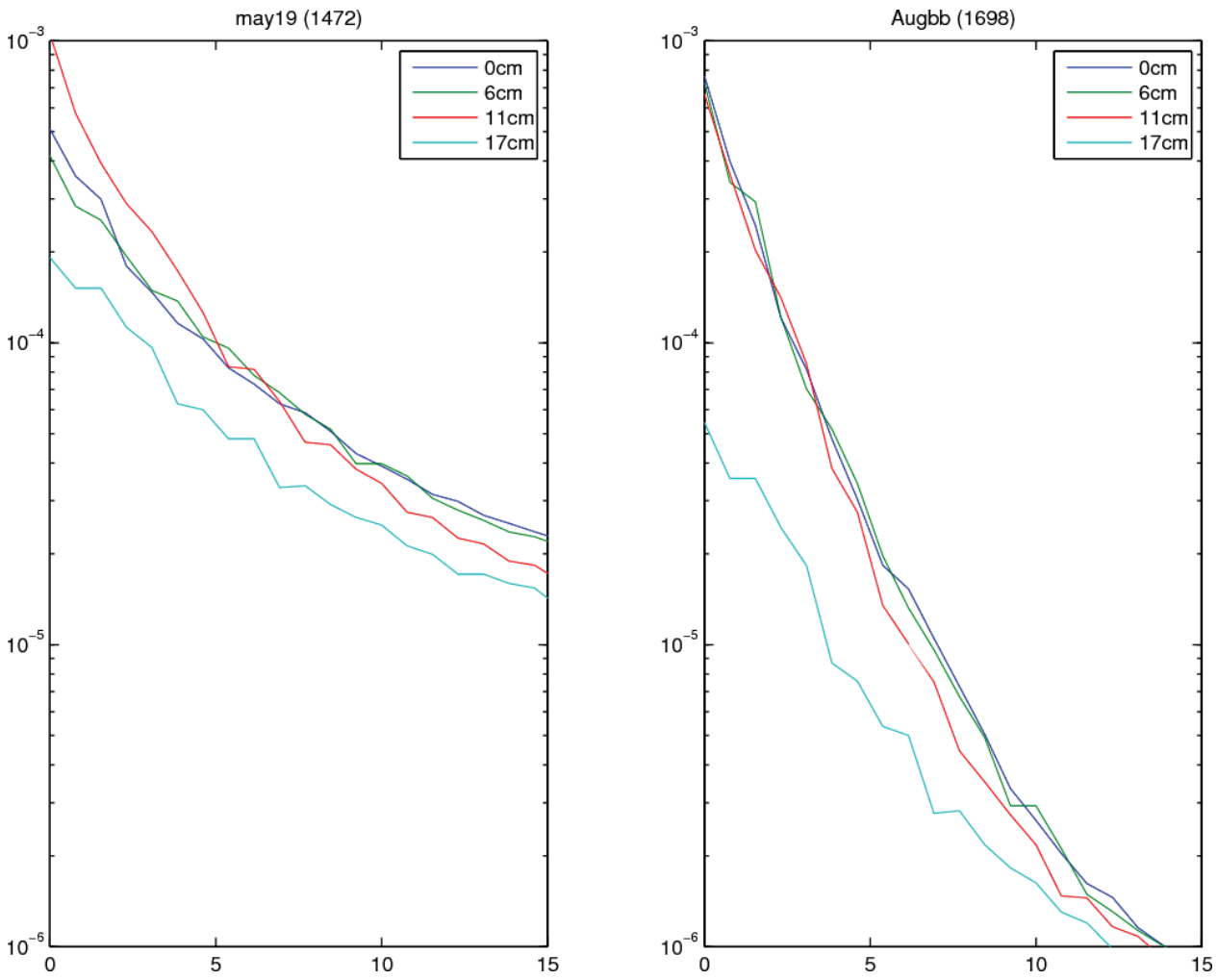

Figure 11. Sensitivity vs. depth at four different points under the array. Depth in centimetres is plotted on the *x* axis and sensitivity is on the *y* axis. Data is plotted at distances of 0cm, 6cm, 11cm, and 17cm from the centre of the array (the 17cm plot is off the edge of the array).

The new stimulation pattern results in moderately improved reconstruction images, but the improvement is not as marked as expected given the increased sensitivity. Figure 12 shows reconstructions from two data acquisitions, one taken using the May 19th pattern and one taken with Augbb. The Augbb reconstruction places the target closer to the edge of the array than its true location, whereas the May 19th reconstruction has better localization accuracy. The strength of the signal does not appear greatly improved at depth, however. (Note that the higher sensitivity of the new pattern causes greater susceptibility to the effects of the aquarium walls and floor. As these effects have not been disruptive in the past, no great effort has gone into modelling and compensating for them; a better model may become necessary as this research progresses.)

To learn why reconstructions did not improve as expected, the modelling error of both scans was studied. The simulated and measured transimpedance values are plotted together for comparison in Figure 13; discrepancies indicate modelling error. We first observe incidentally that the transimpedances are larger in absolute value for the May 19th pattern, which is consistent with the increased sensitivity resulting from more distantly spaced measurement

electrodes. The error between the simulated and measured values, however, is not greatly different from that of the augbb pattern. This finding suggests that the modelling error, not the sensitivity, is now the dominant performance limiter.

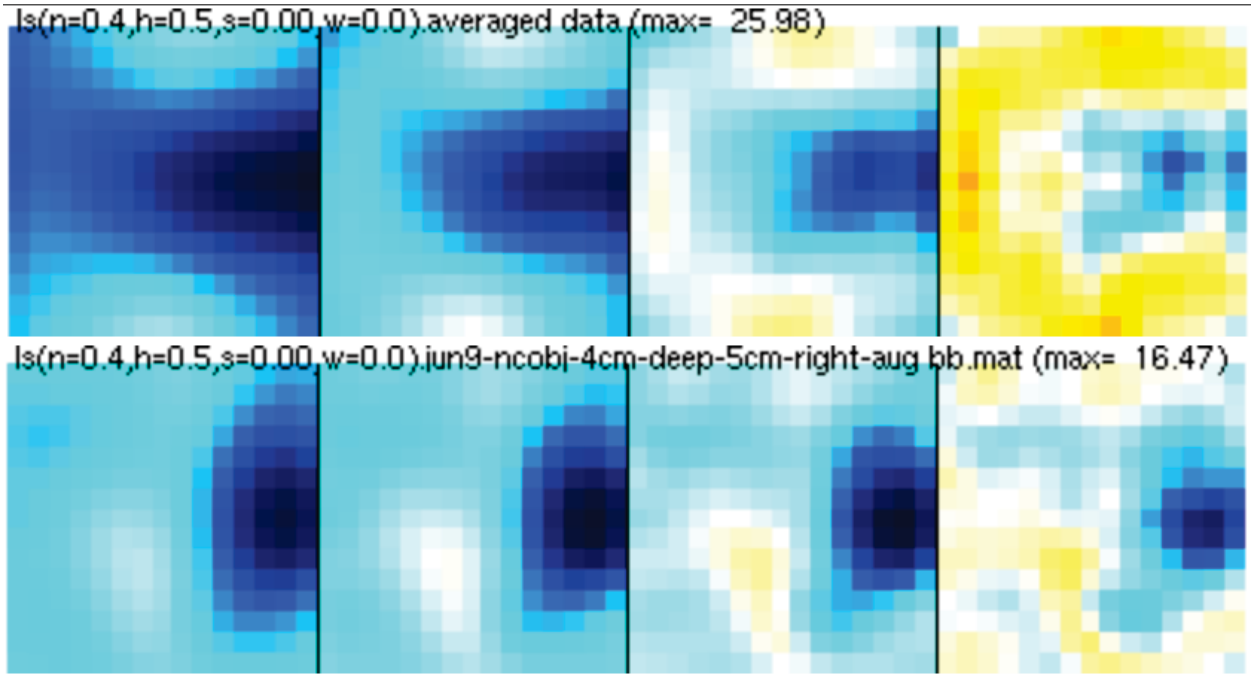

Figure 12. Reconstructions of a non-conductive target buried 4cm deep and 5cm to the right of centre. Data is acquired using the May 19th stim pattern (top) and the augbb stim pattern (bottom). Images show increasing depth from left to right of 3cm, 4cm, 5cm, and 6cm.

In the previous contract some work was done to improve the model accuracy with more precise models of the electrode size and shape, using Finite Element Modelling (FEM). The resulting model did not improve reconstructions greatly, and was therefore not used for subsequent research.

The next hypothesis to test is that the electrical interface between the electrodes and the soil medium is the dominant source of model inaccuracy. It was found during the tunnel investigation in this contract (see Section 5.5.2) that electrode contact is both highly influential on reconstruction quality and difficult to achieve in a soil medium. As illustrated in Figure 11, sensitivity near the surface is at least an order of magnitude greater than at a depth equal to half the dimension of the array. Contact impedances at the electrodes therefore introduce an error that is amplified by a factor of ten compared to the signal created by the target object.

Improving the electrode design to facilitate good contact is one avenue of study to improve performance. Another important step is to build more accurate models of the electrode-soil interface, including electrical properties of the interface and physical relative positions of electrodes. Some preliminary work has been begun on this topic and is discussed in Appendix E.

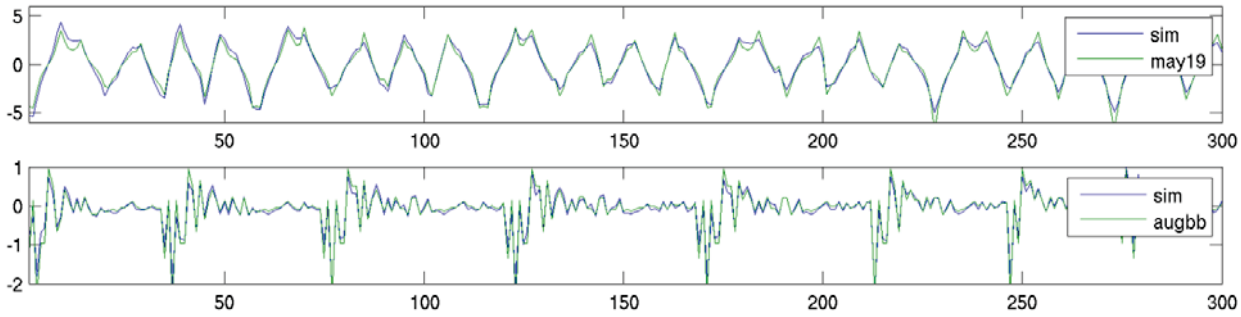

Figure 13. Simulated and measured transimpedance values for the May 19th pattern (top) and the Augbb pattern (bottom). Note different *y*-axis scales.

5.2.2 Algorithm variants

The EIDORS code structure provides a convenient framework in which variants on image reconstruction procedures can be implemented and tested. Many algorithms and variants have been implemented already by contributors to the open-source suite, and testing is often a relatively simple matter of selecting algorithms and parameters within a high-level script. For this research several algorithm variants of primary interest were identified and investigated (a theoretical definition and development of these algorithms is presented in Appendix C):

- Normalization (effectively weighting by transimpedance value)
- Smoothed image prior
- Total variation
- Robust data norm

Before investigating these algorithms a check was performed to evaluate the measurement error of the instrument in comparison with medium modelling error. Acquisitions were recorded using a given stimulation pattern and a variation on it in which both stimulating and recording pairs were reversed. Differences between these acquisitions indicate measurement errors within the instrument, as the transimpedances are theoretically of identical magnitude in both cases. As shown in Figure 14, the images are very similar for both acquisitions, indicating that measurement error is small compared to medium modelling error.

In Figure 14 and all reconstructions shown in this section, the four images from left to right are cross-sections of the reconstruction at depths of 3cm, 4cm, 5cm, and 6cm. The non-conductive target is buried approximately 4cm deep and 5cm to the right of centre. The ‘max’ value listed in the text string above each reconstruction represents the strength of the strongest signal within the medium. The colour map is scaled between zero and this value for each reconstruction.

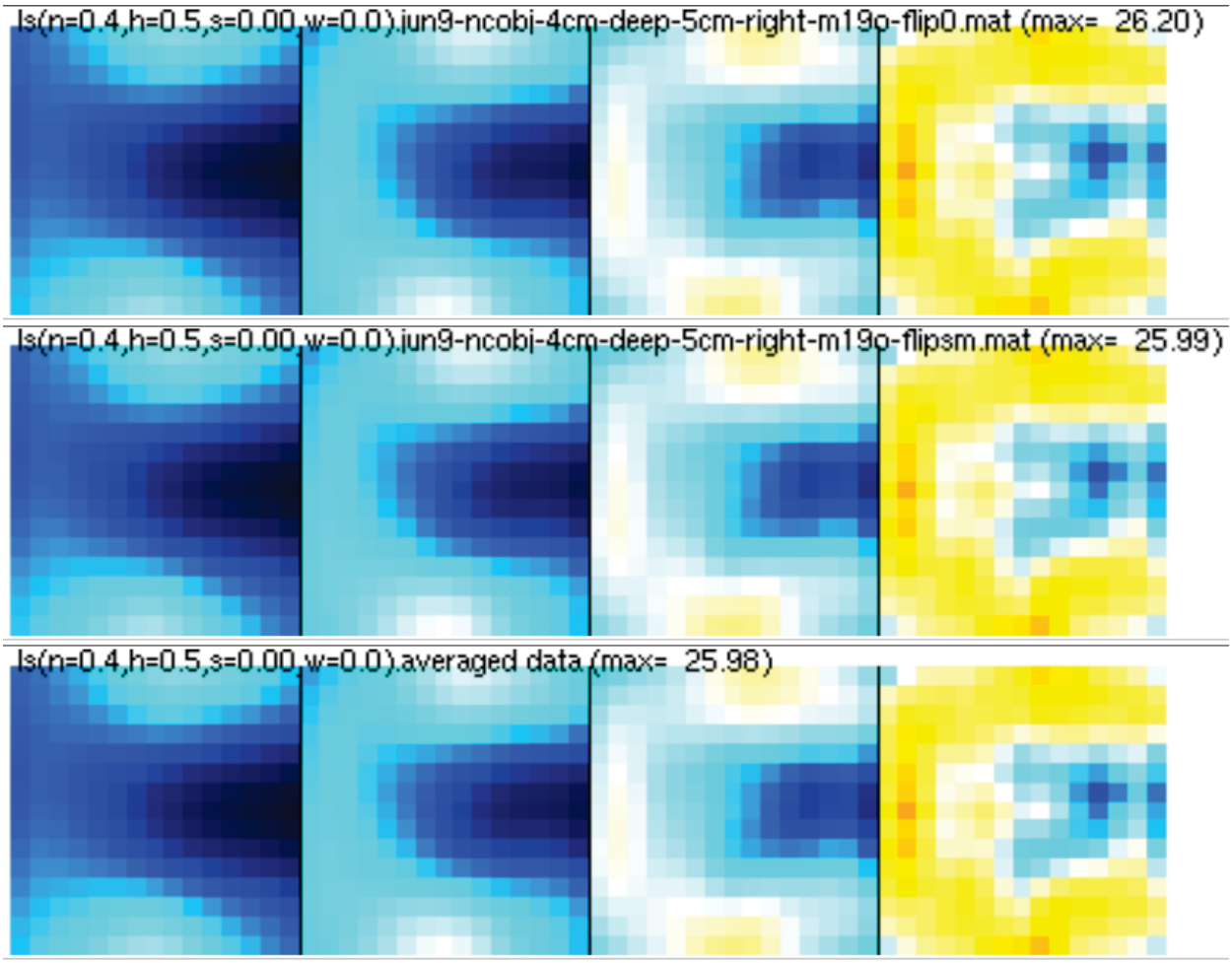

Figure 14. Image reconstructions for the original stimulation pattern (top), the stimulating and recording pairs both reversed (middle), and the mean of these two acquisitions (bottom). Stimulation pattern used: may19_stim.

The first algorithm variant tested was normalization of measured transimpedance values to the model. Reconstruction is performed not with absolute transimpedance values but with values expressed as a fraction of the predicted model transimpedance raised to the exponent *w*, where *w* usually varies between zero and one (the case *w*=0 corresponds to no normalization, and *w*=1 corresponds to normalization to the model transimpedance). Greater values of *w* cause low transimpedance values to be more heavily weighted compared to the no-normalization case. Figure 15 and Figure 16 show the reconstruction result using three levels of normalization between zero and one.

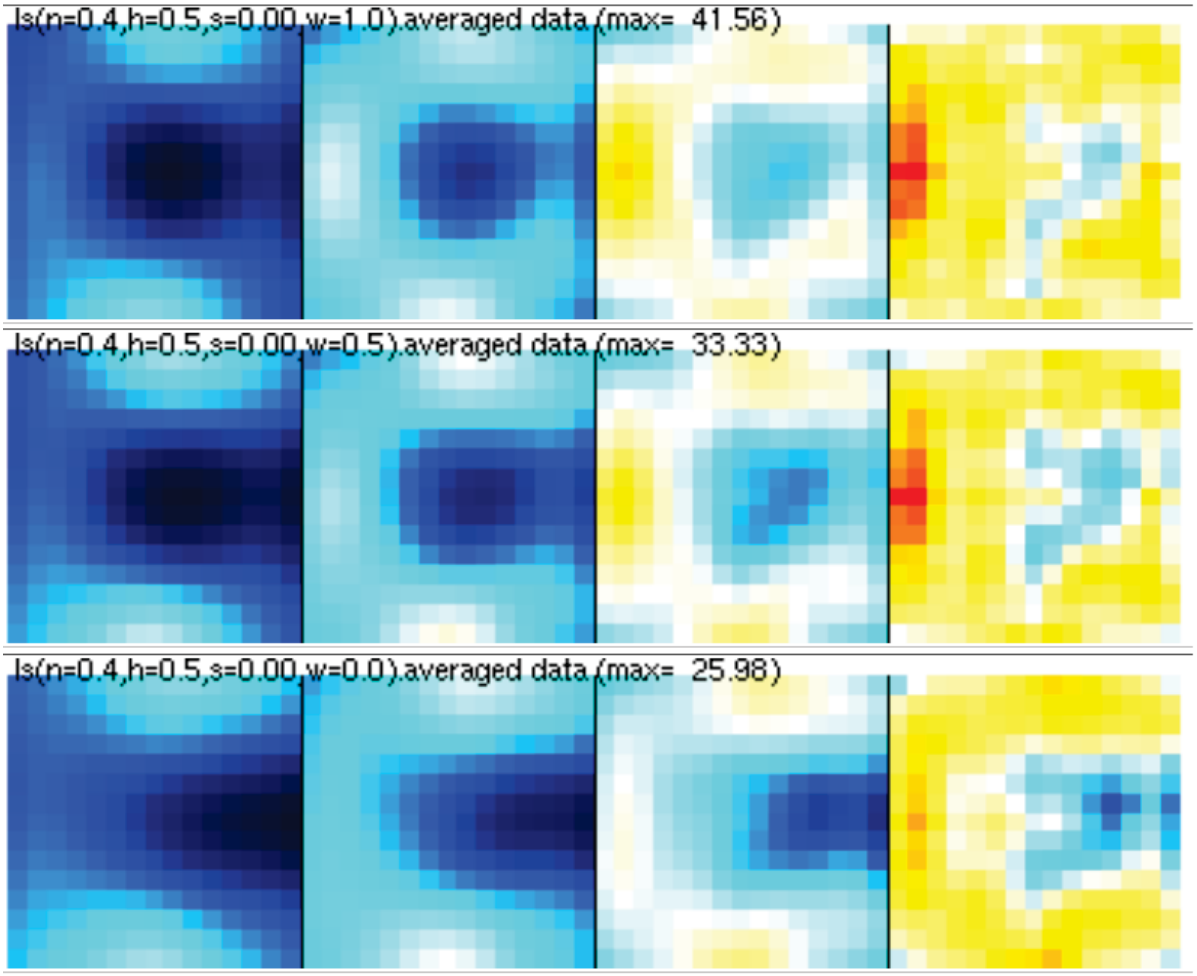

Figure 15. Reconstructions using normalization. Top: *w*=1. Centre: *w*=0.5. Bottom: *w*=0. Stimulation pattern: may19_stim.

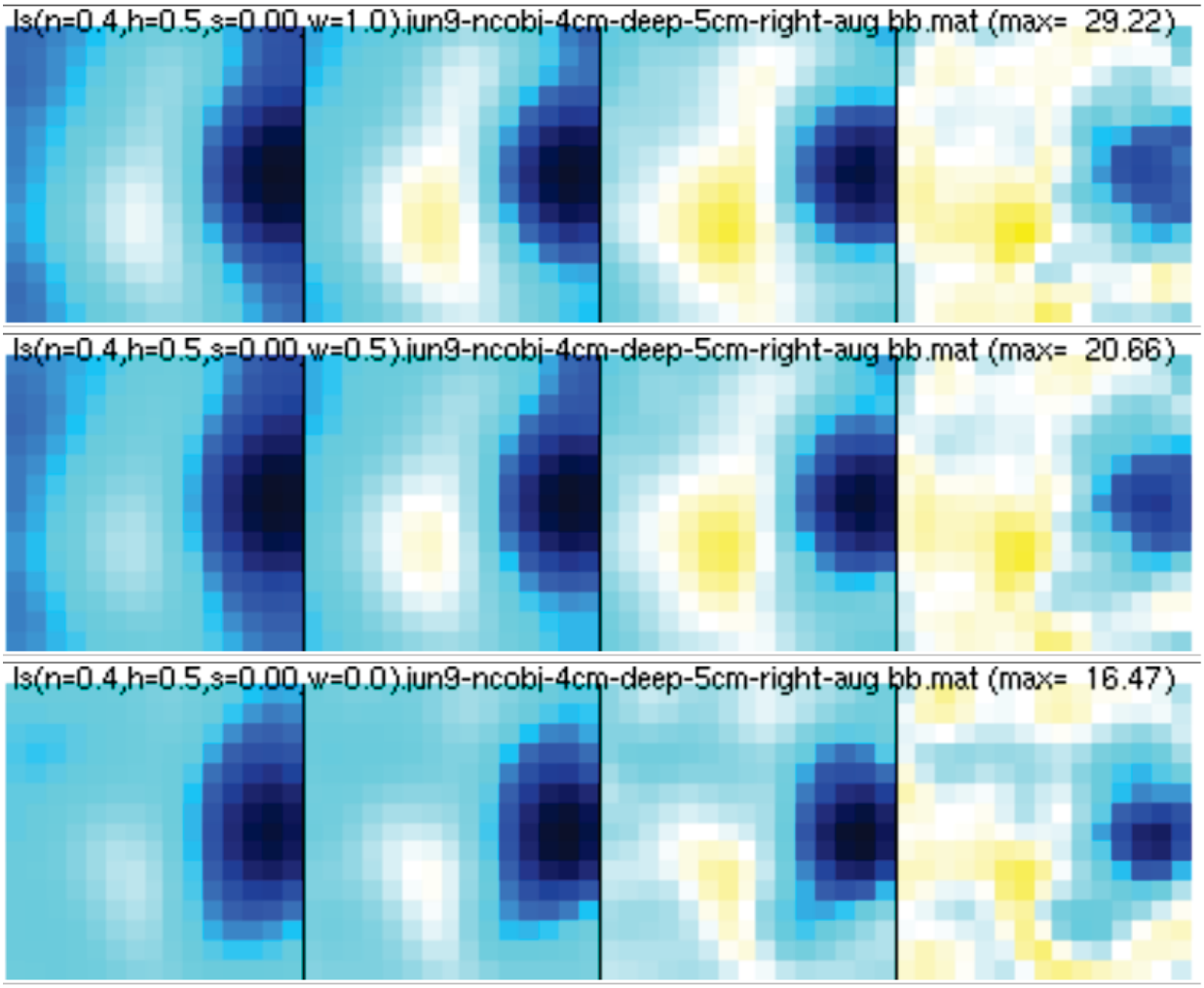

Figure 16 Reconstructions using normalization. Top: *w*=0. Centre: *w*=0.5. Bottom: *w*=1. Stimulation pattern: augbb.

Using the May 19th stimulation pattern, normalization slightly degrades the strength of the signal at depth. With the original augbb pattern the normalization does not have a strong effect. Note that the augbb pattern localizes the object further towards the edge of the array than its true location. (This effect is consistent across the algorithm variants investigated, and appears to be a characteristic of the stimulation pattern; the reason for this effect is not currently known.) Normalization does not appear to be advantageous.

The second reconstruction technique studied is smoothing of the image prior. The smoothing parameter *s*, as described in Appendix C, is varied. Figure 17 and Figure 18 show the results; increased smoothing appears to improve the clarity of the image at greater depths for the May 19th stimulation pattern, although it degrades the deeper image for the augbb pattern. The use of a smoothed image prior is unlikely to create a clear target signature out of a reconstruction that is unclear, but it does offer some improvement in the image when a target signal is present.

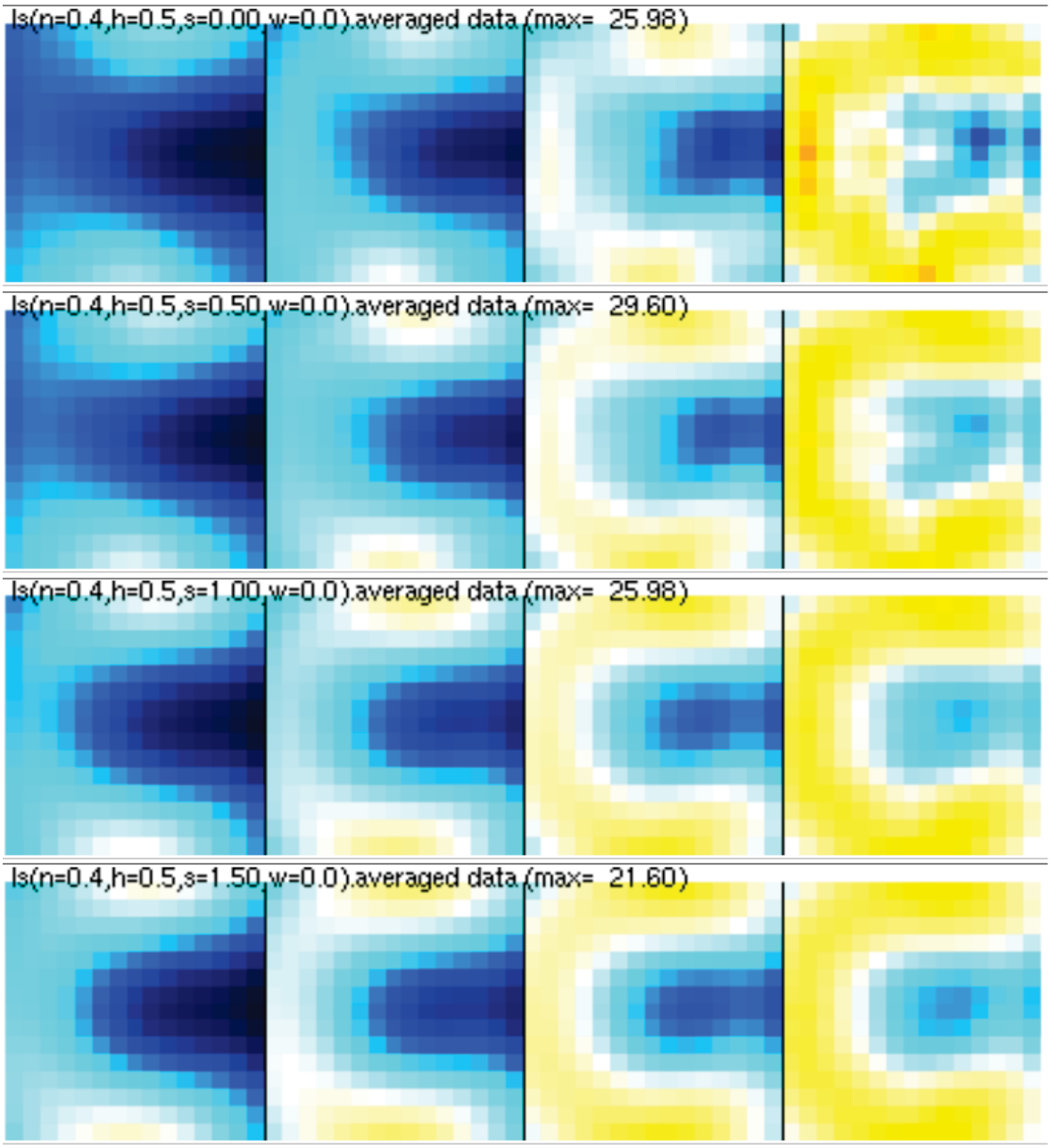

Figure 17. Reconstructions using smoothed prior. Top to bottom: *s* = 0, 0.5, 1.0, 1.5. Stimulation pattern: may19_stim.

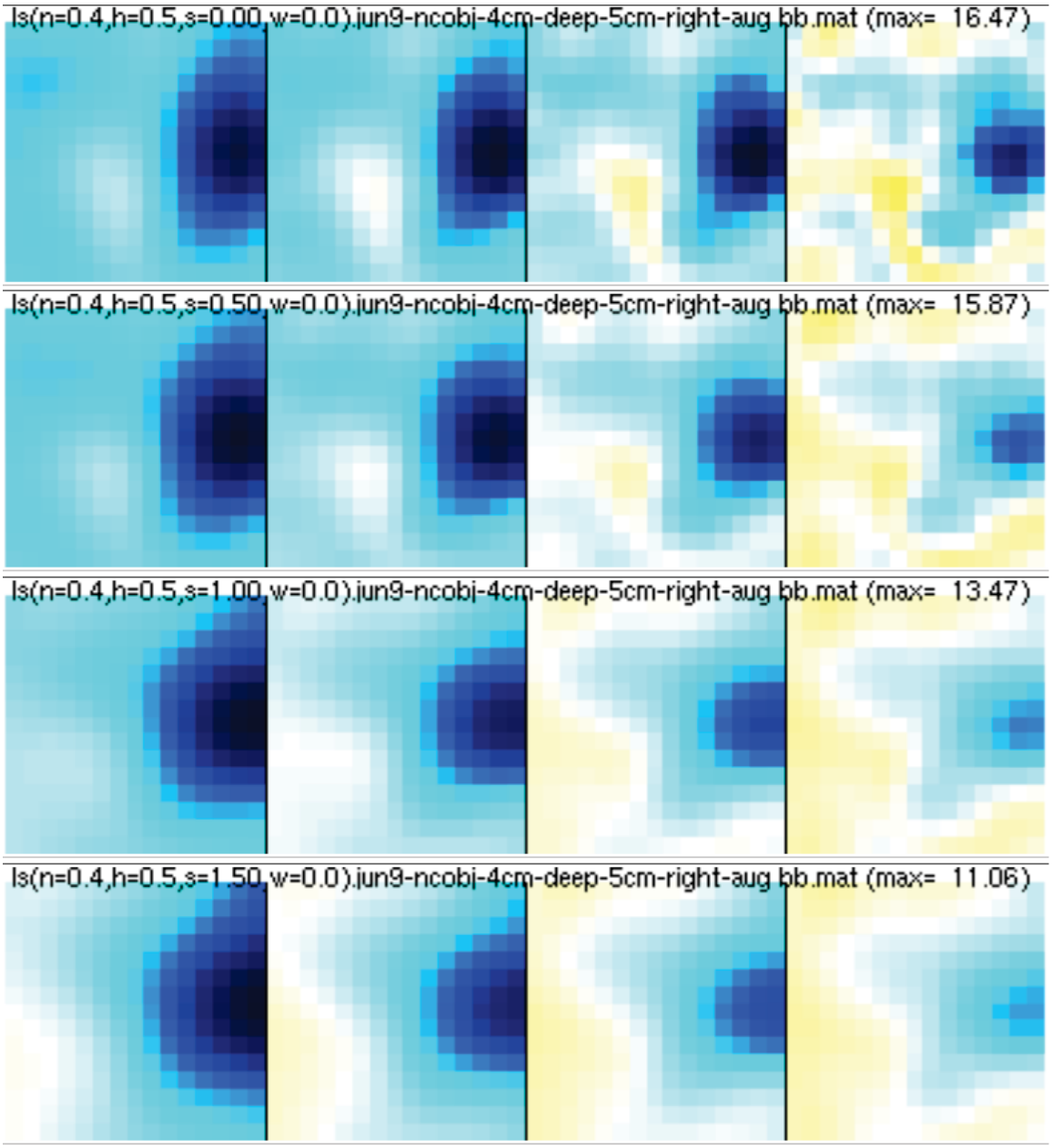

Figure 18. Reconstructions using smoothed prior. Top to bottom: *s* = 0, 0.5, 1.0, 1.5. Stimulation pattern: augbb.

Third, the total variation algorithm was investigated, also known as compressed sensing. This method tends towards producing hard edges in the image, which can help in identifying the extent of a target but may also lead to false positives and can misrepresent the signal strength. Results are shown in Figure 19 and Figure 20; the technique is not strongly recommended for this application.

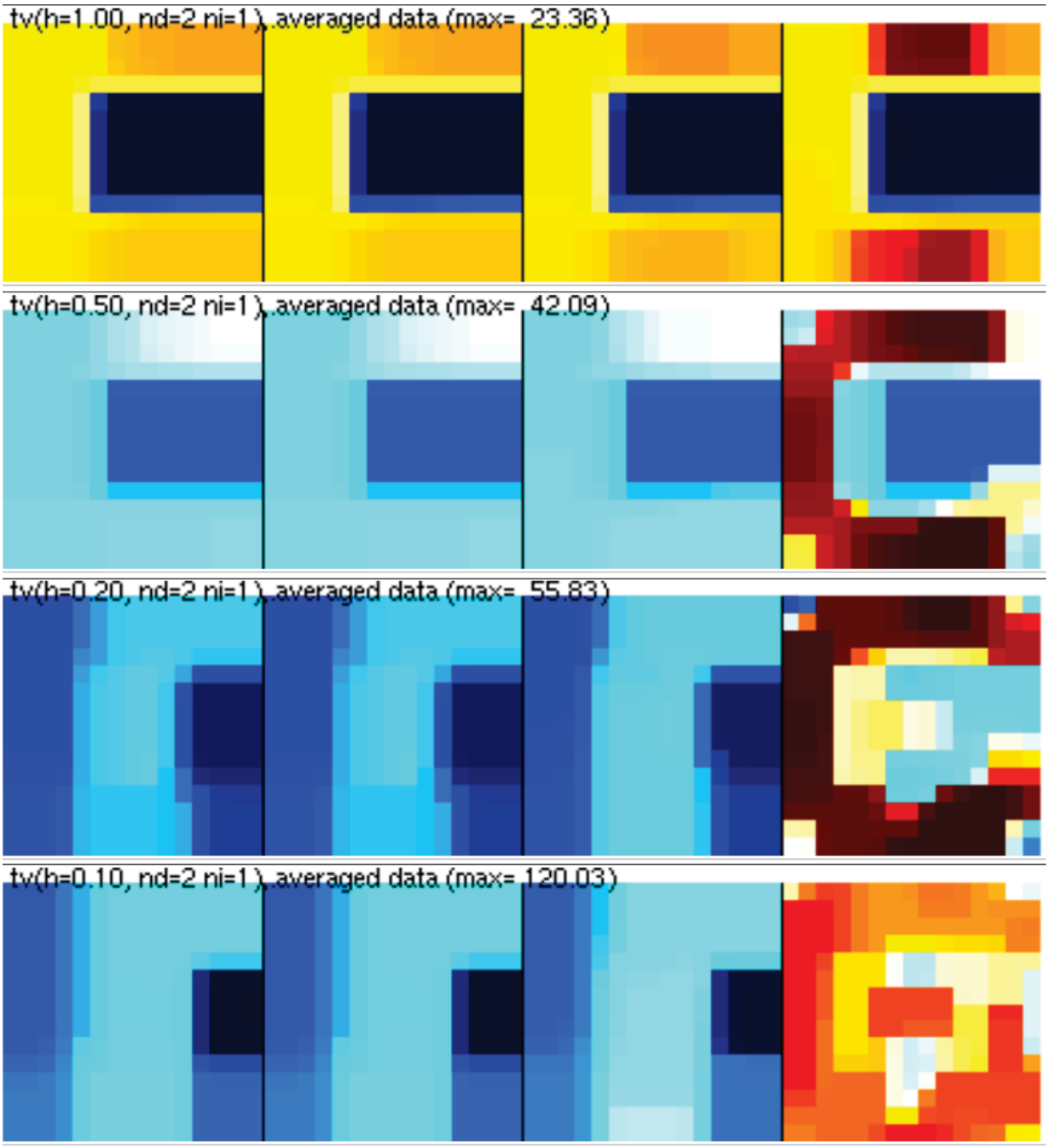

Figure 19. Reconstructions using total variation. Top to bottom: *h* = 1.0, 0.5, 0.2, 0.1. Stimulation pattern: may19_stim.

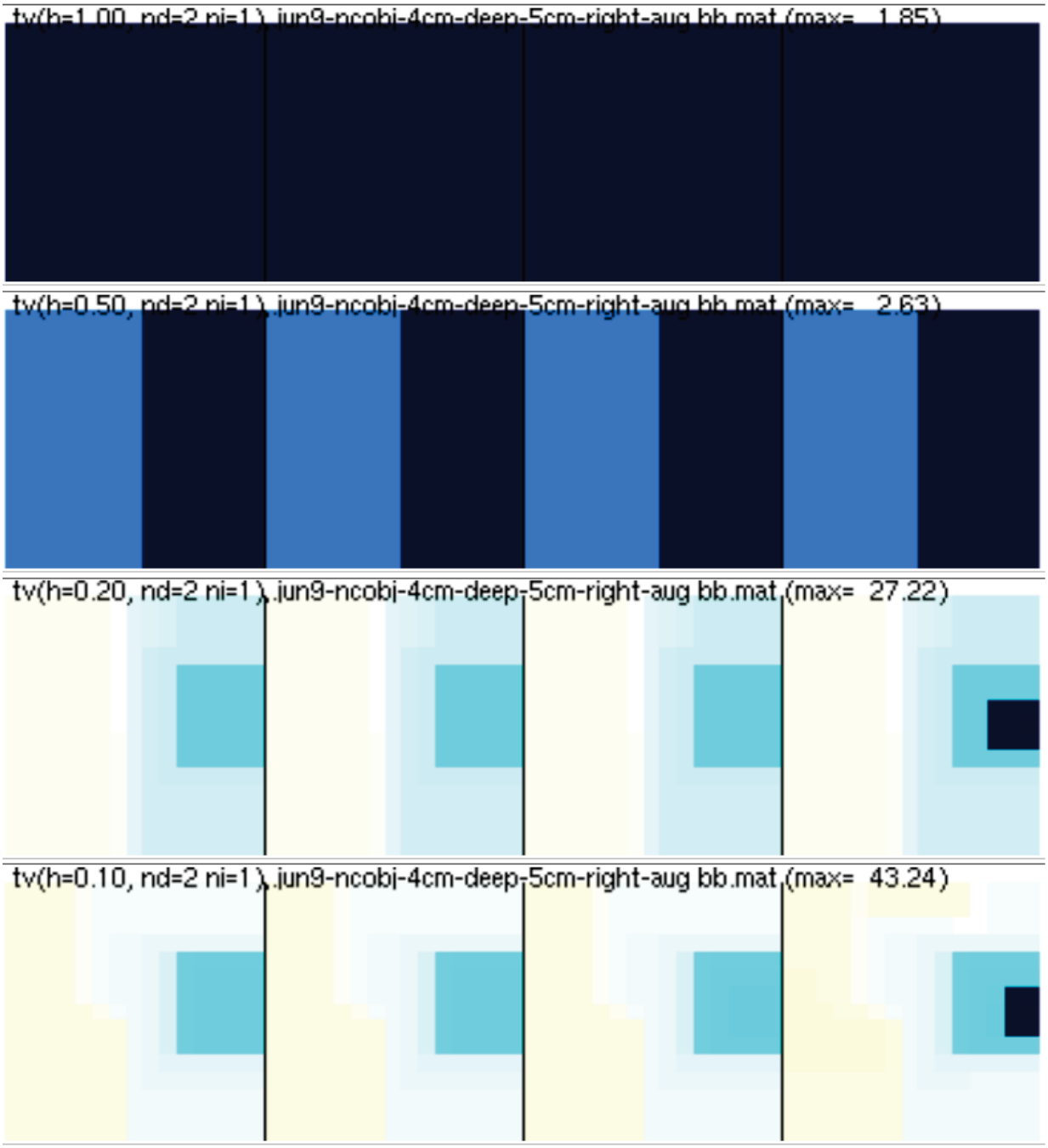

Figure 20. Reconstructions using total variation. Top to bottom: h = 1.0, 0.5, 0.2, 0.1. Stimulation pattern: augbb.

Fourth and finally, the robust data norm algorithm was investigated. As shown in Figure 21 and Figure 22, the target signal appears improved for some values of the data norm parameter. This algorithm is good at eliminating outliers in a data acquisition. There are not many outliers in the data collected to date, but this technique may become useful as a strategy for working around bad electrode contact (see Section 5.5.2).

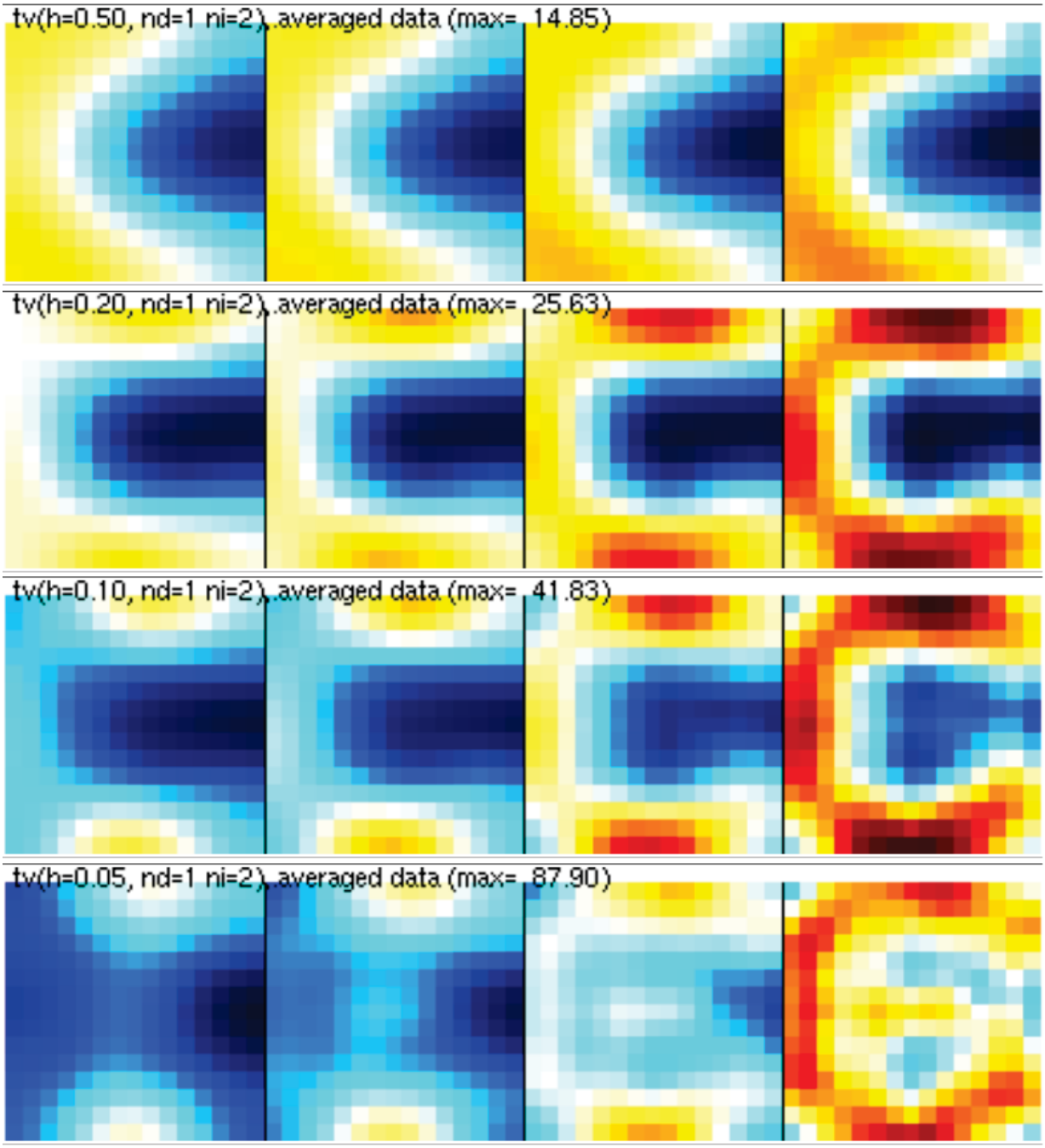

Figure 21. Reconstructions using robust data norm. Top to bottom: h = 0.5, 0.2, 0.1, 0.05. Stimulation pattern: may19_stim.

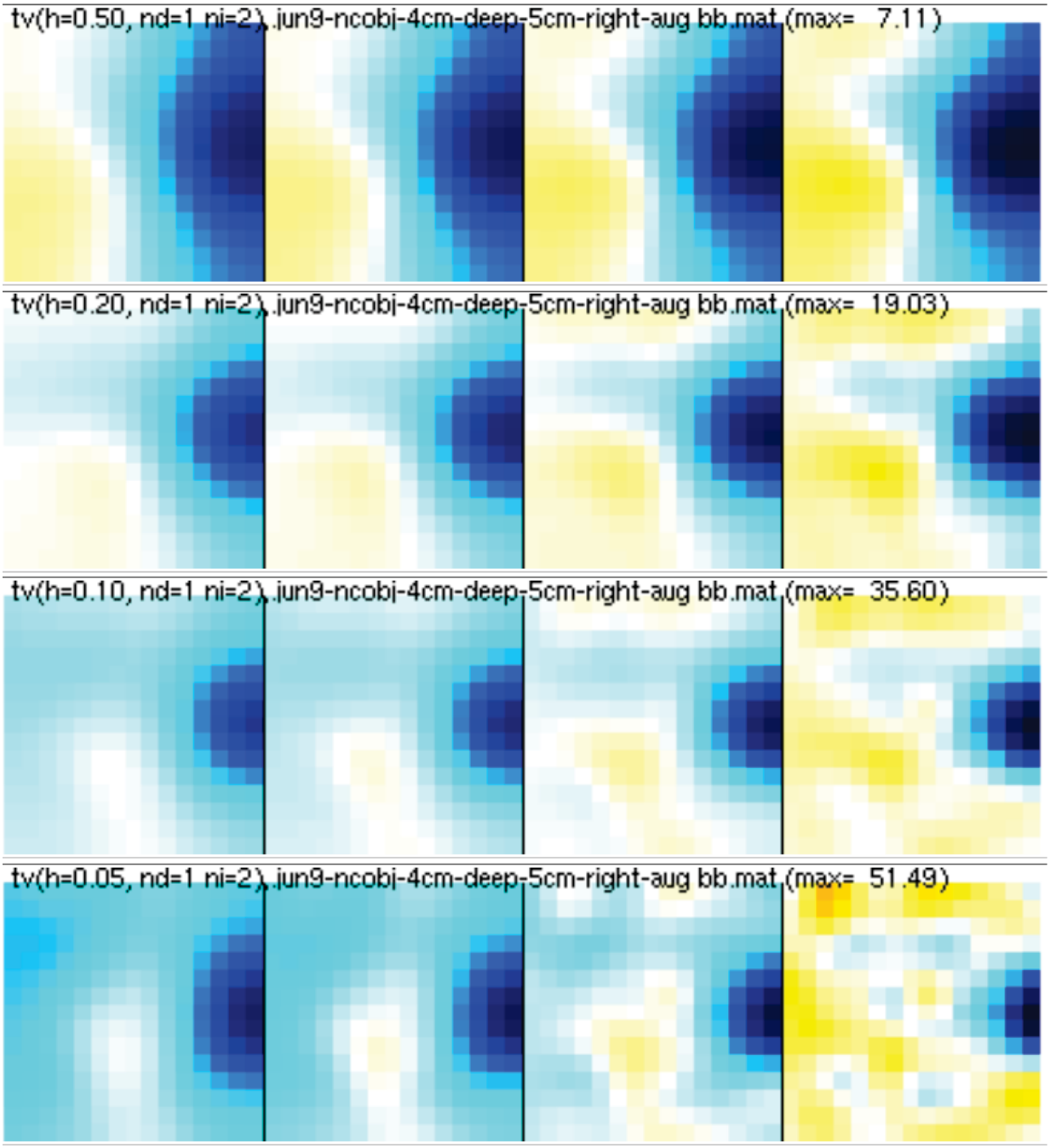

Figure 22. Reconstructions using robust data norm. Top to bottom: h = 0.5, 0.2, 0.1, 0.05. Stimulation pattern: augbb.

Of the algorithm variants studied none provides dramatic improvement, though the smoothed image prior and robust data norm may be of benefit. Of more importance in improving reconstruction quality is the modelling of the electrode interface, as discussed in Section 5.2.1. An improved model may more clearly show the advantages of various reconstruction algorithms.

5.3 Polarization task

5.3.1 Characterization of polarization behaviour

Acquisitions were performed to study the polarization behaviour of the system in a tap water medium. A stimulation pattern was used that measures one configuration ten times then swaps its stimulating and recording pair, then repeats the original configuration *n* times, as shown in Figure 23. This stimulation pattern allows comparison of the behaviour of a recording pair before and after being used for stimulation.

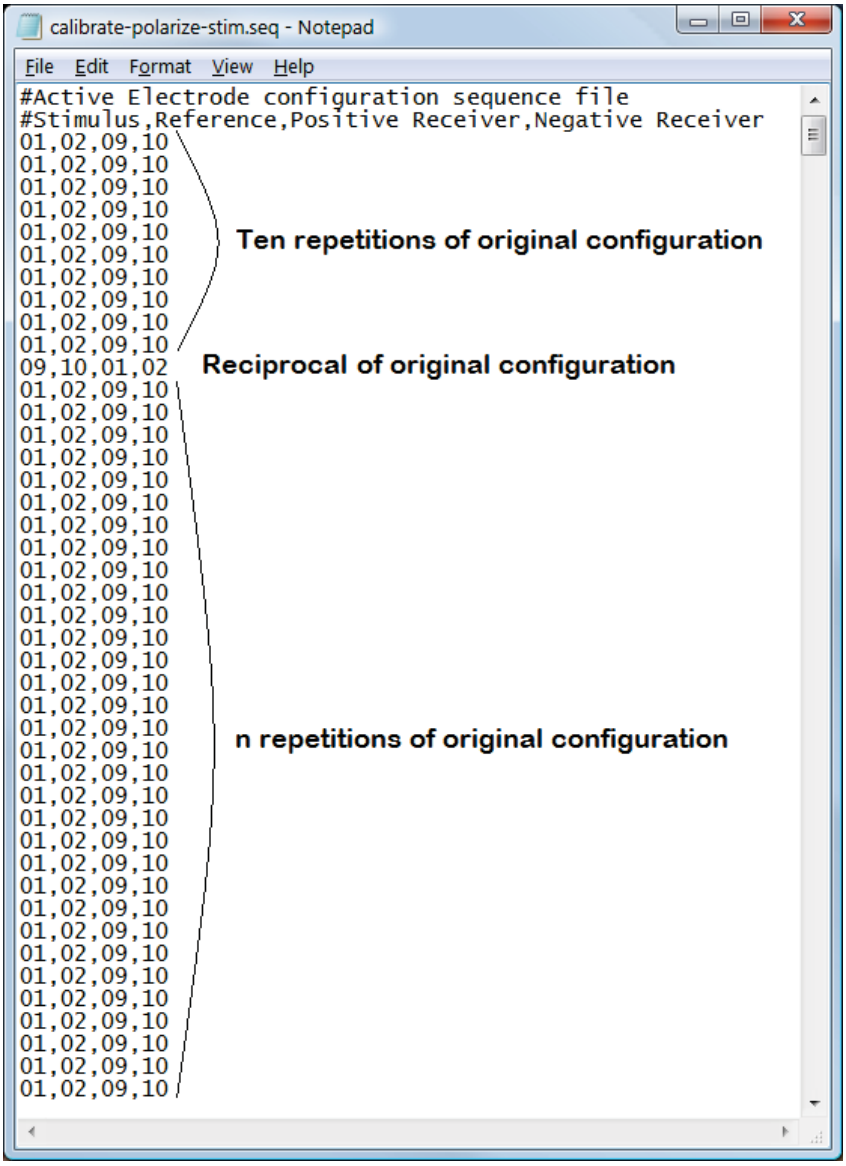

Figure 23. Stimulation pattern used to investigate polarization effects of stimulating on an electrode pair. Numbers in the file represent electrode indices (see Figure 4).

An acquisition was performed using n = 1000 repetitions of the original configuration; at a sampling frequency of 200Hz these repeated configurations continued for approximately 5s. Figure 24 shows the raw voltage readings for all configurations. Each plot on the axes represents one configuration within the stimulation pattern; those at the top in magenta are the ten original instances of the configuration, before swapping the stimulating and recording pairs. The remaining plots are the post-swap configurations; the voltage recorded from the reciprocal (swapped) configuration is not shown.

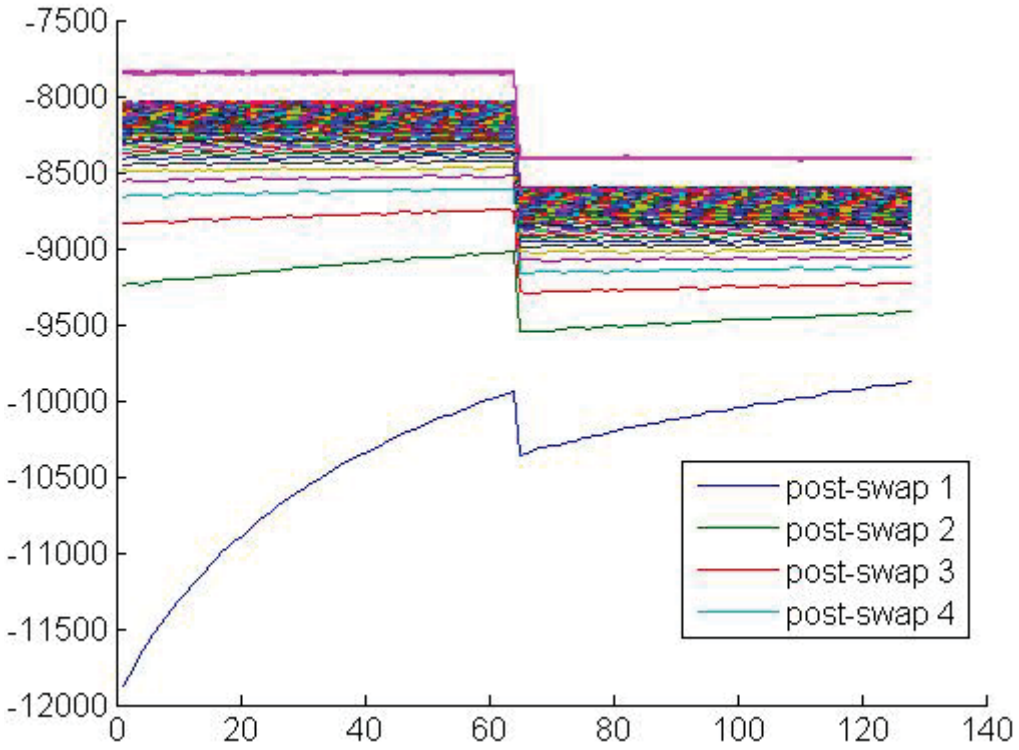

Figure 24. Raw voltage measurements before and after stimulating on the voltage recording pair.

The original configuration shows consistent voltage measurements across both the positive and negative phases of the measurement; the step between positive and negative phases is the signal containing the transimpedance information, and it is distinct.

The post-stimulation repetitions of the configuration, especially the early ones, exhibit voltage readings that are not constant but appear to change logarithmically. This behaviour makes the voltage measurement unreliable. Furthermore the step between phases is smaller than in the original configuration, obscuring the signal still more under the effects of electrode polarization.

The voltage measurements improve with each subsequent configuration, that is with time. The voltage of each phase becomes more constant and the step between phases greater. The waveform appears not to converge towards the original pre-stimulation behaviour, however; the voltage measurements converge to within approximately 3% of the original voltage, indicating a long-term polarization effect of about 3% on electrodes that have been stimulated.

Note that this acquisition was performed several minutes after another acquisition with n = 600. The ‘original’ value of this acquisition is not the same as the original value from the first scan, suggesting that a long-term transient lasts on the order of minutes.

It has been demonstrated that stimulating an electrode pair affects subsequent voltage recordings on the same pair. An additional check was done to confirm that recording on the electrodes does not affect subsequent voltage recordings. The same acquisitions as above were repeated but with a variation on the post-stimulation configurations. Rather than taking n identical repetitions of the original configuration, the repetitions were interspersed with a ‘dummy’ configuration that used different stimulating and recording pairs, as shown in Figure 25; the dummy configuration was chosen to be in a different area of the array from the original configuration. A total of n/5 original repetitions were captured, with four dummy configurations after each one. These dummy configurations were then discarded and the repeated readings of the original configuration were compared to the readings from the initial experiment. The experiment was also performed using n/20 original repetitions interspersed with nineteen dummy configurations.

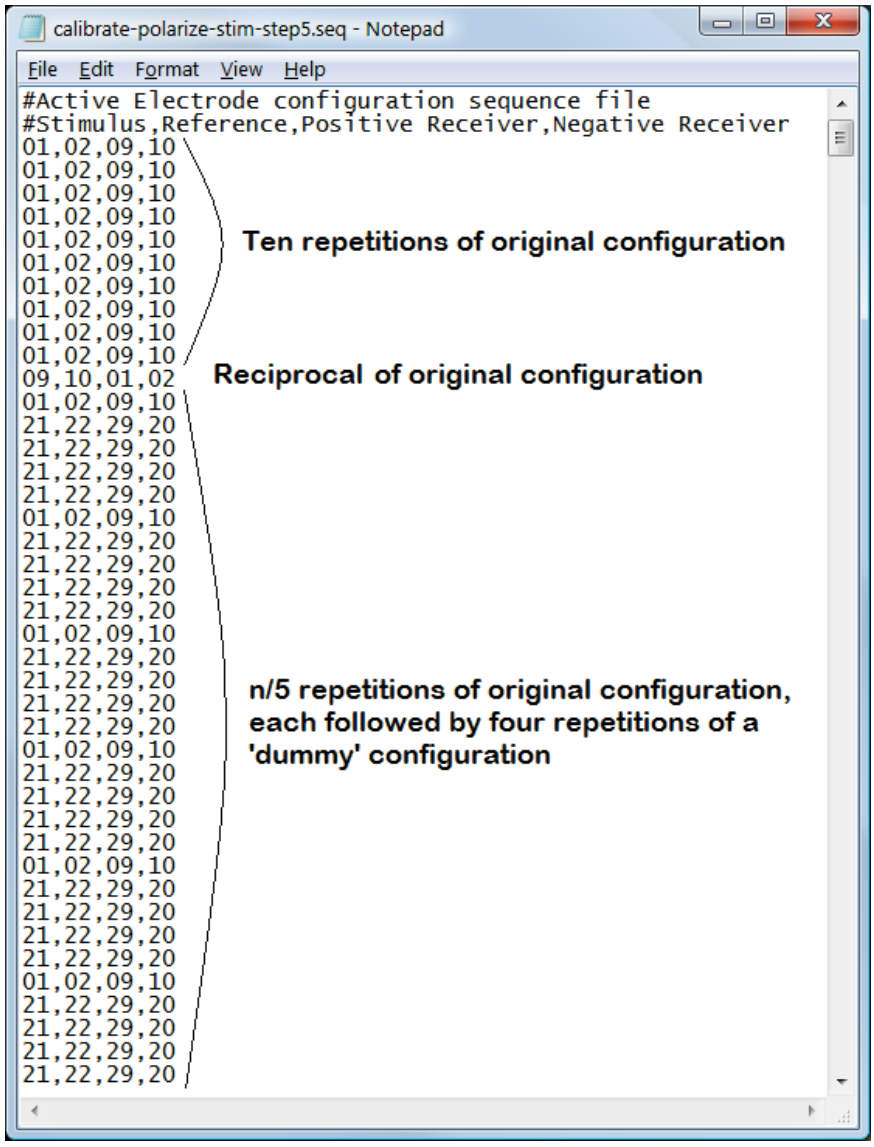

Figure 25. Stimulation pattern used to investigate polarization effects of recording on an electrode pair.

This comparison was designed to show whether the action of recording on an electrode pair changes the reading of subsequent recordings. As expected and as shown in Figure 26, the recorded values were not affected by whether the same electrode pair was previously used for recording. The figure shows voltage measurements from four acquisitions. The blue and green plots show acquisitions taken with *n* identical repetitions of the original configuration. The red plot shows an acquisition with *n*/5 repetitions interspersed with four dummies, and the pink plot shows *n*/20 repetitions interspersed with nineteen dummies (the dummy configurations have been removed). The *n*/5 and *n*/20 data points are coincident with the corresponding data points from the identical-configuration scans, demonstrating that recording on an electrode pair does not alter the voltage reading on subsequent recordings.

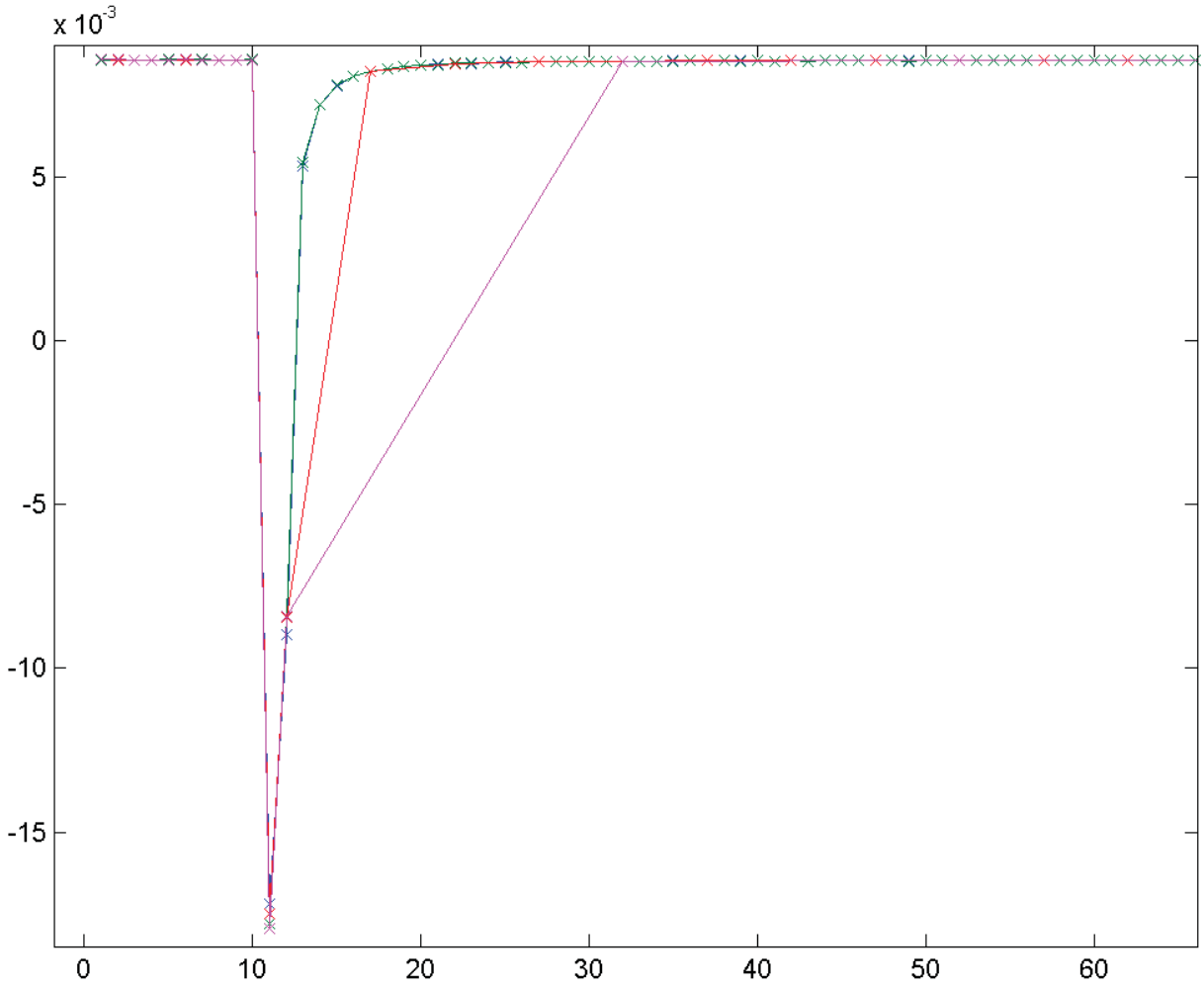

Figure 26. Polarization effects of recording on an electrode pair.

The polarization investigation was carried out in order to characterize the polarization induced on an electrode pair by stimulation (and by recording). It was found, as expected, that recording on an electrode pair does not induce polarization and does not affect subsequent voltage recordings. The polarization induced by stimulation on an electrode pair was found to introduce an error of approximately 3% in subsequent voltage recordings, with this error continuing to affect readings for potentially several minutes.

5.3.2 Reducing polarization by current balancing

During experimentation it was observed that the stimulation current was not perfectly balanced; the absolute value of the positive phase of stimulation was not equal to that of the negative phase. A hypothesis was raised that this imbalance may affect polarization of the electrodes, and experiments were carried out to test this hypothesis.

The current balance was adjusted by setting the offset voltage of the output current amplifier (U6 in the schematic; see Appendix A, sheet 6). The voltage compensation pin was connected to the voltage supply rails (+/-12V) via a potentiometer, and the overall current balance was then controlled by the potentiometer. The pot was adjusted to various levels and scans were taken. The current balance for each scan was calculated as the percentage difference between the absolute values of the positive and negative phases of the current stimulation. The convergence of the voltage to its original value was measured as the percentage difference between the pre- and post-stimulation voltages, where the post-stimulation voltage is taken as the average of the final ten configuration measurements; in these scans the final measurements occurred 1000 configurations and approximately 5s after the swapping of stimulating and recording pairs. Voltage convergence was measured separately for the positive and negative phases of stimulation, and is plotted versus current balance in Figure 27 and Figure 28. The point at which voltage converges to zero does not occur when current is perfectly balanced, possibly a result of hardware or medium imperfections. More importantly, however, there is a zero-crossing of voltage convergence, indicating that voltage convergence can be brought as close to zero as desired with sufficiently fine tuning of the current balance.

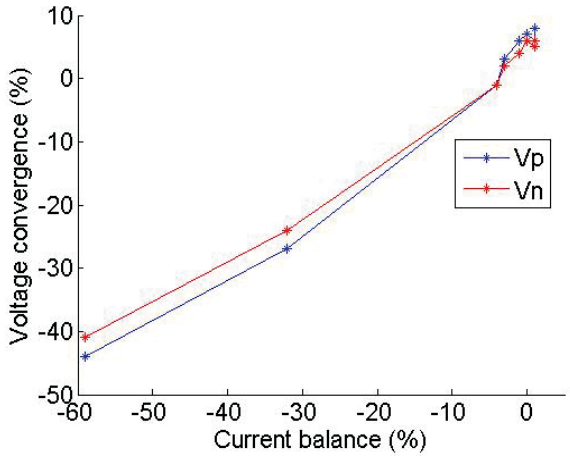

Figure 27. Effects of current balancing on polarization.

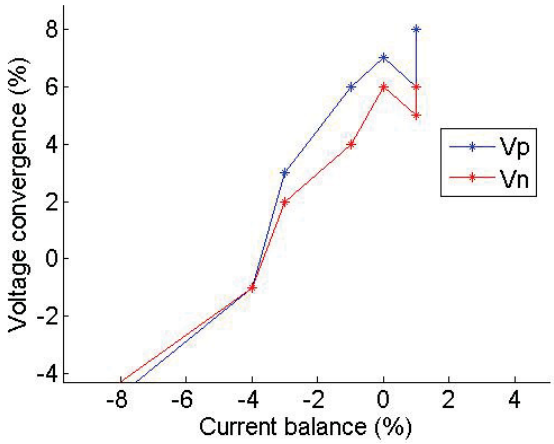

Figure 28. Detail of Figure 27.

Of the scans acquired and shown in Figure 27 and Figure 28, the one with the closest voltage convergence is shown in Figure 29. In this scan the current was balanced to within 4% and the voltage converged to within 1.8% of its pre-stimulation value, a 45% improvement over the unbalanced current scan shown in Figure 24.

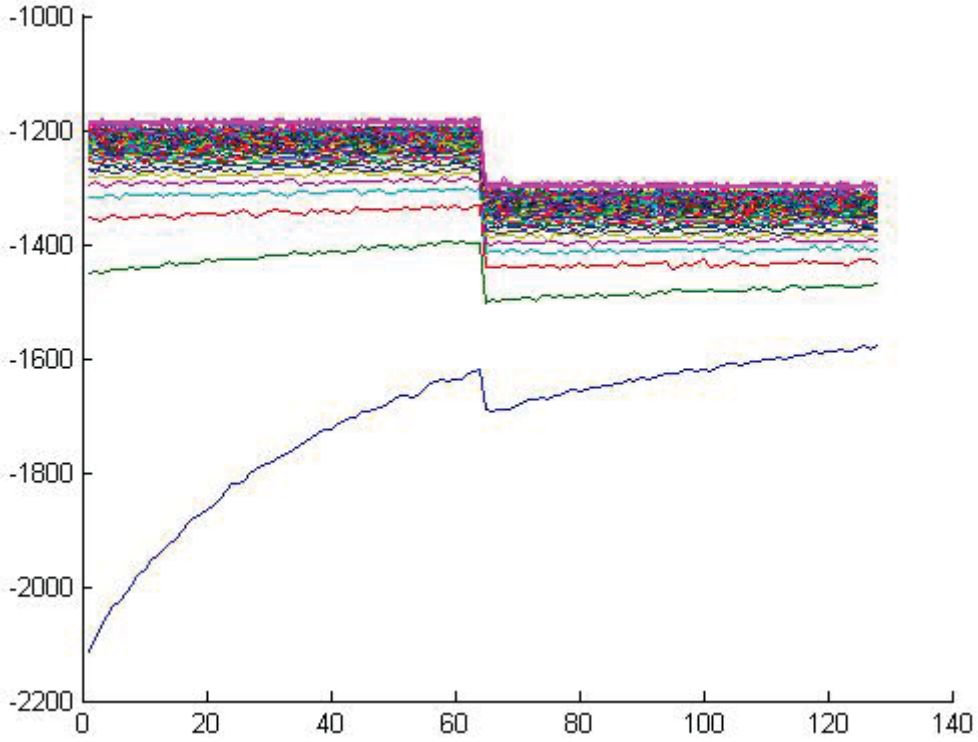

Figure 29. Raw voltage measurements before and after stimulating on the voltage recording pair. Current is balanced to within 4%.

These results indicate that the polarization induced on an electrode as a result of stimulation can be made to attenuate more quickly by balancing the current input. The quick attenuation of polarization transients allows stimulation patterns to be used that record on previously stimulated electrodes, a useful option that has not been available in the past.

To achieve reliable reconstructions it is desirable to maintain measurement error below 1%. For practical implementation of stimulation patterns it is desirable to have a recording electrode available within several hundred configurations (typically several seconds) of using it for stimulation. An appropriate objective in balancing the current input is therefore to provide voltage convergence to within 1% within a time on the order of seconds. The work carried out on this task does not achieve this objective but does indicate that such an objective is achievable. It is recommended for future work to implement hardware improvements that enable sufficiently precise current balancing.

These improvements can be made by developing more precise and sophisticated current stimulation electronics. The existing hardware implementation of the current balancing solution is a temporary and low-precision implementation set up for research purposes. Tuning of the current balance is coarse and must be verified and tweaked each time the instrument is used, a time-consuming manual process. A more finely adjustable current balance, implemented more permanently in the hardware, would enable use of current balancing in a field-operable system and thus enable the use of more varied stimulation patterns.

5.3.3 Reducing polarization with good electrode contact and electrode 'warm-up'

A detailed, seemingly unrelated investigation of electrode-medium contact grew out of the tunnel experimentation task. The difficulty and benefits of achieving good contact were discovered and several work-arounds were developed for poor-contact situations, including electrode 'warm-up.' It was discovered during this research that good electrode contact and electrode warm-up are also effective in reducing polarization effects. These concepts are fully developed in Sections 5.5.2 and 5.5.3, and the results relating to polarization are presented in 5.5.3.1.1.

5.4 Ammunition round experiments

In the previous contract experiments were carried out using a 20mm and a 40mm ammunition round, to determine if unexploded ordnance is detectable using EIT. The rounds were not detected and it was hypothesized that the partial coating of paint on the rounds was the reason. Both rounds tested were painted with non-conductive paint but the paint was worn off in many places, exposing underlying conductive metal. The rounds were partially conductive and partially non-conductive in this state, and therefore did not give a clear signature in the EIT image.

To confirm this hypothesis the rounds were entirely stripped of paint and re-imaged, then fully painted again with non-conductive paint and imaged again. Stripped of paint the rounds are fully conductive, while fully painted they act as an insulator. The smaller round still did not show up clearly in the images but the 40mm round gave a clear signature, as shown in Figure 30 and Figure 31.

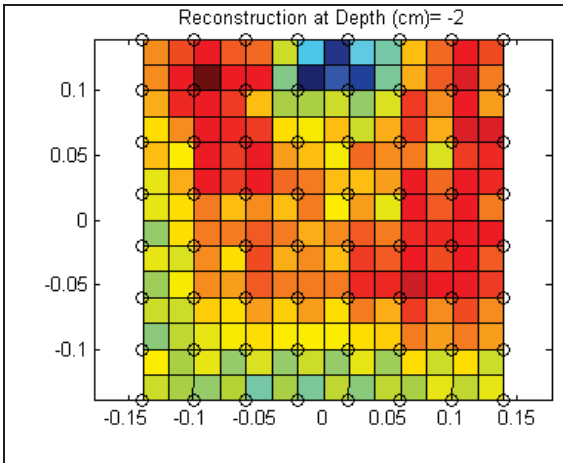

Figure 30. Reconstruction of 40mm round stripped of paint. The round is buried near the top of the array, at centre, in a 'horizontal' orientation. The conductive round appears in blue and its long, narrow shape can be seen.

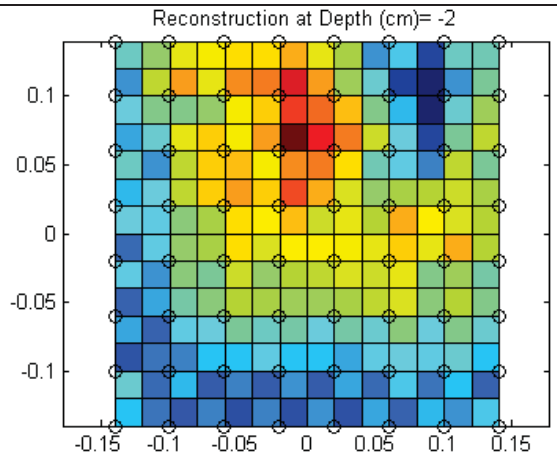

Figure 31. Reconstruction of 40mm round fully painted. The round is buried near the top of the array, at centre, in a 'vertical' orientation. The insulative round appears in red and its long, narrow shape can be seen.

It is concluded that ammunition rounds with a complete coat of paint or no paint at all are detectable using EIT, provided the round size is large enough with respect to the array electrode

pitch. Rounds with a near-complete coat of paint or with almost no paint are likely also detectable, but rounds with a mix of painted and exposed spots cannot be detected as a result of their hybrid conductor-insulator characteristics.

5.5 Tunnel and culvert experiments

The detection of tunnels and culverts in soil is in essence the same problem as detection of mine-like objects in soil, the only difference being in the size and shape of the targets of interest. Successful detection of mines and mine surrogates has been performed in the field using EIT [contract W7702-04R040/001/EDM], and successful detection of tunnel surrogates was achieved under this contract. Initial failure to detect tunnel surrogates and subsequent investigation have led to a greater understanding of the nature and requirements of EIT in a soil medium.

This section begins with a description of the experimental set-up then describes the lessons learned about electrode contact with the medium and its effects in a soil environment, including the presentation of lab and field results from a good-contact scenario. Some work-around solutions are then proposed for situations with poor electrode contact, including preliminary results. Finally a voltage clipping phenomenon is discussed, which was discovered in the hardware and characterized during tunnel testing.

5.5.1 Experimental set-up

Lab experiments were carried out using an aquarium filled with garden-variety topsoil, as shown in Figure 32. Four cylindrical objects were used as tunnel surrogates (Figure 33).

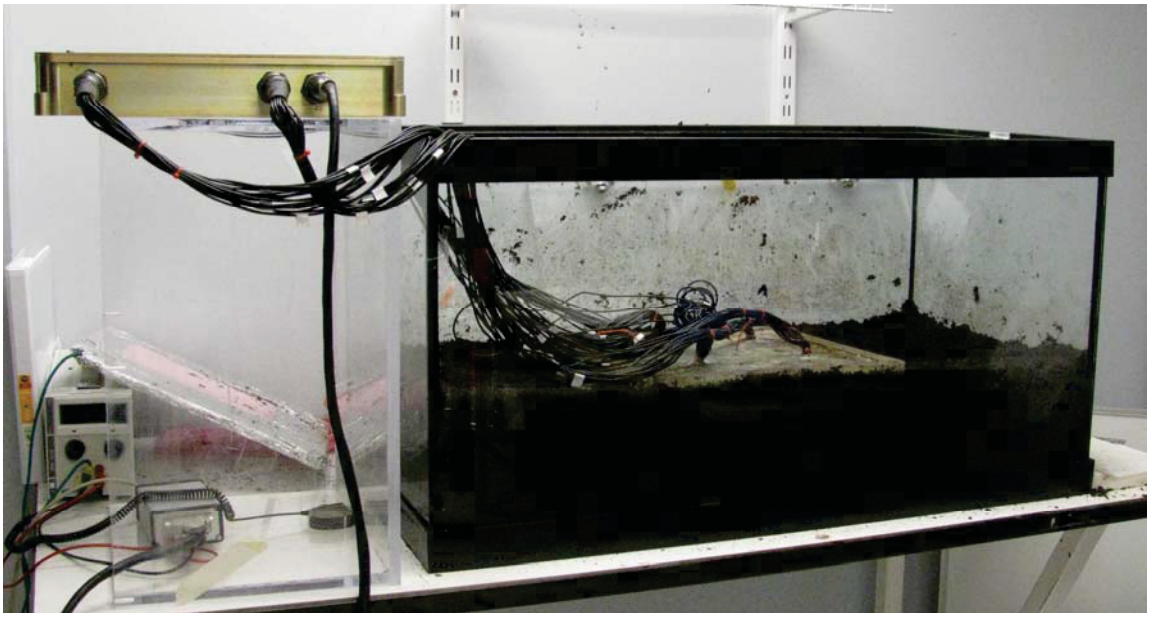

Figure 32. Experimental set-up for tunnel/culvert study.

Figure 33. Cylinders used as tunnel surrogates.

Two tunnel surrogates are conductive copper pipes, of 1.5” and 2” diameter. One cylinder is a 2” diameter ABS pipe, and the fourth is a length of 6” diameter builder’s tube used for pouring concrete posts. It is made of heavy cardboard. These targets were buried in the soil at various depths and scanned using the lab instrument.

5.5.2 Effects and prevention of bad electrode contact

Performance of the EIT system is highly dependent on acquiring accurate data from the instrument. Without accurate measurements, improvements in reconstruction algorithms or stimulation patterns offer no improvement in overall reconstruction quality. The first priority is therefore to ensure the accuracy of the transimpedance measurements, either by achieving good contact with the soil or by using work-around solutions to collect reliable measurements even with some bad contacts.

When using the instrument in a soil medium, it is useful to consider the problem in two cases. In the ‘good electrode’ case contact impedance is low between electrodes and the medium and current stimulation follows the desired square wave, producing accurate transimpedance measurements. In the ‘bad electrode’ case one or several electrodes fail to make good contact with the medium, which prevents the current stimulation from behaving as intended and introduces error in the transimpedance measurements.

5.5.2.1 Analysis of electrode contact

Initial lab experimentation with tunnel surrogates gave reconstructions in which the target was not discernible; it was found that these scans fell into the 'bad electrode' case, failing to make reliable contact with the soil. In these cases the current stimulation behaves as in Figure 34 and Figure 35; these figures show the current injected into soil for a stimulation pattern that repeated the same configuration one hundred times (stimulating on electrodes 2 and 3, recording on 9 and 10 [see Figure 4 for an electrode numbering map]). Sixty-four positive and negative samples were taken for each stimulation. The hundred current stimulations are shown superimposed; ideally these waveforms are identical. For comparison, Figure 36 shows the current from the same stimulation pattern run in tap water.

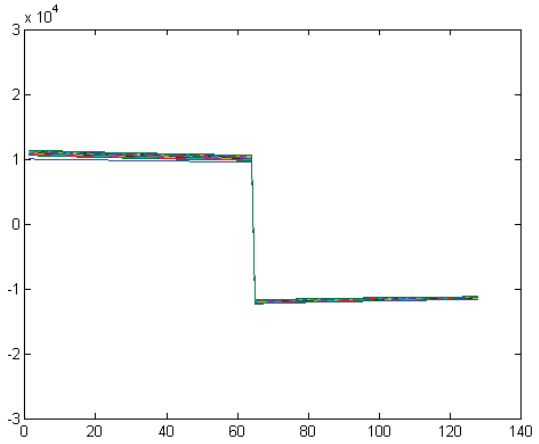

Figure 34. Current stimulation in soil medium with poor electrode contact.

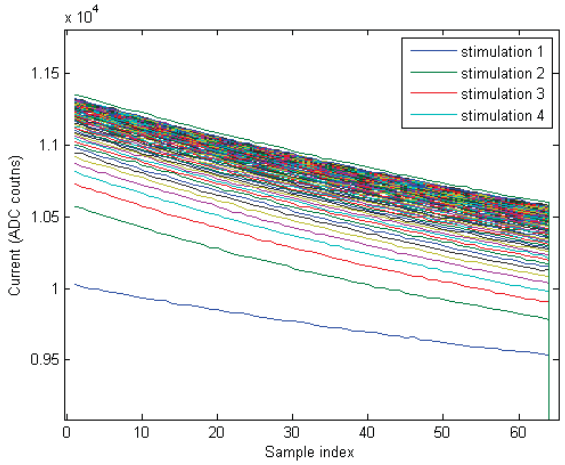

Figure 35. Detail of Figure 34, showing positive phase of current stimulation.

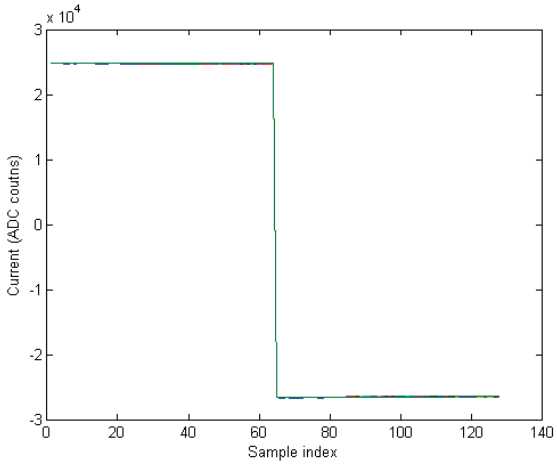

Figure 36. Current stimulation in water medium (good electrode contact).

The first observation of interest in Figure 34 is that the positive and negative phases of current stimulation are not symmetric – the current does not behave the same way during positive and negative stimulation, meaning that voltage measurements are not consistent. The second phenomenon (Figure 35) is that successive stimulations on the same electrode pair appear to converge. The first few stimulations differ significantly from one another, and after several stimulations have elapsed the current waveform becomes consistent. Finally, even once the current waveform converges it fails to deliver a square wave; current amplitude steadily drops through each phase of stimulation (this drop appears exponential but was found to fit poorly to an exponential model). By comparison, the stimulation current in water is a crisp and repeatable square wave.

The inconsistent behaviour of the current in the soil medium compromises the transimpedance measurements. To confirm this finding, fifty-six test acquisitions were performed using different stimulation patterns, target objects, and burial depths. The acquisitions were performed once in soil and once in water, and the standard deviations of the transimpedance measurements were recorded and averaged over all configurations of the scan. The transimpedance standard deviations in water and soil are compared in Figure 37 and Figure 38; the two figures show the same data on different vertical axis scales. On average the transimpedance has a much greater variability in soil than in water, by a factor of approximately 200. Even when the worst soil cases are ignored (cases where the standard deviation is greater than twice the mean standard deviation across all scenarios), the standard deviation in soil is still on average ten times greater than in water.

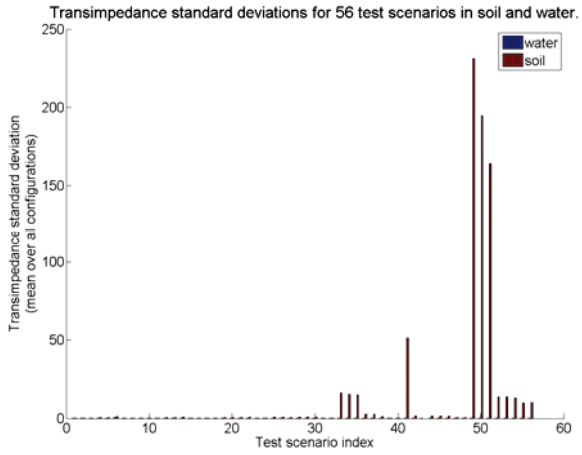

Figure 37. Comparison of transimpedance standard deviation in soil and water.

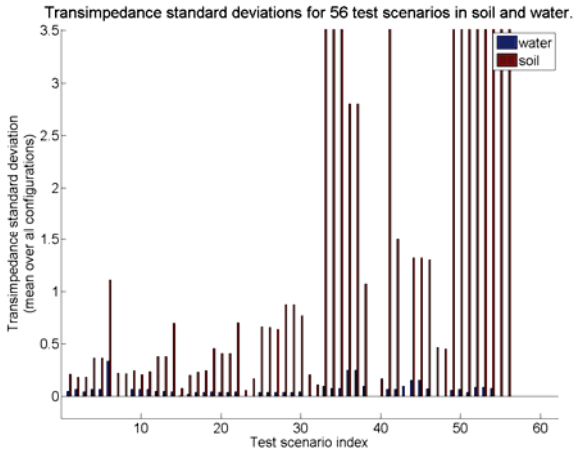

Figure 38. Comparison of transimpedance standard deviation in soil and water – detail of vertical axis near zero.

This result shows that transimpedance measurements are unreliable in the soil medium when current input fails to follow the intended square wave. This 'bad' current behaviour is a consequence of poor electrode contact with the medium.

5.5.2.2 Good contact through wet soil surface

Electrode contact can vary unpredictably in a soil medium over the course of days or even hours. Methods attempted to improve contact include pushing down on the array before or during scanning and dropping the array into the soil from varying heights (2cm to about 10cm). These attempts yielded inconsistent results, sometimes improving reconstruction quality and sometimes not.

An approach of pouring water on the soil surface immediately before scanning was investigated in detail. It also yielded mixed results in the final reconstructed images but showed great improvement in the raw current and voltage measurements. The raw voltage measurements are discussed first, followed by presentation of some reconstructed images.

Acquisitions were taken in soil, with and without water poured onto the surface immediately before scanning. In both cases the soil medium was moderately moist throughout the tank; only the surface moisture was changed between scans. Figure 39 and Figure 40 show the current injected in the medium with the unmoistened and the watered surface respectively. The current stimulation with a watered surface is more repeatable from one configuration to another and more consistent within one configuration than the unmoistened case, matching closely the behaviour of current stimulation in water (Figure 36). This result demonstrates that surface water greatly improves current stimulation in a soil medium.

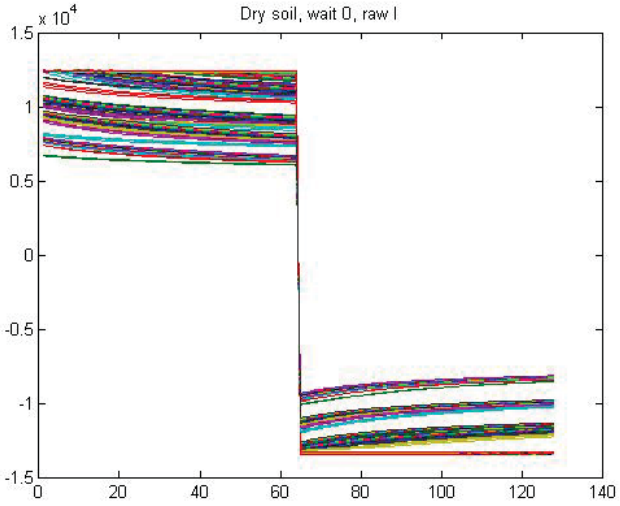

Figure 39. Current stimulation in soil medium with unmoistened surface.

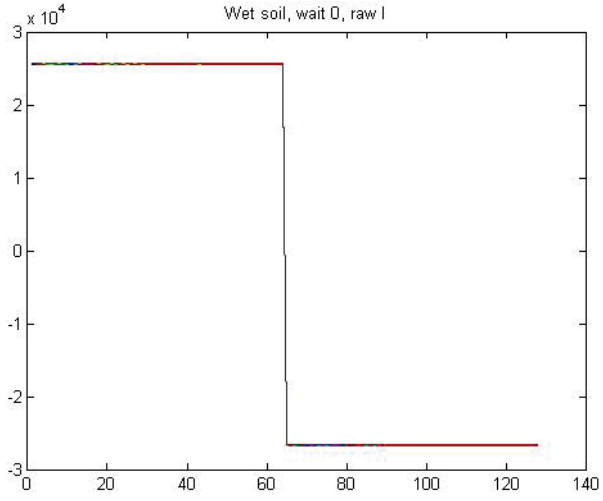

Figure 40. Current stimulation in soil medium with water poured on surface.

Voltage measurements were also evaluated, with a focus on the effects of good contact on electrode polarization. A stimulation pattern that has been effective in the lung imaging field was modified for this testing purpose. The pattern uses only the electrodes around the outer edge of the array; for simplicity only every second electrode was used, effectively producing a square of fourteen electrodes as shown in Figure 41.

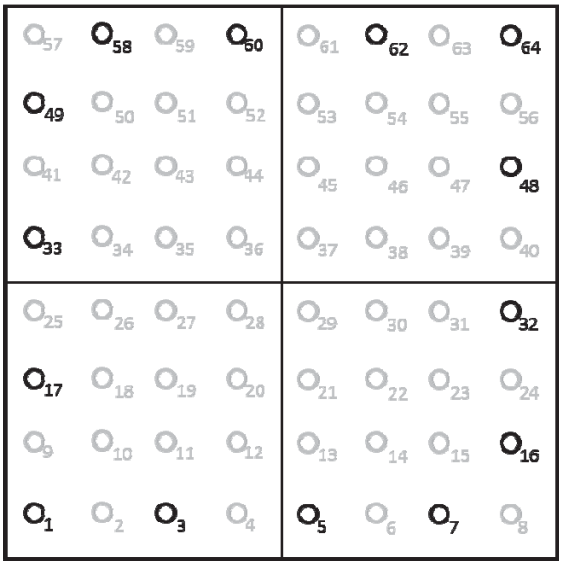

Figure 41. Electrodes used for contact investigation.

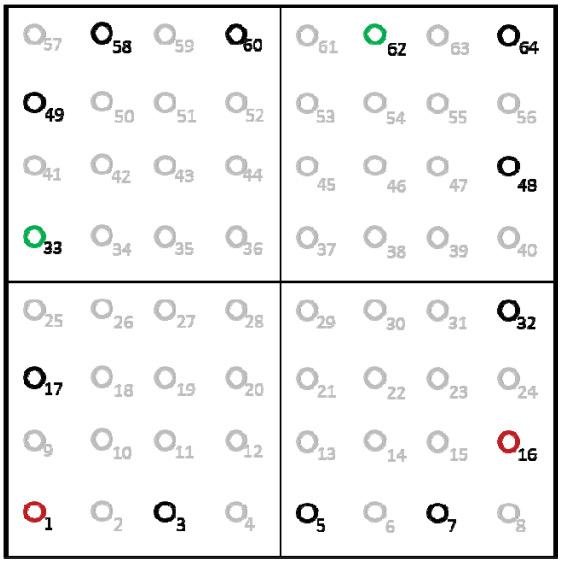

Figure 42. One sample stimulation pair is shown in red and another is shown in green.

Stimulation pairs are formed using any electrode and the fourth electrode over from it, counting in a counter-clockwise direction around the square. There are fourteen such pairs, and all are used in the stimulation pattern. Two sample stimulation pairs are shown in Figure 42. For each stimulating pair, recording pairs are formed using the same rule. All eleven such pairs are used in the pattern, producing 154 distinct configurations; Figure 43 illustrates several recording pairs for the stimulating pair (1, 16). Figure 44 shows a portion of the stimulation pattern text file.

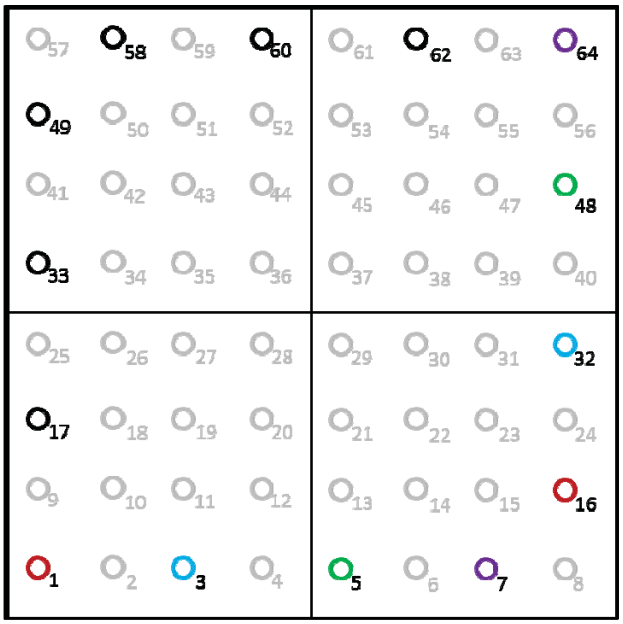

Figure 43. Sample recording pairs (blue, green, and purple) for the stimulation pair (1,16) (red).

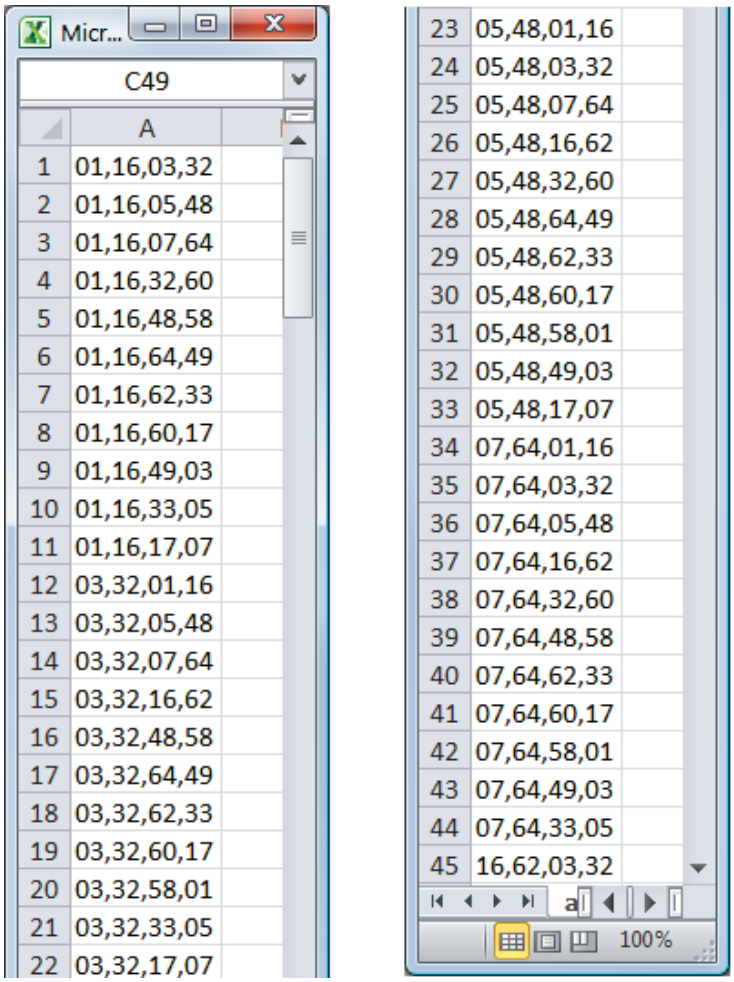

Figure 44. Stimulation pattern used for surface contact investigation. The current stimulation, current reference, positive voltage recorder, and negative voltage recorder electrodes are listed respectively for each configuration.

The stimulation pattern runs through these configurations three times in succession for a total of 462 configurations. During each of the three cycles each configuration and its reciprocal is acquired once; the time between acquisition of a given configuration and its reciprocal varies depending on the configuration and is not calculated.

Figure 45 and Figure 46 show the transimpedances acquired from this stimulation pattern. The soil moisture was at a moderate level during these scans, but no water was poured on the surface before scanning. Vertical lines mark every switch of stimulating pair. The 154 distinct configurations are shown, and their three repetitions are plotted separately in blue, red, and green. For comparison, each configuration's three reciprocal measurements are also plotted in blue, red, and green.

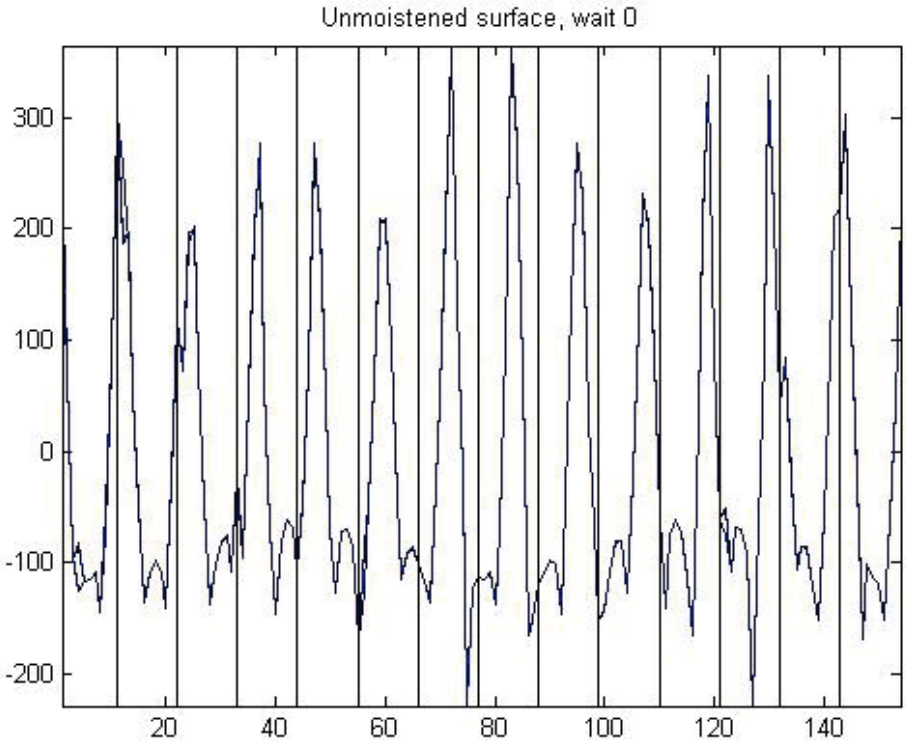

Figure 45. Transimpedances from reciprocal acquisition.

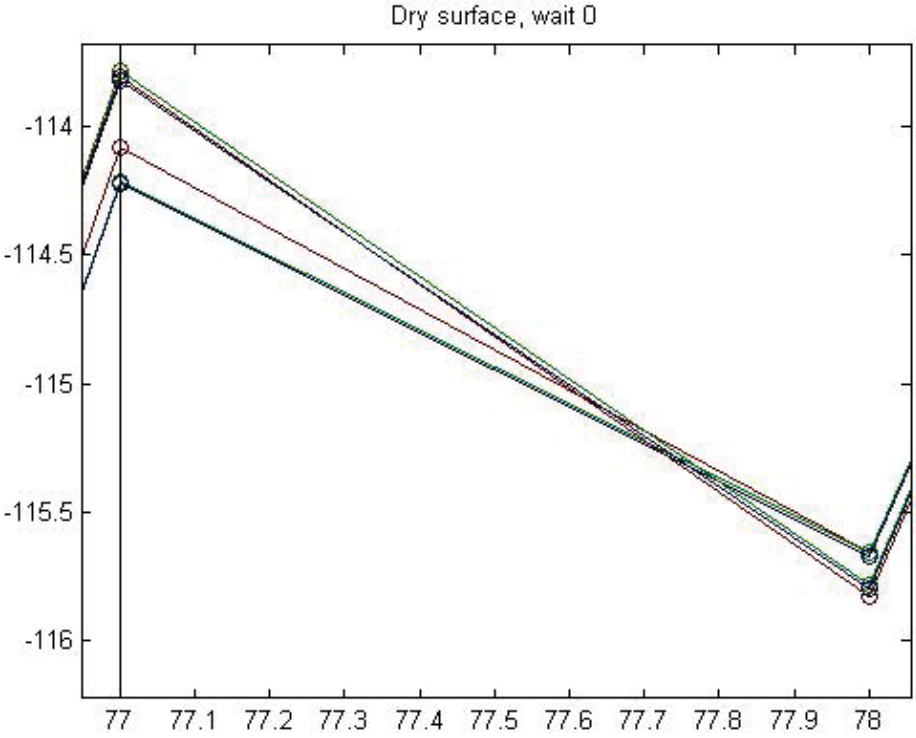

Figure 46. Detail from Figure 45. Data points are marked with circles and connected with solid lines. One set of three functions is the original configuration while the other set of three is its reciprocal.

As shown in Figure 46, both the original and the reciprocal configurations are moderately repeatable, giving somewhat differing measurements each time through the measurement cycle (the standard deviation of the three measurements averages 0.11 over all configurations). This behaviour indicates that the polarization induced by the reciprocal measurement has partially but not fully attenuated by the time the original configuration is stimulated the next time around. (Original measurements are separated by 154 configurations or approximately 0.8s; the interval between reciprocal and original stimulation is between zero and this upper bound.)

Figure 47 and Figure 48 show the transimpedance measurements from a similar acquisition before which water was poured on the surface of the soil. Enough water was used to make the surface muddy. As shown in Figure 48, both the original and the reciprocal measurements are much more tightly grouped; on average they remain within a standard deviation of 0.01 across the three measurement cycles.

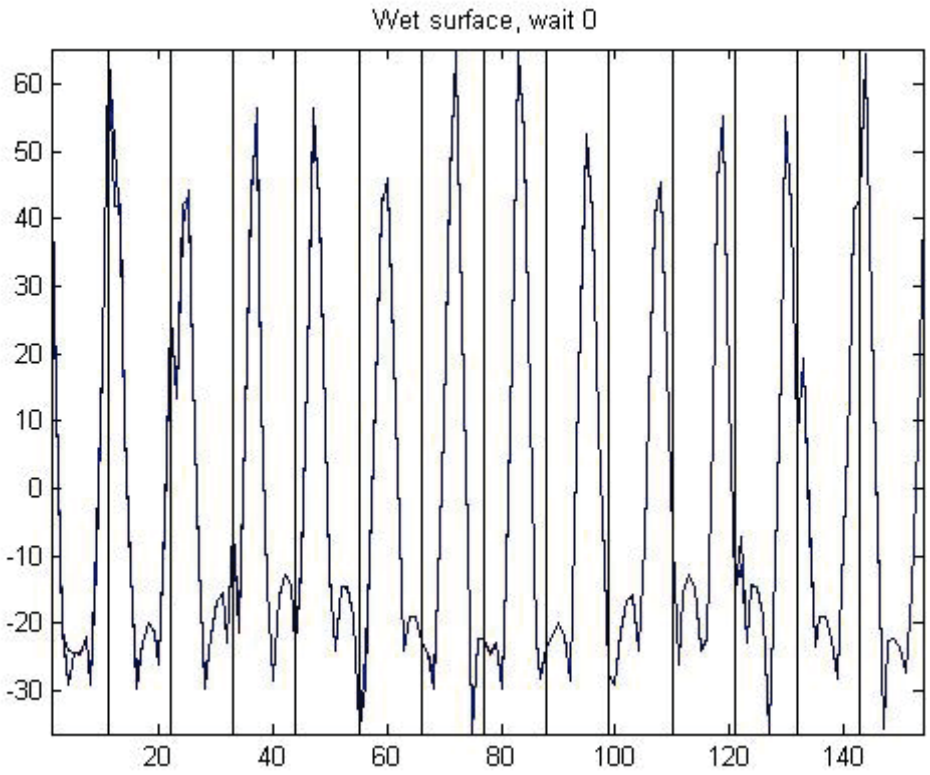

Figure 47. Transimpedances from reciprocal acquisition, wet soil surface.

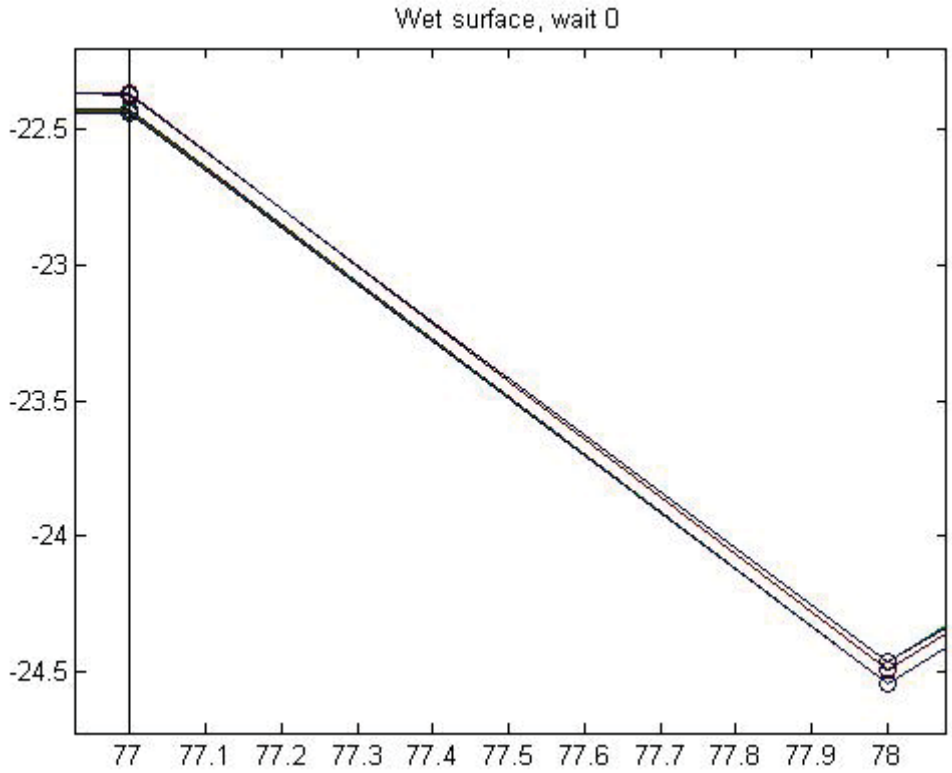

Figure 48. Detail from Figure 47.

This result is an order-of-magnitude improvement over the unmoistened soil surface case; ensuring good contact by pouring water on the soil surface effectively attenuates stimulation-induced polarization within at most 154 configurations. Good contact is therefore a very important requirement for collecting reliable voltage data as well as providing reliable current stimulation.

Despite providing high-quality transimpedance measurements, good contact with a wet soil surface yielded mixed results in final reconstruction quality, as shown in Figure 49 through Figure 58. Figure 49 and Figure 50 show reconstructions of the 2" copper pipe buried approximately 4cm deep in soil, near the front of the tank and lying in the *x* direction. Figure 49 shows the original scan, and Figure 50 shows the scan taken with water poured on the soil surface immediately before scanning (these scans were acquired using Neptec's augbb stimulation pattern). With a wet surface the metallic cylinder appears clearly as a conductive region across the bottom of the scan, while in the original scan the target is not discernible. A similar improvement was found scanning the builder's tube (Figure 51 and Figure 52, showing the tube buried at a depth of 2cm). Some reconstructions were not improved by the addition of surface water, however. Figure 53 through Figure 58 show reconstructions of the ABS pipe with and without water on the soil surface. The presence of surface moisture does not appear to improve detection.

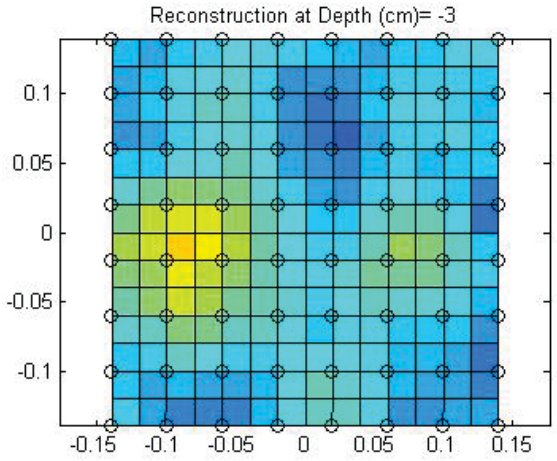

Figure 49. Reconstruction of copper pipe with unmoistened surface.

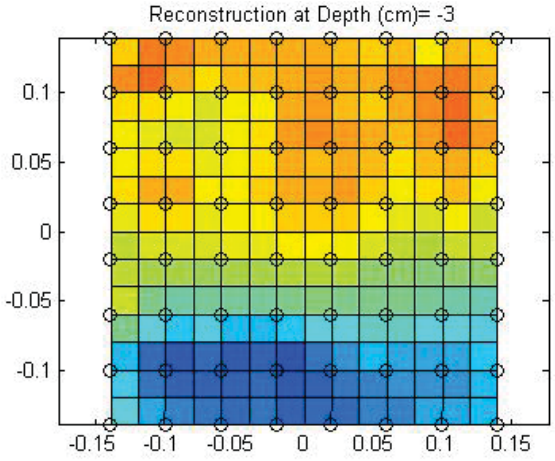

Figure 50. Reconstruction of copper pipe with water on surface.

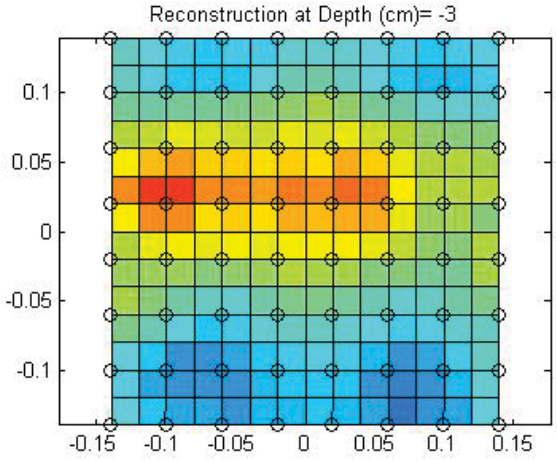

Figure 51. Reconstruction of builder's tube with unmoistened surface.

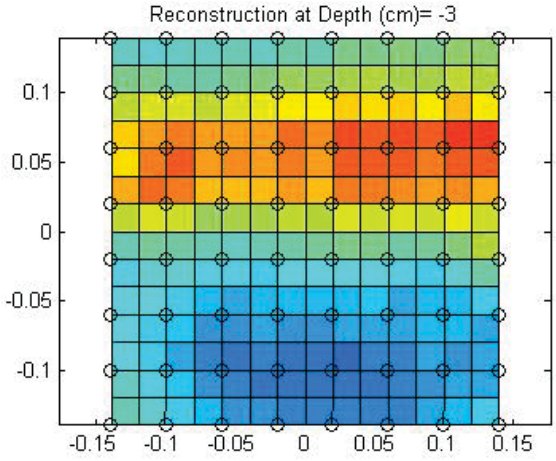

Figure 52. Reconstruction of builder's tube with water on surface.

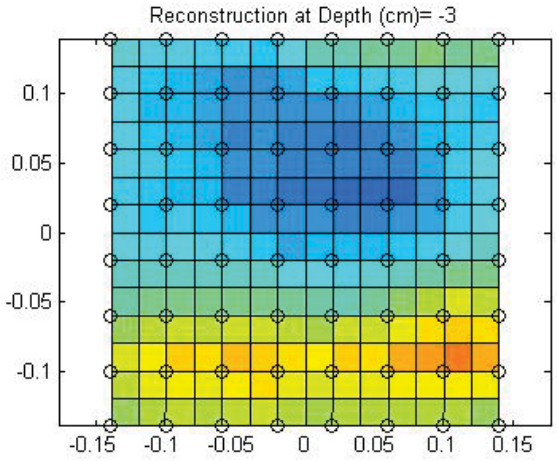

Figure 53. Reconstruction of ABS pipe with unmoistened surface: 2cm burial depth.

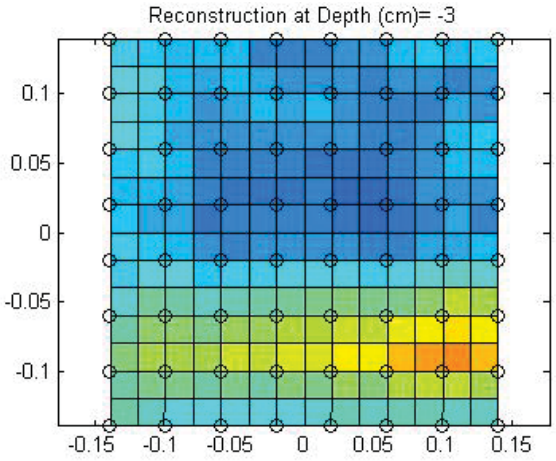

Figure 54. Reconstruction of ABS pipe with water on surface: 2cm burial depth.

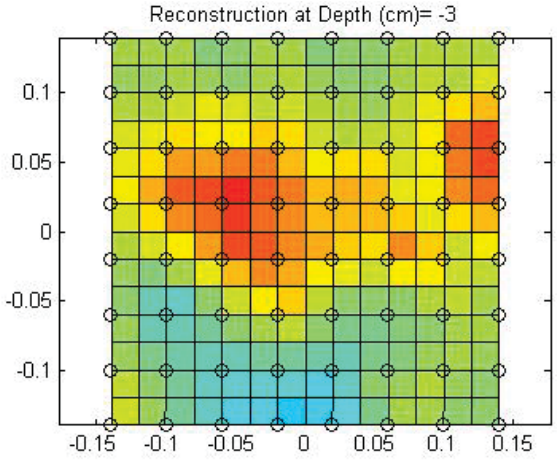

Figure 55. Reconstruction of ABS pipe with unmoistened surface: 4cm burial depth.

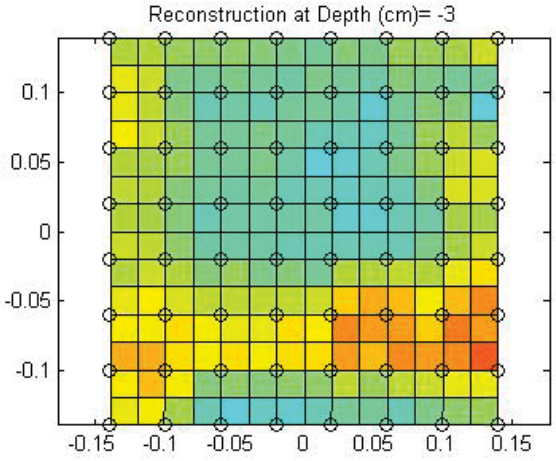

Figure 56. Reconstruction of ABS pipe with water on surface: 4cm burial depth.

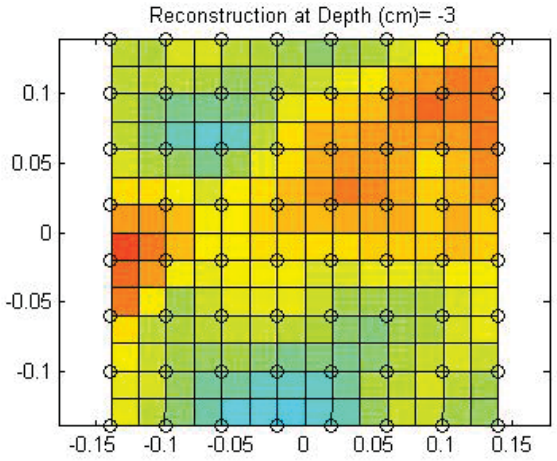

Figure 57. Reconstruction of ABS pipe with unmoistened surface: 6cm burial depth.

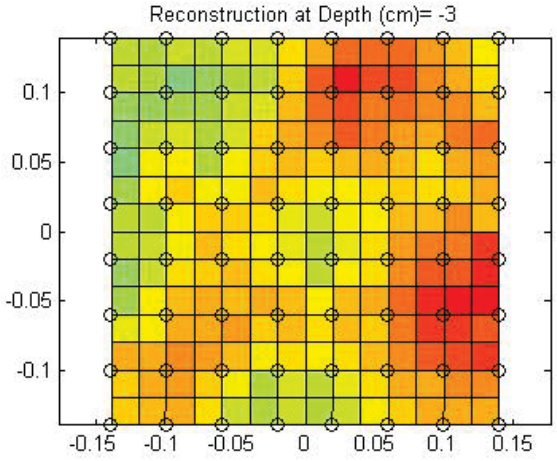

Figure 58. Reconstruction of ABS pipe with water on surface: 6cm burial depth.

It is concluded that good contact between the electrodes and a soil medium enables accurate measurements, and one means of promoting good contact with the lab-scale instrument is to put water on the soil surface immediately before scanning. This step is not sufficient to produce high-quality reconstruction images, however. Further discussion on this result is at the end of the following section.

5.5.2.3 Good contact through electrode shape

Another means of ensuring good contact is using long, tapered electrodes such as those found on the field-scale instrument. These electrodes are also spring-loaded for better contact. Scans of the tunnel surrogates were taken outdoors using this larger array, and yielded reliable measurements. Figure 59 and Figure 60 show the experimental set-up, including the tunnel surrogate. The surrogate is a 24" length of 6"-diameter builders' tube intended for pouring concrete posts. It was buried at a depth of approximately 10cm.

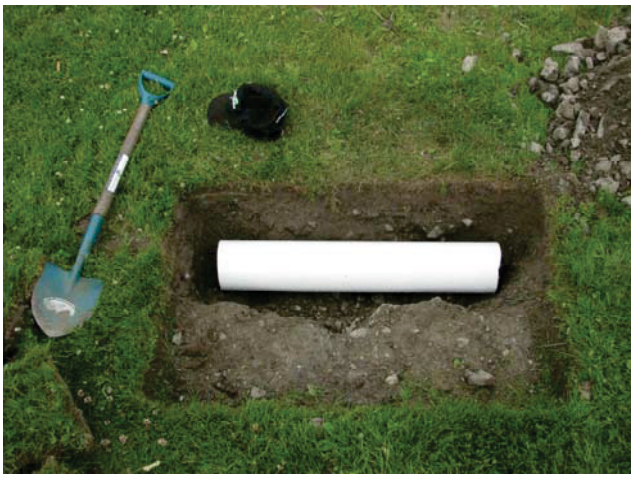

Figure 59. Tunnel outdoors.

Figure 60. Outdoor lab set-up

Initially acquired scans did not exhibit the crisp, repeatable square wave that is a signature of good contact (Figure 61), although later acquisitions did (Figure 62). The medium is less controlled and uniform than in the lab set-up, and it is surmised that soil chemistry variations required some initial data acquisitions to allow transient polarization effects to attenuate before reliable current measurements could be taken. Only one scan was acquired of each stimulation pattern under investigation, so this supposition cannot be confirmed; however the sequence in which the acquisitions were taken and the reliability of current stimulation in the successive scans supports this hypothesis.

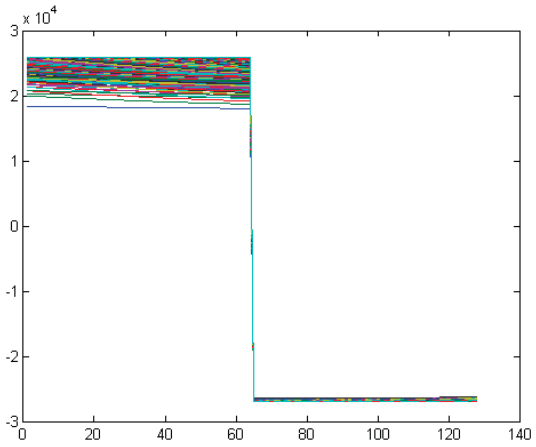

Figure 61. Current stimulation for scan of builders' tube using outdoor array (augbb stimulation pattern).

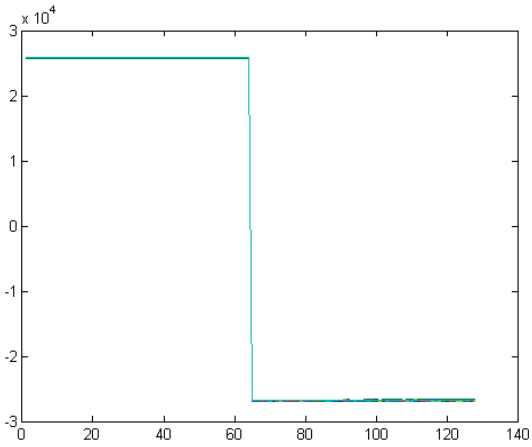

Figure 62. Current stimulation for scan of builders' tube using outdoor array (may19 stimulation pattern).

Conductivity images were reconstructed from these measurements. Unsurprisingly, the scan with inconsistent current measurements did not yield an image with the target clearly visible (Figure 63), while the 'good contact' acquisition clearly showed the buried builders' tube as a non-conductive region (Figure 64). The long, narrow shape of the tube does not show up with great clarity. This may be because the tube length is only 60% of the dimension of the array; a tube extending beyond the instrument would likely display its shape more clearly.

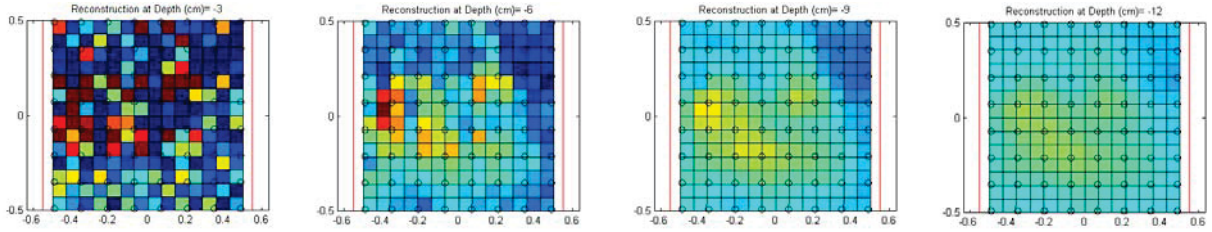

Figure 63. Reconstructed image of buried builders' tube (augbb stimulation pattern). Images are cross-sections of the medium at depths of 3cm, 6cm, 9cm, and 12cm.

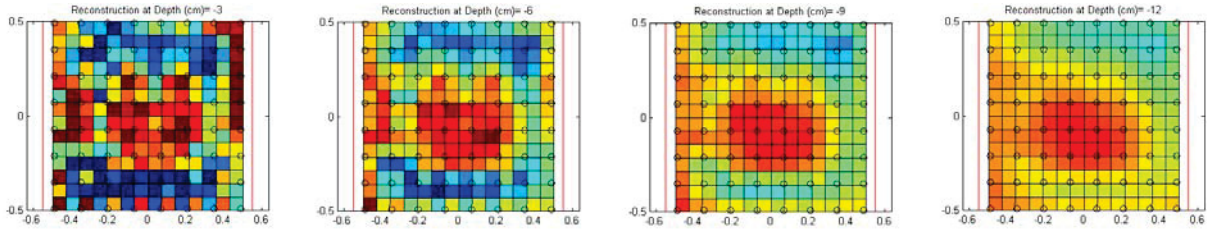

Figure 64. Reconstructed image of buried builders' tube (may19 stimulation pattern). Images are cross-sections of the medium at depths of 3cm, 6cm, 9cm, and 12cm.

Experiments with electrode contact yielded improved reconstruction quality in some cases and not in others. It is concluded that good contact enables but does not guarantee accurate imaging. The electrical properties of the electrode-medium interface are still not well understood, however, and the effects of these properties are highly influential on reconstruction quality. A thorough investigation into accurate models of this interface is required.

5.5.3 Work-arounds for bad electrode contact

When good electrode contact with the medium cannot be established, other work-around solutions may still enable the collection of reliable transimpedance data.

5.5.3.1 Electrode warm-up

As shown in Figure 35, when electrode contact with soil is poor the stimulation current requires several repeated configurations to converge to a consistent waveform; this phenomenon was observed to occur with each change of current stimulating pair (stimulation patterns are typically ordered by grouping consecutively all configurations sharing a stimulating pair). Imposing a 'warm-up' time by recording and discarding *n* 'dummy' configurations after every change of stimulating pair could ensure that the current stimulation is consistent for all configurations acquired. Investigation into this approach was carried out, examining the effects of electrode 'warm-up' first on voltage measurements and then on final reconstructed images.

The effects of electrode warm-up on voltage measurements were evaluated using the stimulation pattern shown in Figure 44 and many of the same scans used in the surface moisture investigation (Section 5.5.2.2). Scans were taken using the original stimulation pattern of Figure 44 and one in which twenty dummy configurations were recorded and discarded at each change of stimulating pair, before recording the legitimate configurations of the sequence.

Consider the original stimulation pattern with no warm-up configurations. A given configuration is the i^{th} one to occur after the most recent change of stimulating pair. Its reciprocal configuration is acquired elsewhere in the stimulation pattern and is the j^{th} one to occur after its most recent change of stimulating pair, where *i* is not necessarily (nor likely) equal to *j*. Since $i \neq j$, the effect of changing stimulation pairs has attenuated to different degrees for the original and the reciprocal measurements. These two measurements will therefore not be equal in practice, although they are identical in theory. The degree to which they differ indicates the strength of the effect of changing stimulating pairs on subsequent measurements.

The introduction of *n* warm-up configurations should attenuate the effect of changing stimulating pairs before recording any legitimate configurations; for both the original and the reciprocal

configurations this effect should have attenuated to effectively the same degree. Although $i \neq j$, the introductions of warm-up configurations means that $n+i \approx n+j$.

We therefore expect to see reciprocals differ from original measurements to a greater extent in the non-warm-up stimulation pattern than in the warm-up pattern. As shown in Figure 65 through Figure 68, this is the case. The figures show the transimpedance measurements of the original and the reciprocal configurations in the same display format as Figure 45 and Figure 46, but in these figures the mean of the original configuration has been subtracted. The original configurations all appear close to zero and the reciprocal configurations, while grouped tightly together, are farther away from zero.

Without using a warm-up protocol (Figure 65 and Figure 66) the reciprocal measurements differ significantly from the originals, on average by about 3%. With a warm-up protocol (Figure 67 and Figure 68) this difference is reduced by an order of magnitude to an average of 0.4%.

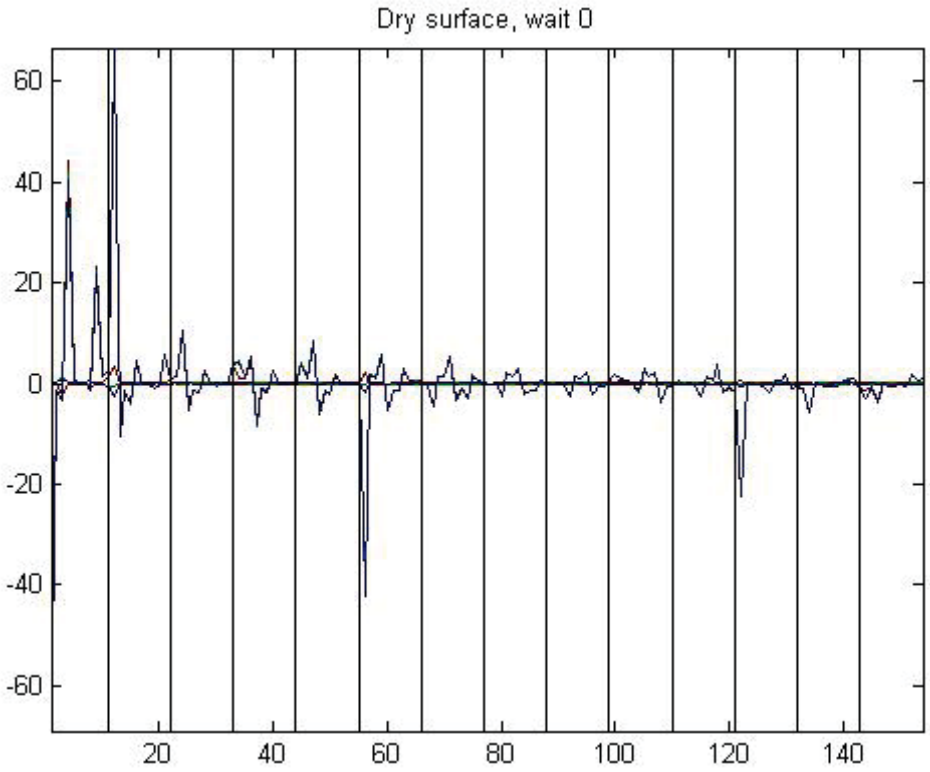

Figure 65. Transimpedances with mean of original subtracted (no warm-up).

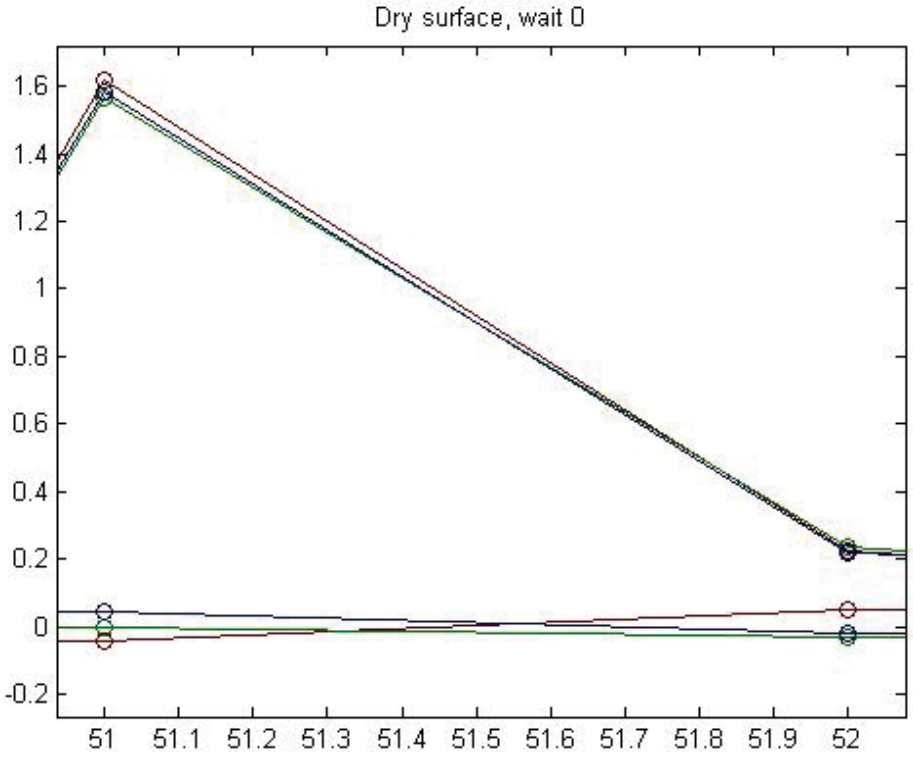

Figure 66. Detail of Figure 65.

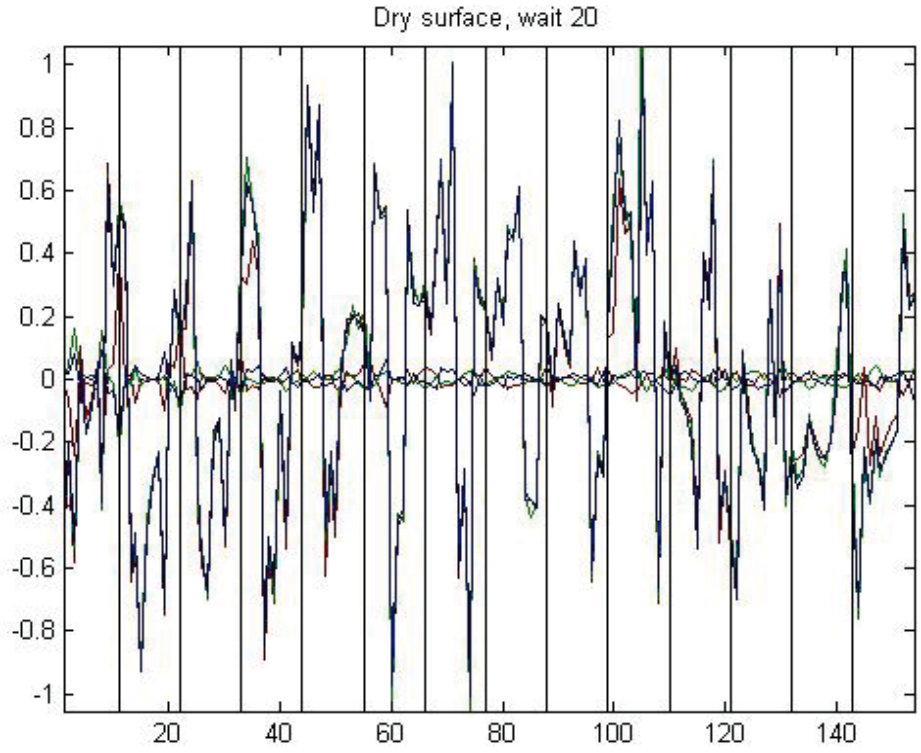

Figure 67. Transimpedances with mean of original subtracted (with warm-up). Note difference in *y*-axis scale from Figure 65.

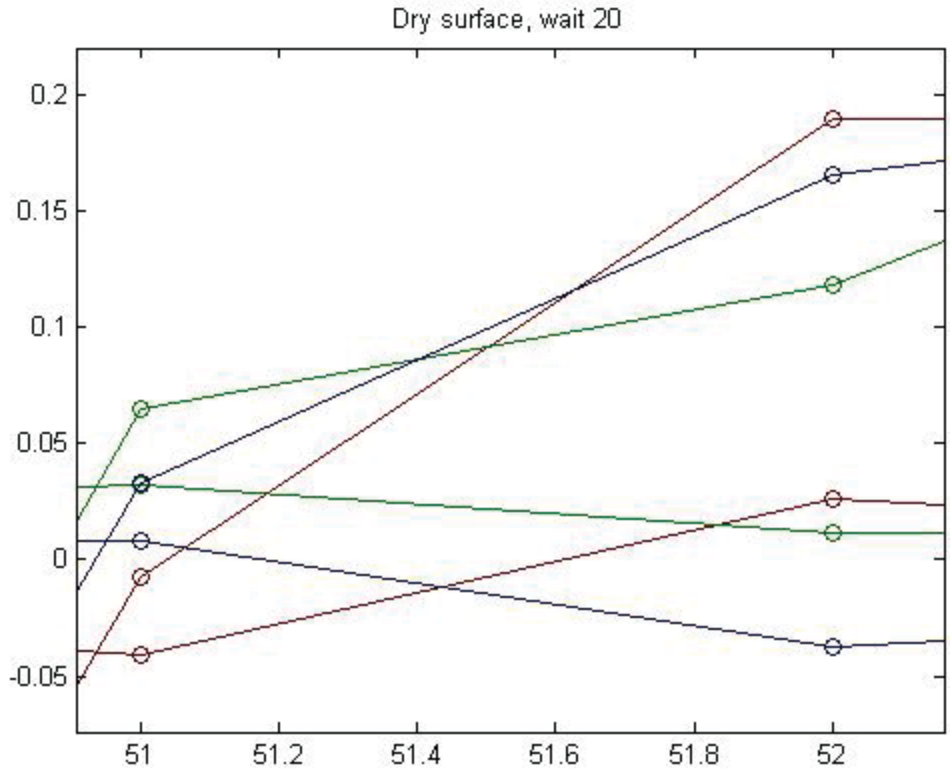

Figure 68. Detail of Figure 67. Note difference in *y*-axis scale from Figure 66.

These experiments were carried out both with and without pouring water on the soil surface before scanning. Table 2 summarizes these results, showing the difference between mean reciprocal and mean original transimpedance measurements, expressed as a percentage of the original measurements. The use of a warm-up protocol reduces by an order of magnitude the effect of changing stimulating pairs, while the quality of electrode contact does not significantly affect this effect. Since polarization induced by stimulation on an electrode pair is mitigated with good electrode contact, this result indicates that stimulation-induced polarization is a distinct phenomenon from the effect of changing stimulating pairs.

	Unmoistened surface	Wet surface
No warm-up	3.3%	2.9%
Warm-up	0.4%	0.4%

Table 2 - Effects of surface moisture and electrode warm-up on stim-pair switching-induced error.

5.5.3.1.1 A note on polarization

Although stimulation-induced polarization is a separate phenomenon from the effect of changing stimulation pairs, good electrode contact and use of the warm-up protocol mitigate both effects. Additional investigation was undertaken to evaluate the benefits of electrode warm-up for

reducing polarization in a soil medium. The same stimulation patterns and scans as above were used for this purpose.

Figure 69 and Figure 70 show the transimpedance measurements using the warm-up pattern on an unmoistened soil surface (compare to Figure 45 and Figure 46 with no warm-up). When a twenty-configuration warm-up is imposed the measurements are more closely repeatable by approximately a factor of four, with a repetition standard deviation of 0.030 compared to 0.11 for the non-warm-up stimulation pattern. Warming up a new stimulating electrode pair therefore reduces polarization effects in addition to mitigating the effects of bad electrode contact (recall that the variation of the three original configuration measurements indicates polarization effects and the variation between mean original and mean reciprocal indicates stim-pair-switching effects). This result is not surprising: the imposition of warm-up configurations at every change of stimulating pair increases the time delay between stimulation on an electrode and future recording, giving the polarization effect more time to attenuate.

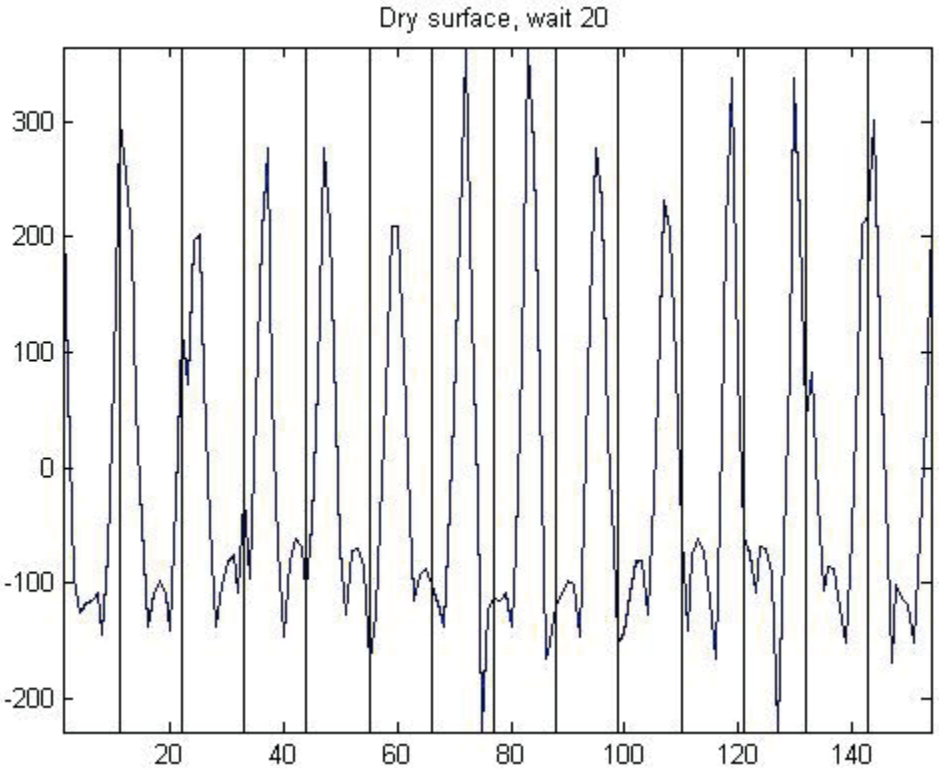

Figure 69. Transimpedances from reciprocal acquisition, unmoistened surface, 20 warm-up configurations.

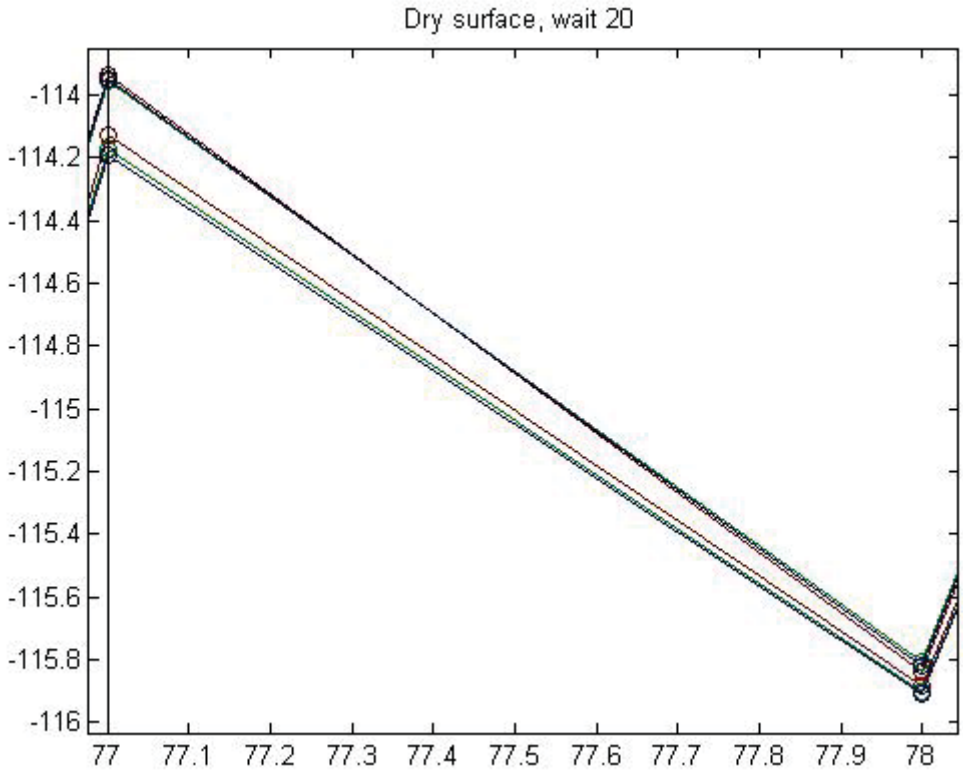

Figure 70. Detail from Figure 69.

Furthermore, imposing a warm-up time reduces polarization effects even when surface contact is good. Figure 71 shows a detail of the transimpedance measurements acquired using a warm-up stimulation pattern with water on the soil surface. Compared to the wet surface with no warm-up period (Figure 48), measurement repeatability improves by approximately a factor of three, from 0.011 to 0.004 standard deviation. These results are summarized in Table 3; values in the table are the standard deviation of the three repetitions of the transimpedance measurements taken of each configuration, averaged over the 154 distinct configurations in the stimulation pattern. A consistent pattern of improvement is evident: good contact through a wet surface reduces polarization by a factor of ten while electrode warm-up time does so by a factor of three to four.

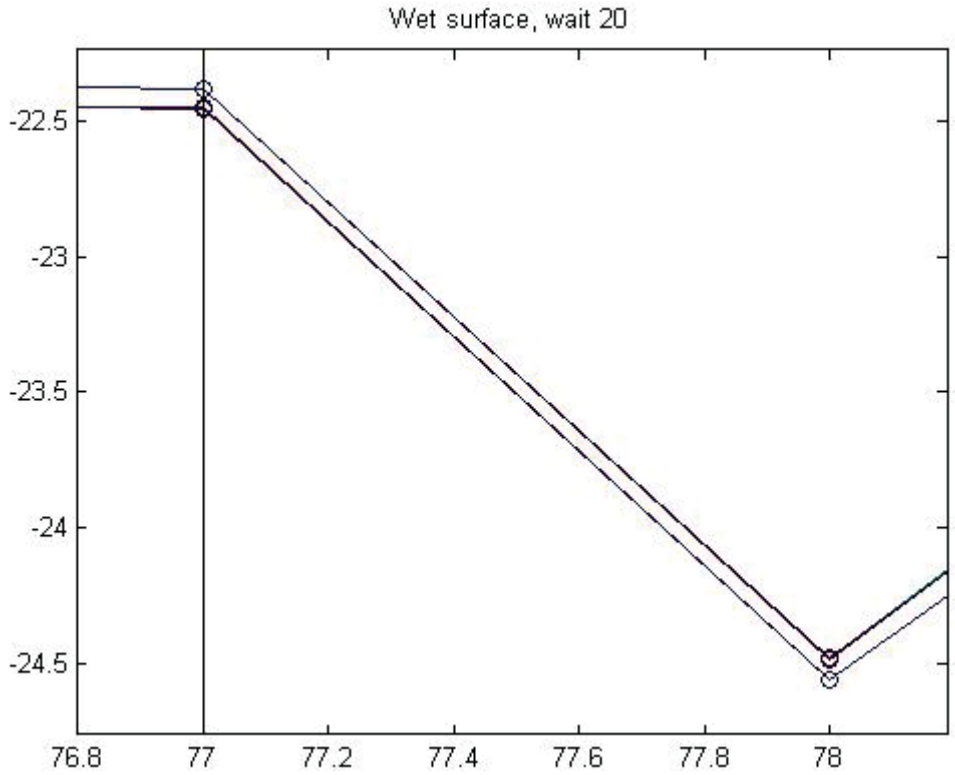

Figure 71. Detail of transimpedances from reciprocal acquisition, wet surface, 20 warm-up configurations.

	Unmoistened surface	Wet surface
No warm-up	0.112	0.011
Warm-up	0.030	0.004

Table 3 - Effects of surface moisture and electrode warm-up on polarization-induced error.

Reconstructions using the warm-up protocol suggests promise for objects buried deep in soil, as shown in Figure 72 through Figure 77. These figures depict a non-conductive round Tupperware container buried in soil at depths of 3cm, 7cm, and 10cm. The figures on the left show an acquisition without imposing a warm-up time; those on the right had twenty warm-up stimulations recorded and discarded at every change of stimulation pair. At 3cm depth both acquisitions are good and the warm-up period does not offer improvement. At the greater depths the warm-up acquisitions appear to localize the target more clearly. It is hoped that future improved modelling of the electrode interface will help manifest the measurement improvements even more clearly in the final reconstructed image.

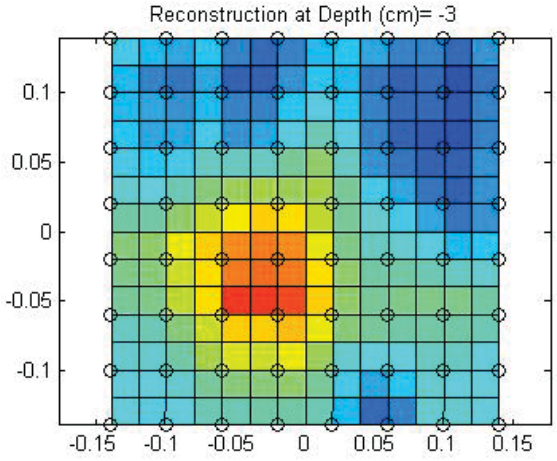

Figure 72. Object buried 3cm deep, no warm-up time.

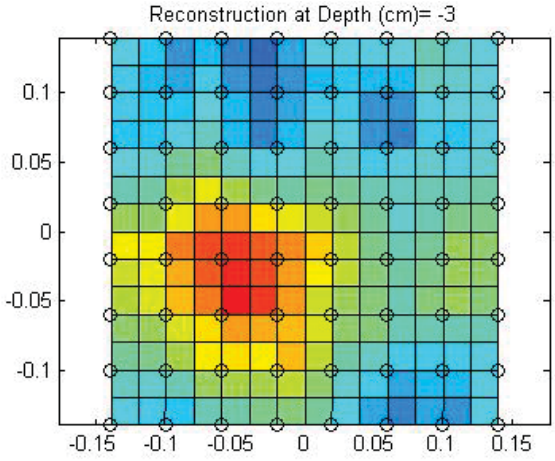

Figure 73. Object buried 3cm deep, with warm-up time.

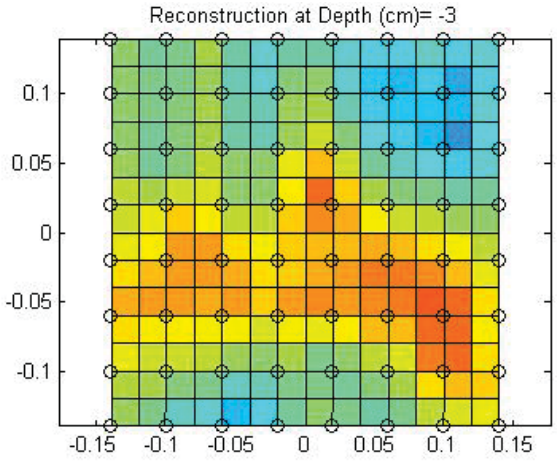

Figure 74. Object buried 7cm deep, no warm-up time.

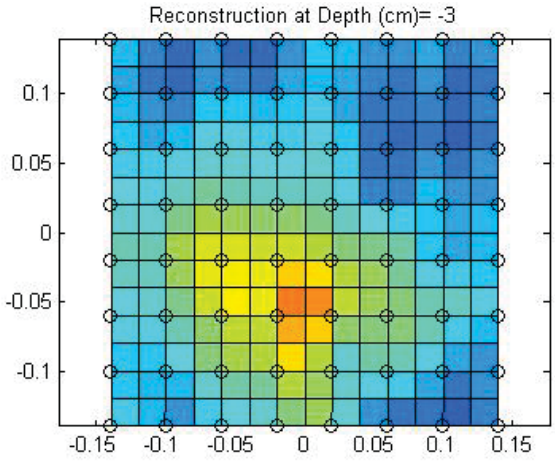

Figure 75. Object buried 7cm deep, with warm-up time.

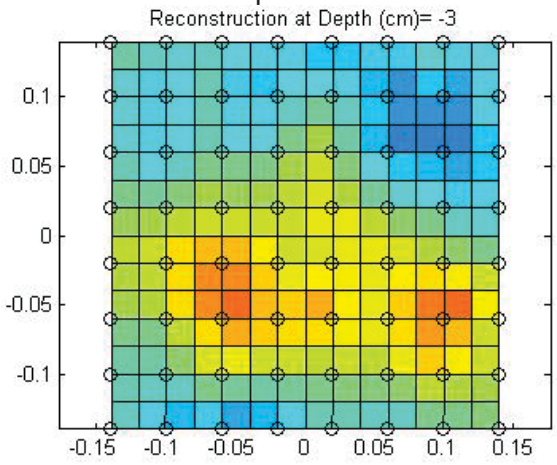

Figure 76. Object buried 10cm deep, no warm-up time.

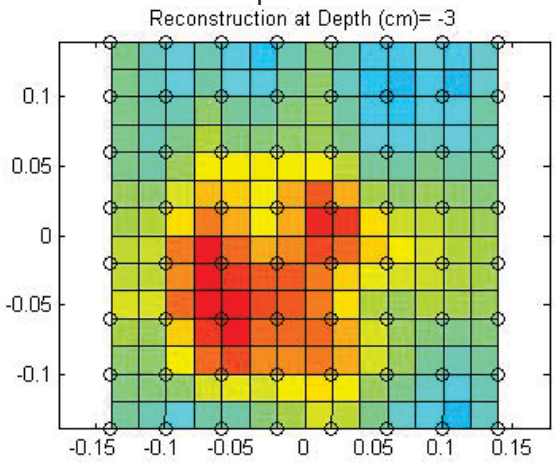

Figure 77. Object buried 10cm deep, with warm-up time

5.5.3.2 Reject bad configurations

Another approach to dealing with poor contact is to reject 'bad' configurations from a dataset before processing. Data quality metrics could be developed to reject unreliable measurements. Preliminary investigation of this technique was undertaken and showed some promise, and use of this technique in other EIT applications has produced substantial improvement [1,2]. For these reasons it is recommended for future work to study in detail the detection and rejection of unreliable configurations.

In the preliminary investigation undertaken during this project, configurations were filtered by a transimpedance standard deviation threshold and a current threshold (high transimpedance standard deviation and low current have both been indicative of unreliable measurements). The reconstruction algorithm was modified to carry out this thresholding operation and to remove the rejected configurations from consideration. Resulting reconstructions are shown in Figure 78 through Figure 81 for the Tupperware container buried 7cm deep in soil.

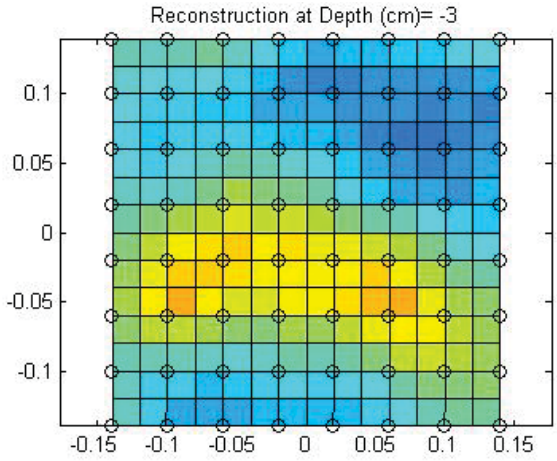

Figure 78. Reconstruction with no thresholding.

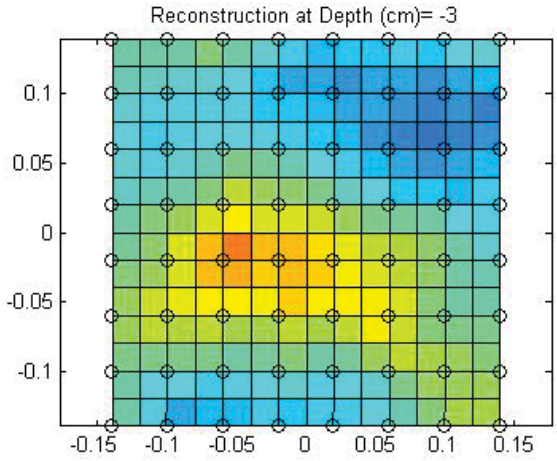

Figure 79. Reconstruction using current threshold.

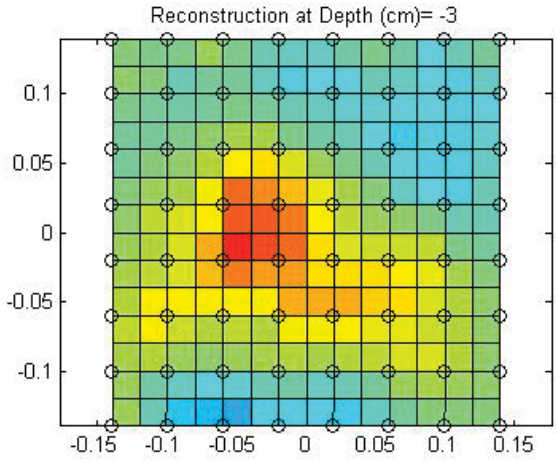

Figure 80. Reconstruction using threshold on transimpedance standard deviation.

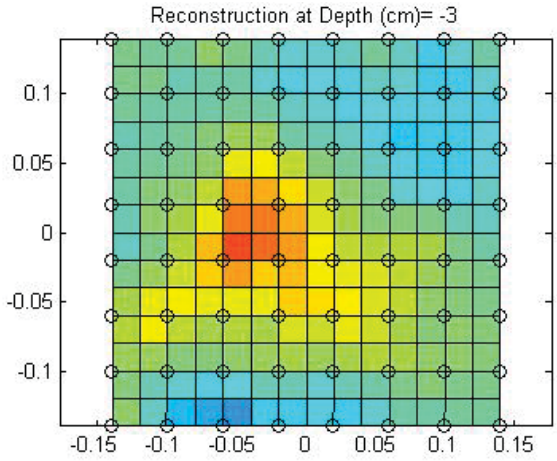

Figure 81. Reconstruction using both thresholds concurrently.

The reconstructions using these two thresholds, individually or together, appear to localize the target more clearly. These preliminary results indicate that thresholding may offer improved performance in cases where good electrode contact is not reliable. The poor-contact configurations can be identified and removed from the reconstruction to improve image quality. Further development of this capability may be of interest in future research.

5.5.3.3 Reciprocal measurements

Another filtering criterion to investigate is reciprocity: a configuration theoretically produces the identical measurement to one with its stimulating and recording pairs swapped, that is by recording on the stimulating pair and stimulating on the recording pair. If both of these configurations are acquired and their measurements are found to differ by more than a given threshold, the configuration could be deemed unreliable; this phenomenon could be a result of intermittent electrode contact, physical damage to an electrode, or imbalances in electronics. To rely on such a measurement it is necessary to use an electrode warm-up protocol as described in Section 5.5.3.1 and to ensure that stimulation-induced polarization has attenuated before measuring the reciprocal configuration. The possible use of reciprocity to identify unreliable configurations is recommended for further study.

5.5.4 Voltage clipping and voltage offset

During the course of tunnel experimentation a phenomenon was discovered whereby the measured voltage signal saturates at an amplifier stage before reaching the AD converter. This behaviour only occurs under certain conditions of signal amplitude and amplifier gain, and is not believed to have affected a great number of scans collected in the past; furthermore each scan's data file contains the information needed to determine whether this voltage clipping occurred. A second observation was made during the clipping investigation, namely that the amplifiers introduce a systematic offset into the voltage measurement. This offset is likely the dominant error source in measurements, but the overall error is still within typical ranges for EIT systems and does not likely compromise reconstruction quality greatly. This section first describes the voltage clipping phenomenon and procedures to prevent it, then describes the voltage offset phenomenon and analyses the error it introduces.

5.5.4.1 Voltage clipping

Figure 82 shows the voltage recording circuitry between the measurement electrodes ("AE_POS_RECORDER" and "AE_NEG_RECORDER", at left) and the ADC input ("V_FILT", at right). (The modifications shown in this schematic were implemented to correct what was initially thought to be the cause of the voltage clipping problem. These mods did not solve the problem but were left in place to minimize potential damage to the electronics and because they had no negative effects on instrument performance.) The voltages of the recording electrodes are passed through a differential amplifier U26 with a gain of 0.5. This amplifier stage removes the common mode and passes the difference signal into an instrumentation amplifier U11 with a user-selectable gain of 1, 10, 100, or 1000. From there the signal goes through a final amplifier stage U10 before going through a low-pass filter to the AD converter. The U10 amp has a user-selectable gain of 1, 2, 4, or 8 and according to its datasheet delivers output between 10V and -10V. The ADC is designed to saturate before +/- 10V, so that any voltage signal not saturating the ADC is known to be a valid measurement not saturated at any earlier amp stages. The

instrument's user interface displays ADC dynamic range so the operator can adjust gains and re-take scans if the ADC saturates.

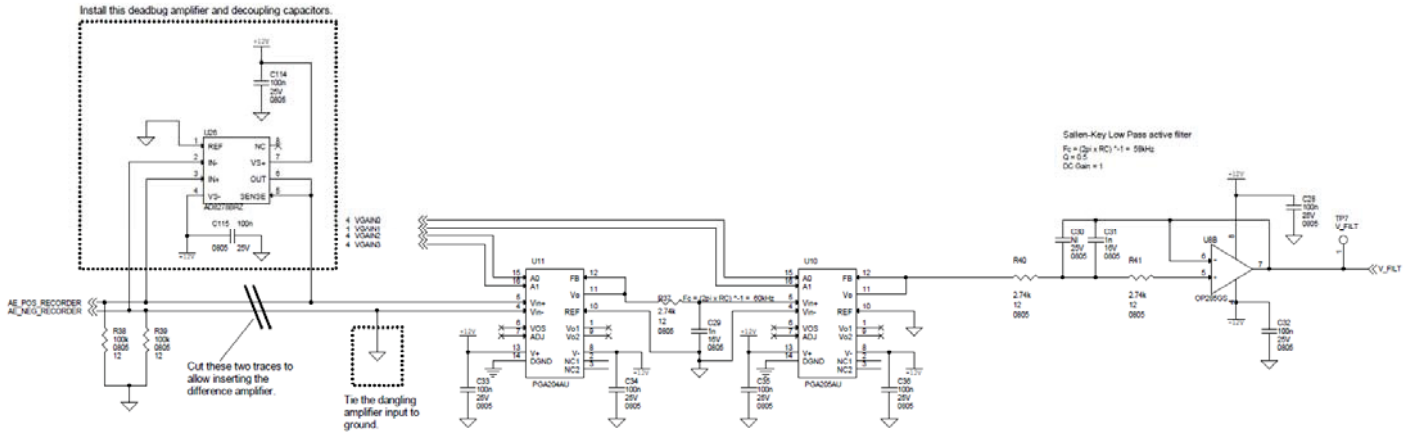

Figure 82. Schematic diagram of the modified voltage recording electronics.

As part of the voltage clipping investigation, various points in this circuit were probed using an oscilloscope during data acquisition. The points measured were

- the two voltage inputs, AE_POS_RECORDER and AE_NEG_RECORDER.
- the output of the instrumentation amplifier, U11 pin 11.
- the input to the AD converter, TP7.

Acquisitions were taken using a stimulation pattern that repeated a single configuration several times. The acquisitions were repeated with increasing gains on U11 and U10 to identify when the voltage clipping begins.

It was found that the U10 amplifier saturates on the negative side at approximately -9V rather than the -10V stated on the data sheet. As a result, voltage saturation can occur that is not indicated by the ADC dynamic range display in the user interface, causing invalid data to pass unnoticed. This phenomenon is illustrated in the figures below.

Figure 83 through Figure 85 show waveforms observed in the circuit for three increasing gain levels. For all three figures, the positive and negative voltage recordings are shown in cyan and red, along with the instrumentation amp output, measured at U11p11, in green. Ideally U11p11 is a scalar multiple of the voltage difference. TP7 is also shown in blue, and should be a scalar multiple of U11p11.

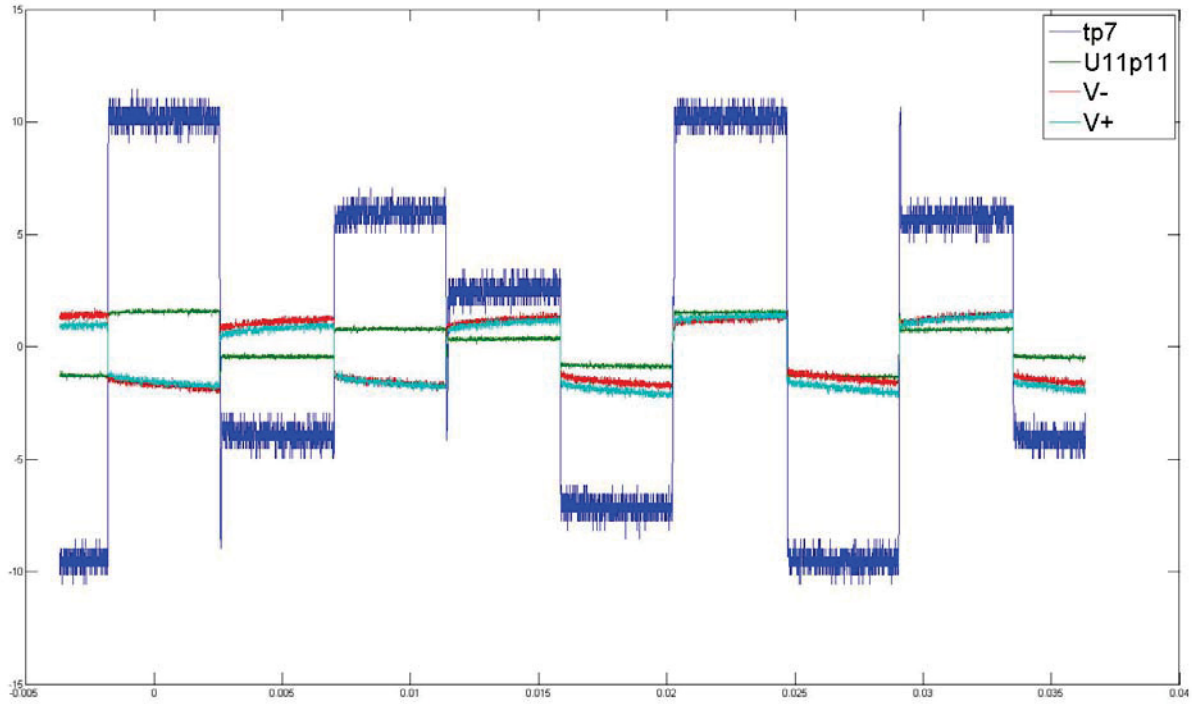

Figure 83. Scope readings, gain of 80 (not including initial diff amp).

As shown in Figure 83, at the first gain level the TP7 waveform behaves as expected. With this gain level TP7 should be eight times U11p11 up to a maximum of 10V. TP7 scales with U11p11 and saturates at 10V as expected.

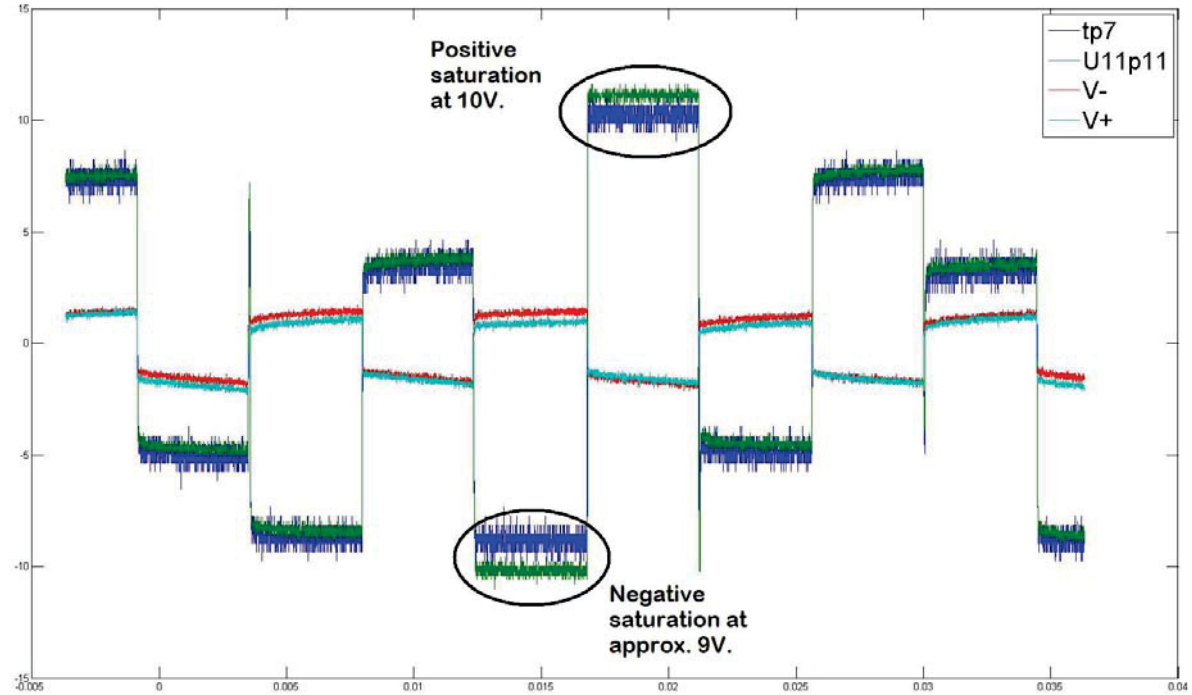

Figure 84. Scope readings, gain of 100 (not including initial diff amp).

At the next gain level of 100 (Figure 84), TP7 should equal U11p11 up to a 10V saturation point. As expected the largest positive voltage is seen to saturate at 10V, unable to match the value of U11p11 when it exceeds 10V. The largest negative voltage also saturates, but at a value less than 10V. This behaviour demonstrates the unexpected early saturation of the U10 amplifier.

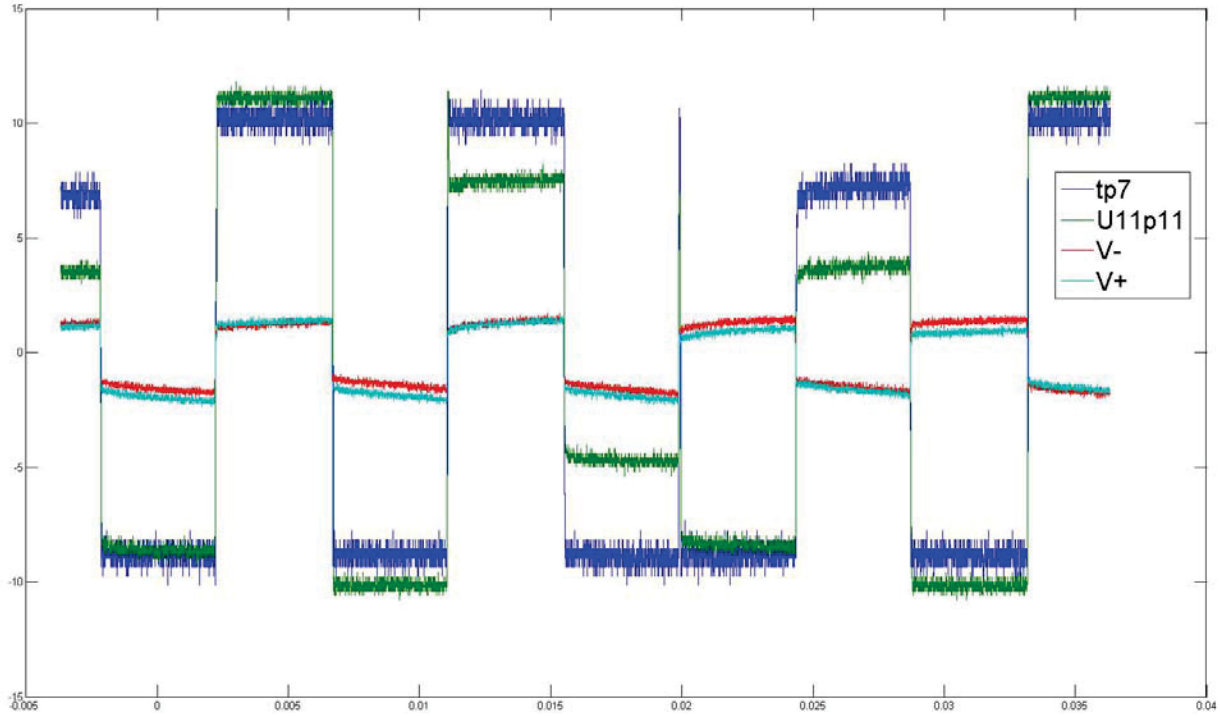

Figure 85. Scope readings, gain of 200 (not including initial diff amp).

Increasing the gain to 200 (Figure 85) shows the early saturation phenomenon on all negative voltage phases. TP7 should be double U11p11 up to a 10V saturation point, but clearly saturates before 10V on the negative phase.

To determine precisely the voltage at which this clipping occurs, acquisitions were taken using three different stimulation patterns. Recall that a pattern usually contains many configurations, each of which is typically sampled 64 times. In this experiment each pattern used a single configuration repeated 100 times (with each repetition sampled 64 times); for each pattern scans were taken at several gain levels.

Table 4 shows the results. The first column lists the configuration used for the scan in the format (*a*, *b*, *c*, *d*) where

a is the electrode index of the current stimulating electrode.
b is the electrode index of the current reference electrode.
c is the electrode index of the positive voltage recording electrode.
d is the electrode index of the negative voltage recording electrode.

The second column shows the voltage gain applied; the third and fourth columns show the maximum and minimum raw voltage measurements acquired during the scan (raw voltage measurements are the individual samples of the configurations in the stimulation pattern).

Table 4 - V measurements for varying V gain levels

Configuration (current stim, current reference, voltage +, voltage -)	Voltage gain (U11 gain x U10 gain, not including U26 gain)	Max raw V Measurement (% of ADC range)	Min raw V Measurement (% of ADC range)
1,8,3,2	20	29.17	5.95
1,8,3,2	40	58.03	11.81
1,8,3,2	80	100.00	23.53
1,8,3,2	100	100.00	29.65
1,8,2,3	10	-2.44	-14.37
1,8,2,3	20	-5.47	-28.74
1,8,2,3	40	-10.22	-56.98
1,8,2,3	80	-20.65	-92.17
1,8,2,3	100	-26.04	-90.16
1,8,2,3	200	-52.71	-89.40
1,8,2,3	400	-89.39	-100.00
1,8,6,7	20	3.63	-16.92
1,8,6,7	40	7.17	-33.79
1,8,6,7	80	14.28	-67.56
1,8,6,7	100	17.61	-85.03
1,8,6,7	200	35.08	-89.48
1,8,6,7	400	69.77	-89.57
1,8,6,7	800	100.00	-89.70

Consider the first configuration, recording on electrodes 3 and 2. As expected, the maximum and minimum voltages increase in approximate proportion to the gain, up to a saturation limit of 100% on the maximum voltage. The maximum voltage of the second configuration also increases roughly in proportion to gain until the final gain level of 400. At this gain level one would expect the voltage to saturate at -100%, but in fact it is limited to -89% in the maximum voltage. The minimum voltage also behaves unexpectedly at high gain levels. Beyond gains of 40 the voltage does not increase proportionally with gain but instead appears limited at approximately -90%, before reaching -100% at the final gain level. Finally, the third configuration shows expected behaviour in the maximum voltage, increasing proportionally to gain until saturation at 100%. Up to a gain of 100 the minimum voltage varies directly with gain, but beyond this point saturation occurs at -89%.

The consistent pattern in this data is the saturation of voltages at 100% (as expected) for positive values and at -89% (unexpected) for negative values. Saturation appears to occur between -85% (the largest ‘known good’ negative value) and -89% (the smallest known saturated value). It is therefore required for reliable data collection to select gains that keep the voltage signal within 85% of the ADC range.

The maximum percentage of the ADC range used for a scan is displayed in the user interface software, making this saturation easily observable by the operator at the time of data acquisition. Current practice is for the operator to verify ADC range levels below 100% for each

scan and to adjust gains and re-scan as necessary to correct saturation. The 'upstream' voltage clipping phenomenon can easily be avoided by changing the re-scan threshold in the acquisition procedure from 100% to 85%. A longer-term solution may include changing the user interface software to reflect this threshold.

5.5.4.2 Voltage offset

During the voltage clipping investigation it was observed that the amplifier chain adds an offset to the voltage measurement, introducing a modest error in the transimpedance measurement. This phenomenon was observed by reversing polarity of the stimulating and recording pairs in a stimulation pattern. Scans were acquired using four different stimulation patterns. The first stimulation pattern was one generated earlier in the project for testing purposes. The second pattern was modelled on the first but had the recording pairs flipped; the positive recording electrode became the negative recording electrode and *vice versa*. The third pattern was modelled on the first but with the stimulating pairs flipped and recording pairs left in their original states. The last pattern had both stimulating pairs and recording pairs flipped.

Note that we refer to 'flipped' electrode pairs when the positive and negative polarity of a pair is reversed, be it a recording pair or a stimulating pair. We refer to the 'reciprocal' of a configuration as one in which the stimulating pair is used for recording and the recording pair is used for stimulating.

Ideally, flipping the recording and/or stimulating electrode pairs causes no change in measured voltage. If the voltage recording circuitry introduces an offset in one direction, however, the reversal of an electrode pair will result in a different voltage measurement.

Figure 86 and Figure 87 show the voltage measurements from these scans; Figure 86 shows the full dataset while Figure 87 shows a representative sample of the dataset in fuller detail. Each of the four stimulation patterns was scanned three times, and the three individual scan results are shown with fine solid lines. The average of the three voltage measurements is shown in a thicker solid line of the same colour. There is a difference in recorded voltages among the four stimulation patterns, and this difference is greater than the variability of voltage within any one pattern. The dominant difference appears to be the flipping of the stimulating pair. The mean SNR of all voltage measurements is approximately 7500, or an error of 0.01% (the calculation of these values is shown in Appendix B, in the Matlab scripting language). This error is low because it is mainly random and is reduced by the averaging of three measurements. The SNR of the voltage measurements compared across stimulation patterns is approximately 330, or 0.3%. This error is not random but systematic, resulting from the offset introduced by the voltage recording circuitry; it is therefore not reduced by averaging. An error over 1% may indicate unreliable data for EIT reconstructions. Errors under 0.1% are usually considered negligible, while errors in the 0.1% to 1% range are significant but not necessarily detrimental to performance. It is therefore concluded that this voltage offset is not an immediate concern, although next-generation electronics design should take this effect into consideration if reduced noise is a goal.

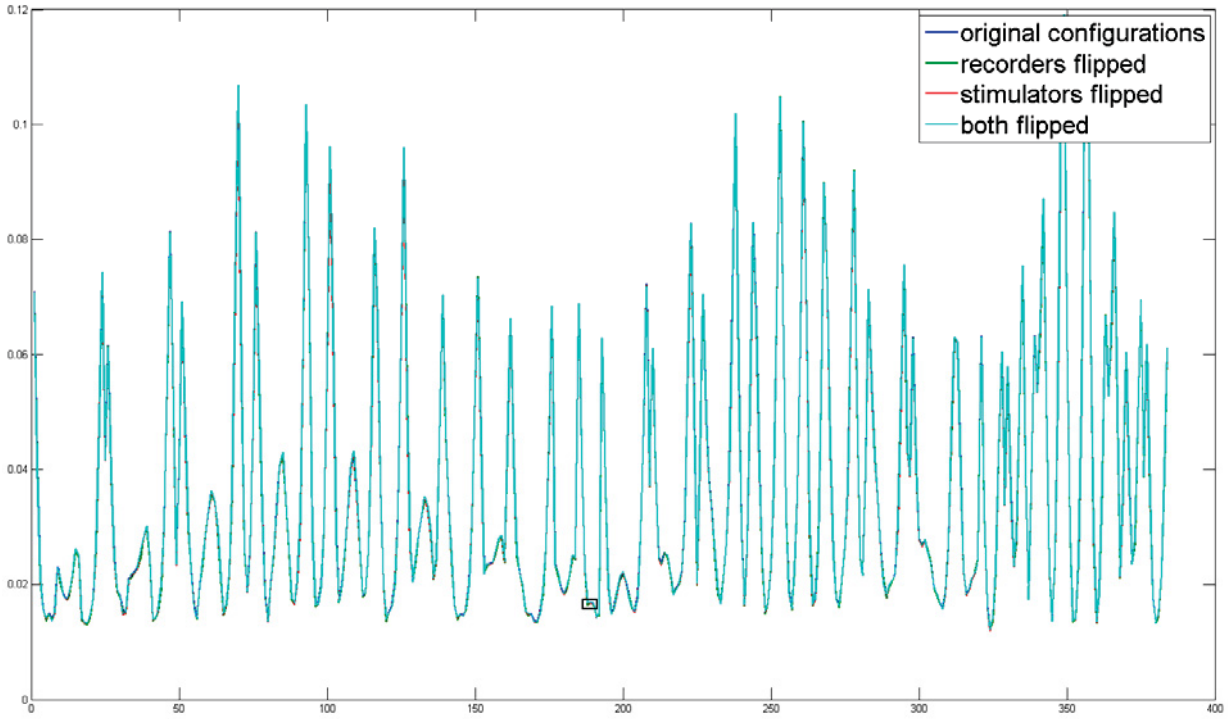

Figure 86 Voltage measurements from flipped recorders and flipped stimulators. The black box indicates the location of the detail shown in Figure 87.

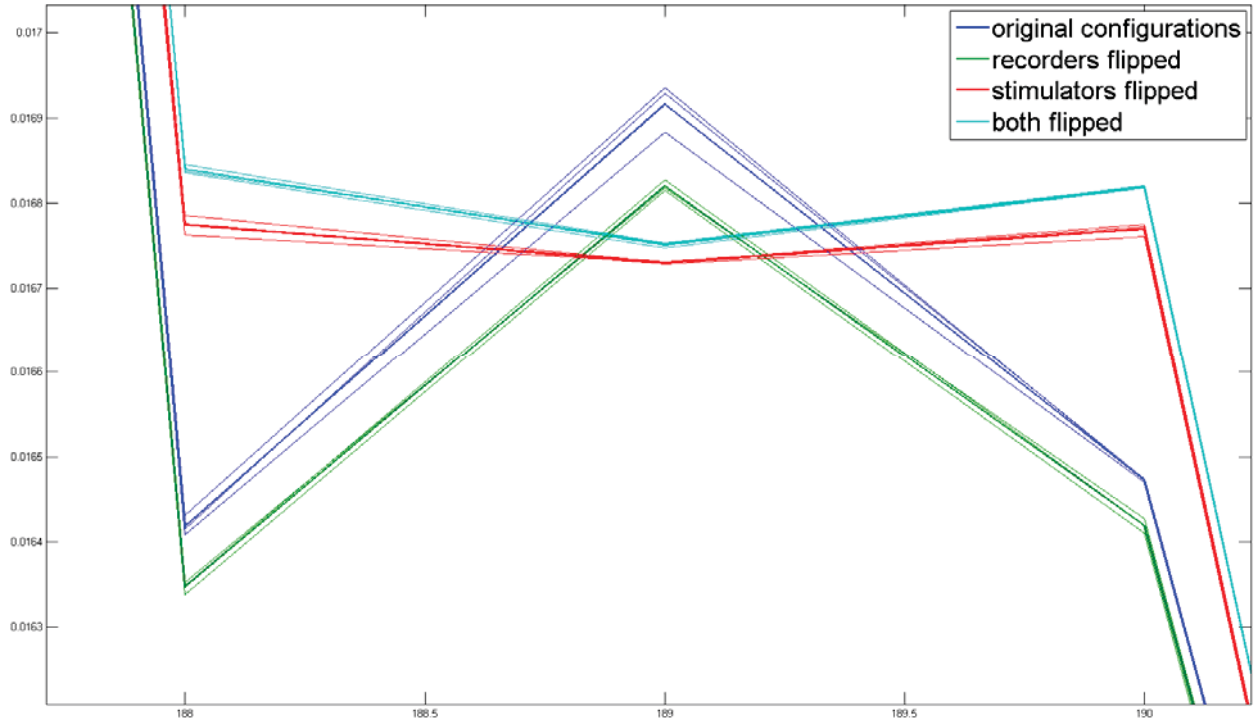

Figure 87. Detail of Figure 86.

5.5.5 Packed tunnels

It is of interest to know whether the presence of packed explosives in a culvert changes its EIT signature. To study this question experiments were performed in the lab with one of the cylinders used as tunnel surrogates. The 2" diameter copper pipe (Figure 33, second from bottom) was buried in topsoil and imaged with the lab-scale instrument at three burial depths. Experiments were taken with the empty cylinder, then the cylinder was packed with solethane potting compound, a non-conductive putty-like substance, to simulate the presence of plastic explosives (see Figure 88 and Figure 89).

Figure 88. Copper pipe filled with solethane compound.

Figure 89. Copper pipe filled with solethane compound - view 2.

The presence inside the cylinder of a non-conductive substance other than air was predicted to have little or no effect on the results. Figure 90 through Figure 92 show the experimental results, confirming this hypothesis. The images from left to right show the reconstructions at burial depths of 2cm, 3cm, and 4cm. The three figures respectively show the target buried at depths of 2cm, 4cm, and 7cm.

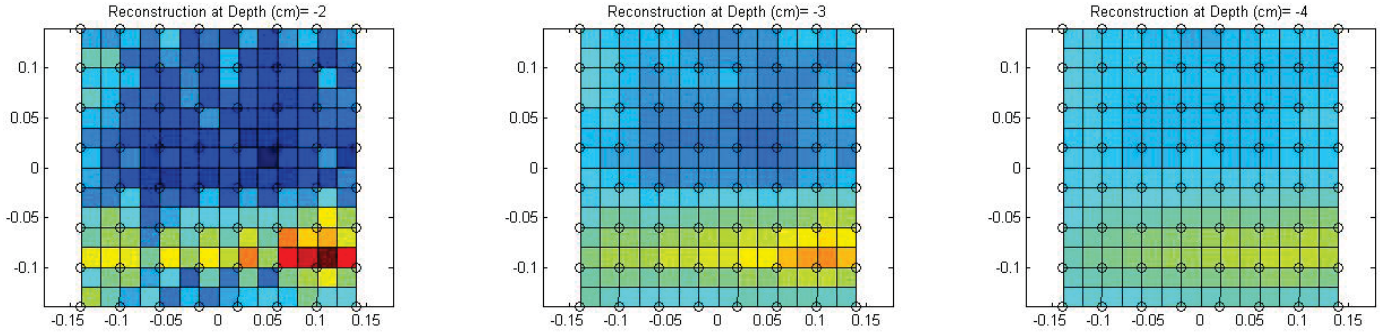

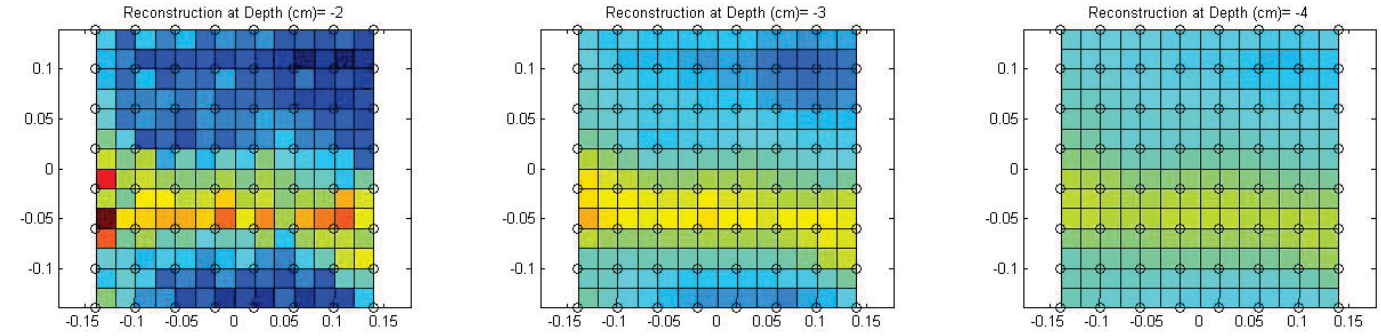

Figure 90. Cylinder without (top) and with (bottom) packed compound: 2cm burial depth.

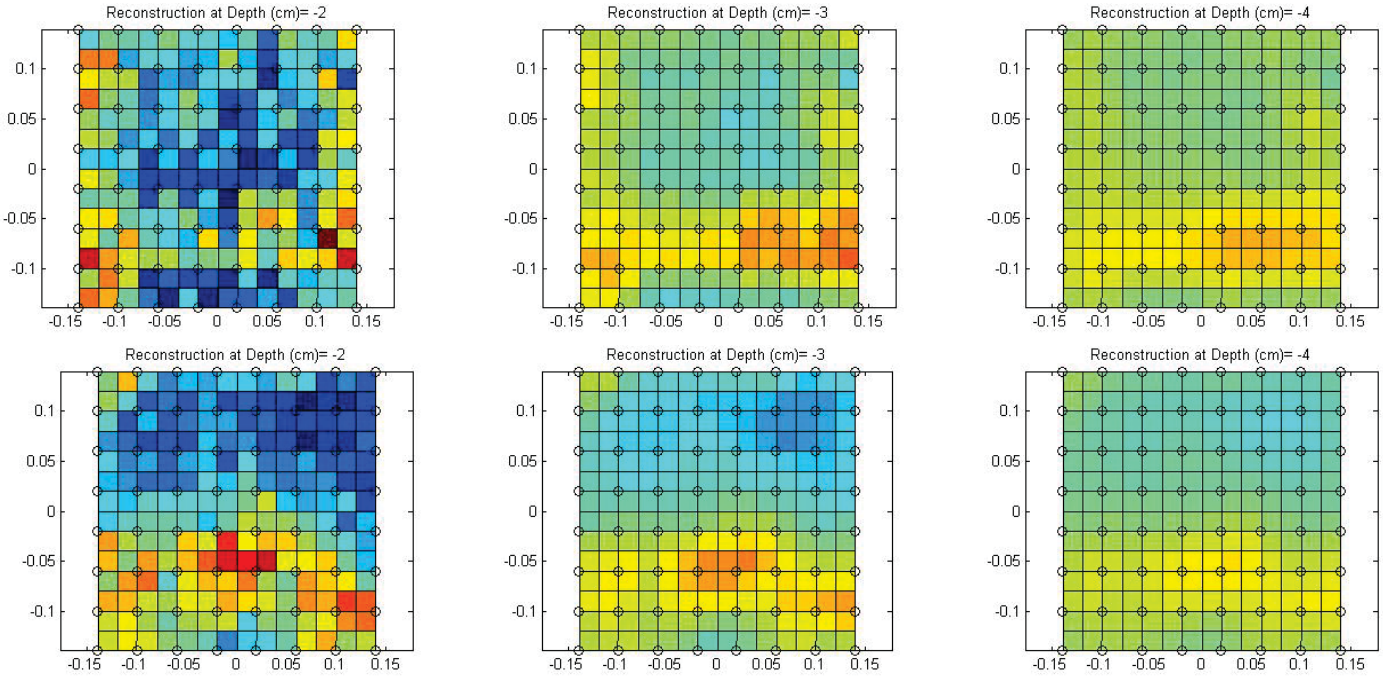

Figure 91. Cylinder without (top) and with (bottom) packed compound: 4cm burial depth.

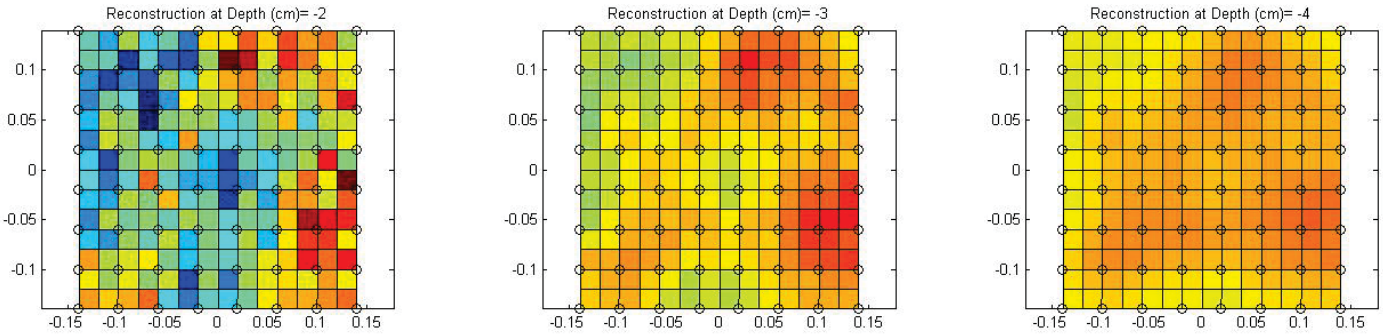

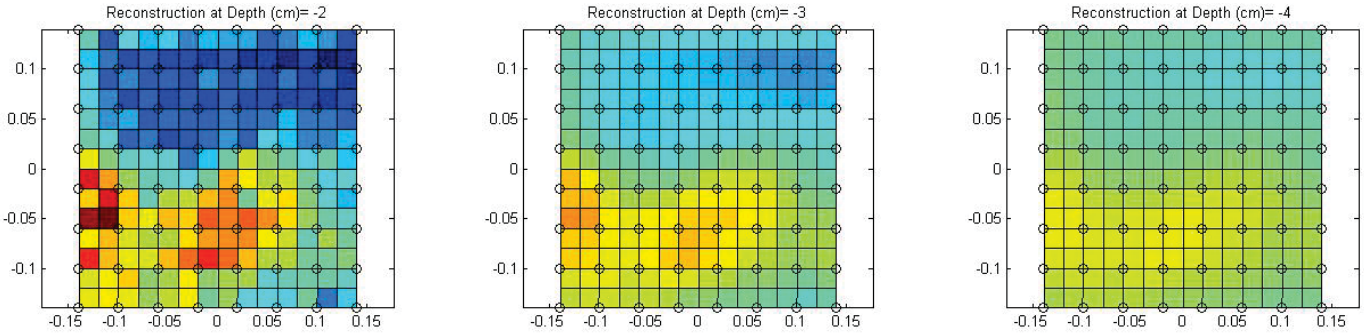

Figure 92. Cylinder without (top) and with (bottom) packed compound: 7cm burial depth.

The presence of a substance inside the cylinder was not detectable based on EIT images collected. This result is as expected. A non-conductive cylinder filled with non-conductive compound is expected to behave the same way as one with open air inside. A conductive cylinder is also not expected to change its signature based on whether it is hollow or filled with non-conductive filler; in both cases the current flows through the surface of the cylinder and not the interior.

No experiments were carried out with conductive filler in the cylinders. In the case of the non-conductive cylinder, the body of the cylinder is an insulator regardless of whether conductive objects are contained inside, so conductive fill is unlikely to be detectable. In the case of a conductive cylinder, current flows near the surface of a conductor and not in its interior, so a solid conductive fill may not affect EIT signature greatly. This latter hypothesis may be worth verifying if conductive explosive materials packed in conductive tunnels/culverts become an operational scenario of interest, but EIT is unlikely to be an effective technology for detecting objects contained within tunnels or culverts.

5.6 Array re-design recommendations

The development of additional data collection hardware could facilitate further research. Improvements in both the electrode array and the electronics may be of benefit, although the dominant factor affecting performance is believed to be modelling of the soil-electrode interface rather than instrumentation.

For research purposes, a re-configurable array may be of high utility and relatively low cost to manufacture. For example, several 2 x 2 sub-arrays of electrodes that can be attached together to form different shapes and sizes of array would afford the study of long, narrow arrays for tunnel detection on flat ground or object detection in berms, where sub-arrays can be placed at different soil angles to cover the top and sides of a berm..

It is recommended to use an electrode shape similar to that on the current 1m x 1m field instrument, namely tapered to a point at the tip. This electrode shape provides much better surface contact with a soil medium than does the flat cylinder shape used in the lab instrument. Before proceeding with design and manufacture it would be of value to test this electrode shape in water to confirm that the shape does not hamper performance in this medium. Such tests could be run using the current field instrument.

It is also recommended to use spring loading on the individual electrodes, as is done on the field instrument. This feature allows all electrodes to make contact in a soil environment even without perfectly flat terrain. An array of the size being considered would certainly encounter terrain variations necessitating this feature even on relatively flat ground.

The electronics associated with the instrument could also be improved to enhance EIT performance. While hardware error and drift were found to be low in the calibration investigation, the polarization phenomenon can be greatly mitigated with precise implementation of certain parts of the electronics. In particular the balancing of the stimulation current source can improve measurement accuracy. A capability not only to balance the current input more finely but also to measure and automatically correct current balance will be an important part of developing a field-deployable system that performs well under a variety of conditions.

Such a capability could be implemented as a process that runs for each scan automatically or as an occasional manual step. The current balance can be evaluated by verifying reciprocity, that is by taking a measurement and then taking a reciprocal measurement. Another means of evaluation is to take a measurement, then measure its reciprocal, then return to the original measurement for a certain number of repetitions; the current balance can be adjusted in one direction if the voltage measurement converges to an undershoot of the original value, and in the other direction for an overshoot.

The balancing of the current stimulation is done by adjusting resistor values of the current source amplifier. Fine adjustment is required, so an electronic design that affords fine resistance variations is needed.

If electronics are being redesigned, a worthwhile effort would be a more precise elimination of amplifier offsets in the voltage recording circuitry; this change would reduce hardware error and could prove useful if future improvements in reconstruction algorithm, stimulation pattern, and system modelling proceed to the point that hardware imperfection becomes the dominant error source.

In the voltage recording circuitry the A/D converter has a resolution of 16 bits. A finer-resolution ADC would not need as high a gain, which would reduce the clipping problem discussed in Section 5.5.4.1. It is therefore recommended to use an ADC with higher resolution in the next hardware implementation.

6 Conclusions and Recommendations

This section summarizes the conclusions of the research undertaken, categorized by task, and some recommendations for future work.

Calibration

Calibration of hardware error in the instrument is unnecessary since this error is on the order of 0.1% or less (instrument error was not discernible above the measured error of the resistor network used for calibration measurements).

EIDORS – stimulation patterns

The first attempt at designing a stimulation pattern more sensitive at depth was successful: the new stimulation pattern has substantially higher depth sensitivity and reconstructed images are somewhat improved, with more accurate target localization. The improvement is not as dramatic as was expected, however: the errors introduced by inaccurate modelling of the electrode-soil interface remain large. Reconstructions are strongly affected by errors at the electrode surface, since sensitivity is inevitably much greater closer to the electrodes. Accurate modelling of this interface, including electrode relative position, contact quality, and electrical properties of the soil-electrode boundary, is therefore of great importance in improving reconstruction fidelity. It is recommended that the next major effort on this program be improved modelling of the electrode-soil interface, especially if use of the technology in a soil medium is desirable.

Research into stimulation patterns may also be of interest. This preliminary investigation produced an improved pattern but no rigorous optimization was carried out, and a more thorough treatment of the problem may yield even better sensitivity performance. This improved sensitivity is expected to further improve reconstructions once the electrode modelling errors are addressed.

EIDORS – algorithm variants

Several algorithm variants were tested. The smoothed image prior appeared to show some potential, and the robust image prior may help reject outliers when electrode contact is poor. It may be that the effects of algorithm variants will become stronger once accurate electrode interface modelling is implemented; at present none of the variants offers dramatic improvement.

Polarization

Polarization of an electrode caused by using it in a stimulating pair can be greatly reduced by balancing the current input, that is keeping the absolute values of the positive and negative currents close to equal. If this can be accomplished more options will become available in stimulation pattern selection; electrodes are currently removed from eligibility as voltage recording electrodes once they have been used for stimulation. Some electronics design effort would be required to implement automatic fine tuning of the current balance to reduce voltage reading error.

Polarization can also be reduced with good soil contact, as demonstrated by pouring water on the soil surface during the tunnel/culvert soil contact investigation. The electrode ‘warm-up’

protocol also reduces the effects of polarization by imposing longer wait time between stimulation and recording.

Ammunition rounds

Ammunition rounds with complete coats of paint appear as insulators; with no paint they appear as conductors. Rounds with partial paint coverage, such as fired rounds with part of the paint worn off in the firing process, do not have an EIT signature. EIT is therefore not useful for the detection of spent ammunition rounds.

Tunnels/culverts

Good electrode contact with the soil medium is required for accurate current stimulation and voltage measurement, but it is not necessarily easy to achieve; simply placing the lab array onto the soil surface does not guarantee good contact. The long, tapered shape of the field-array electrodes helps produce good contact, as does pouring water directly onto the surface of the soil before scanning. As a field-usable strategy, electrode shape is of interest.

Although measurements are improved with good contact, reconstruction images are not necessarily any better. As with other tasks such as the stimulation pattern investigation, it is believed that the model inaccuracies at the electrode-soil interface are large enough, since the reconstruction quality is highly sensitive to these inaccuracies, to prevent the improvements gained with good contact from being manifested in the final image.

When these modelling errors are reduced or eliminated, some further work to improve tunnel detection may offer improvements. The rejection of ‘bad’ configurations by filtering on current amplitude, transimpedance standard deviation, or reciprocity or by implementing the robust data norm algorithm to rejects outliers may offer improvements and could be studied in more detail. The use of an electrode ‘warm-up’ protocol also improves results.

Packed culverts

As expected, a simulated empty culvert gives the same EIT signature as a simulated culvert filled with a non-conductive material intended to simulate plastic explosives. EIT is not capable of detecting explosives or other objects on the interior of a conductive or non-conductive body.

Array re-design

It would be useful for research purposes to have configurable blocks of sub-arrays, for example of four electrodes each, that could be assembled to produce arrays of differing size and shape. This set-up would allow research into long, narrow arrays for tunnel detection or for EIT on berms, where sections of the array can be placed on the top and sides of the berm.

Recommendations for future work

The next important step in improving reconstruction images is the modelling of the electrode-medium interface. This investigation is recommended as the top priority in future work.

Other tasks can also be undertaken in the short term. The design and build of a configurable electrode array for lab research purposes could be done within a modest budget and schedule if robustness to field use were not required. More thorough improvement/optimization of

stimulation patterns for depth sensitivity is also a promising avenue that could be investigated. As a follow-up to the stimulation pattern work the task of modelling the aquarium walls and floor could be undertaken, since improved sensitivity also increases sensitivity to these effects.

A larger task, but also of high potential benefit, is an electronic redesign to perform automatic balancing of the stimulation current. This work would greatly reduce polarization effects.

Another path of research that may be of interest is the rejection of 'bad' measurements before or during the reconstruction, which may be an effective work-around for cases when electrode contact is poor.

In the medium term planning horizon, further investigation into tunnel detection is recommended. With a configurable array more research could be performed into tunnel detection performance as well as appropriate instrument geometry for this application. Further development of the underwater capabilities of EIT is also recommended, especially for salt-water environments.

It may be of interest to test the efficacy of EIT in arctic media such as snow, ice, or frozen soil. Objects may be detectable in these materials, and different layers of snowpack may also be detectable. It may be possible to determine the density and moisture content of terrain such as muskeg and permafrost, which may help determine if terrain is navigable. The best shape of electrodes for use in these materials may differ from the best shape for other media; the tapered shape used in soil is likely a good starting point for these investigations. If these conditions can be simulated in the lab it may be of interest to do preliminary lab assessments.

Another potential application of EIT is in clearing berms. Especially with a reconfigurable array, the exposed sides of a berm make it possible to collect better data on the medium, so mines and unexploded ordnance may be easily detectable.

A SCHEMATIC OF EIT ACQUISITION ELECTRONICS

Double-click the image below to open the schematic in Adobe Reader©.

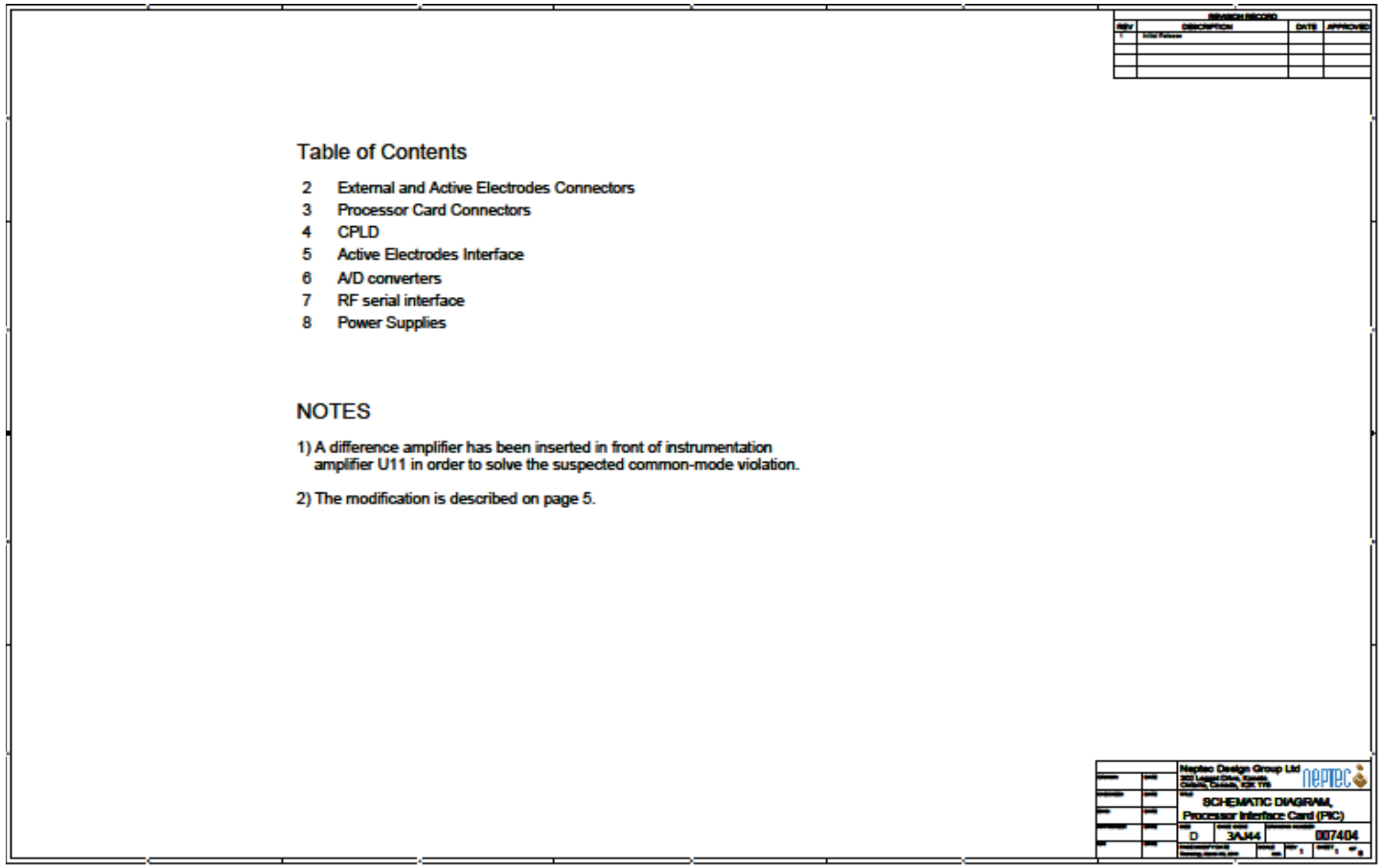

REVISION RECORD

REV	DESCRIPTION	DATE	APPROVED
1	Initial Release		

Table of Contents

NOTES

1) A difference amplifier has been inserted in front of instrumentation amplifier U11 in order to solve the suspected common-mode violation.

2) The modification is described on page 5.

Neptec Design Group Ltd
SCHEMATIC DIAGRAM,
Processor Interface Card (PIC)
D 3AJ44 007404

ANNEX B Calculation of SNR for Voltage offset Investigation

The signal-noise ratios stated in Section 5.5.4.2 were calculated from the acquired data using the following Matlab script. The

```
files = { '10oct06.mat', ...
          '10oct06_2.mat', ...
          '10oct06_3.mat', ...
          '10oct06_fliprec.mat', ...
          '10oct06_fliprec_2.mat', ...
          '10oct06_fliprec_3.mat', ...
          '10oct06_flipstim.mat', ...
          '10oct06_flipstim_2.mat', ...
          '10oct06_flipstim_3.mat', ...
          '10oct06_flipstimrec.mat', ...
          '10oct06_flipstimrec_2.mat', ...
          '10oct06_flipstimrec_3.mat'};

d=[];
for i=1:length(files);
   data=load(files{i});
   d(:,i) = abs(data.Vamplitude);
end

dm=[];
for i=1:3:length(files)
   dm = [dm, mean(d(:,i+(0:2)),2)];
end
plot(dm,'LineWidth',2);
hold on
set(gca,'ColorOrder',kron(get(gca,'ColorOrder'),[1;1;1]));
plot(d);
hold off
legend('original configurations', 'recorders flipped', 'stimulators flipped',
'both flipped')

sm = [];
for i=1:3:length(files)
   sm = [sm, std(d(:,i+(0:2)),0,2)];
end

mean(mean(dm,2)./std(dm,0,2))  %SNR of how flips differ from one another
% 330.9870
mean(mean(dm./sm))  %SNR of measurements in general
% 7534.2
```

ANNEX C Eidors Algorithm Variants

The EIDORS algorithm variants investigated in Section 5.2.1 are defined and developed here. The text is adapted from [3], which focuses on EIT for lung imaging applications. The theoretical development of the algorithm variants is independent of application, however, and therefore applies equally to the landmine and tunnel detection problem.

Our goal is to describe and quantify the impact of the choice of image reconstruction approaches on the reliability and accuracy of EIT measurements. First we review EIT image reconstruction algorithms and develop a taxonomy of approaches. A representative sample of algorithm choices is selected for evaluation. Next we develop an evaluation framework for algorithm performance based on relevant factors.

C-1. EIT image reconstruction

Time difference EIT (TD-EIT) seeks to reconstruct an image of the change in conductivity ($\Delta\sigma$) between $\hat{\mathbf{x}}$, between EIT measurements $\mathbf{v}$ and $\mathbf{v}_r$, where $\mathbf{v}$ represents the current frame of EIT measurements, while $\mathbf{v}_r$ is the reference measurement frame, and is typically calculated by averaging over times when conductivity distribution in the region of interest is stable. We use the notation ($\mathbf{m}$) for the conductivity change image (or model) $\mathbf{m}=\Delta\sigma$ and ($\mathbf{d}$) for time difference data. Since TD-EIT compares two sets of measurements, it is much less sensitive to uncertainties in electrode placement, thorax geometry and some hardware errors (such as gain variability between channels), than algorithms which attempt to reconstruct the absolute conductivity distribution [adler96b]. This paper considers only TD-EIT algorithms.

We consider to algorithms which are applicable to the most common case for which clinical and experimental thoracic EIT measurements have been made. Thus, we assume: 1) TD-EIT measurements; 2) placement of 16 EIT electrodes in a single plane around the thorax; and 3) measurement performed using the adjacent stimulation and measurement (the Sheffield protocol). We also assume reconstruction of images onto a circular domain, since this is common capability of all algorithms. Many TD-EIT algorithms have been proposed (see references of [adler09, lionheart04]). We organize the space of EIT algorithms as in Figure 93; first, algorithms are classified on the features used in the forward problem (and sensitivity matrix) and then on the inverse solution. Two main classes of image reconstruction procedures were chosen for analysis, based on backprojection, and sensitivity matrix (FEM) based solutions; the latter category is subdivided into regularization- and optimization-based methods. We review the formulation of each approach in the following subsections. Clearly, the possible combinations of algorithm variants are very large, and thus difficult to test. Instead, we define a "baseline" algorithm, $\mathbf{R}_0$represents the simplest approach, and consider modifications from it. For each variation, we define a default case (which is part of $\mathbf{R}_0$) and a variant case, which is tested in an algorithm.

We classify these algorithms, based on sensitivity matrix calculation and subsequent inversion, as "direct" EIT reconstruction algorithms, in order to distinguish from approaches such as level sets, monotonicity, or factorization [lionheart06], which do not directly use the model sensitivity. We do not evaluate such approaches, since they have seen little evaluation in thoracic EIT.

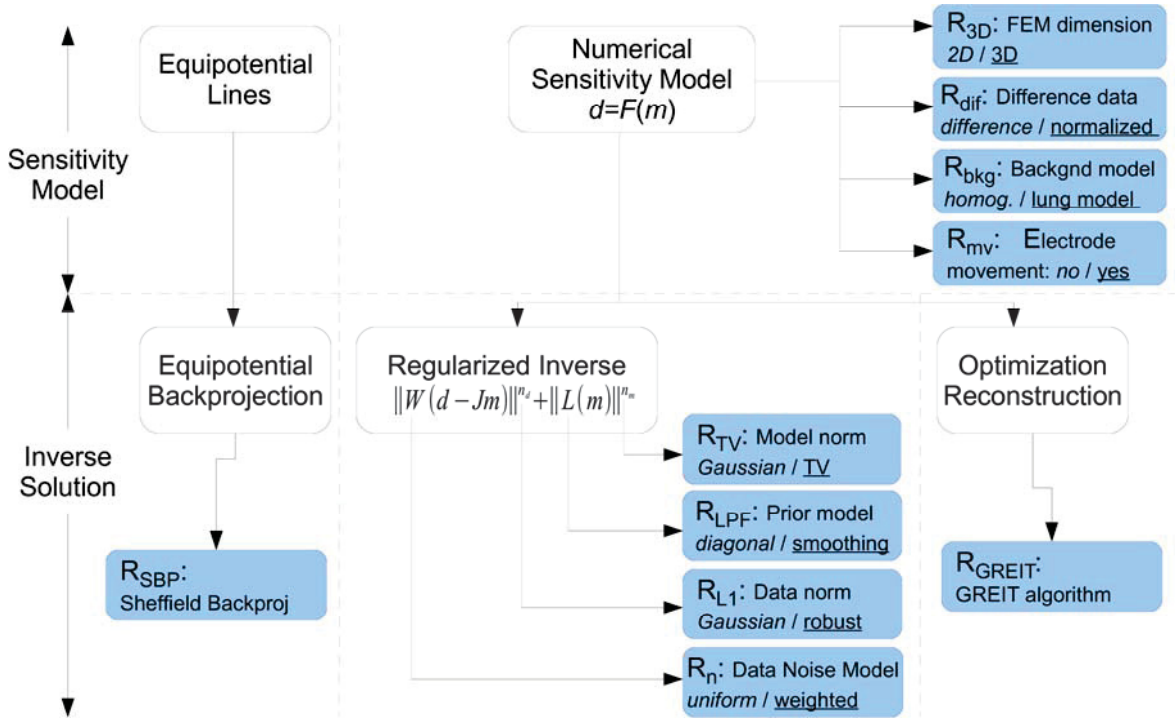

Figure 93. Taxonomy of direct EIT reconstruction algorithms, classified in terms of the selection of forward and inverse model parameters.

C-2. Backprojection Sensitivity Model (Sheffield Backproj)

This algorithm was not implemented for this contract.

C-3. Numerical Sensitivity Model

The forward model, $F(\cdot)$, in EIT simulates the measured data vector **d** for a given vector of model parameters **m**, as $\mathbf{d}=F_{\sigma_r}(\mathbf{m})$. The data vector, **d**, represents each measured voltage for each applied current pattern in a data *frame*; for the Sheffield stimulation protocol on 16 electrodes, this yields 16×13=208 measurements per frame, of which 104 are independent, due to reciprocity [plonsey63]. $F(\cdot)$ is typically based on a finite element model (FEM) and each parameter of the conductivity distribution is modelled in *m* as the piecewise constant conductivity on a tetrahedral element. The forward model is used to calculate a Jacobian, **J**, or sensitivity matrix, which describes the sensitivity of each data element to each model parameter.

$$[\mathbf{J}]_{i,j} = \frac{\partial [F_{\sigma_r}(\mathbf{m})]_i}{\partial [\mathbf{m}]_j}, \tag{1}$$

where the FEM estimate depends on the background conductivity, σ_r, around which the conductivity changes *m* occur. The following section discusses various approaches to numerical (forward) models (F), considering the *baseline* approach and its variants.

1. Model Dimension: *2D FEM* / 3D FEM.

   Since the medium of interest for landmine/tunnel applications is a 3D medium, the model must also be three-dimensional.

2. Difference data: *normalized diff. data* / diff. data

   TD-EIT defines difference data **d** in terms of the current, **v**, and reference, $\mathbf{v}_r$ measurements. The majority of experimental and clinical algorithms (including $\mathbf{R}_{SBP}$have used normalized difference imaging, where $[\mathbf{d}]_i=[\mathbf{v}-\mathbf{v}_r]_i/[\mathbf{v}_r]_i=[\mathbf{v}]_i/[\mathbf{v}_r]_i-1$. If difference imaging (without normalization) is used, then $\mathbf{d}=\mathbf{v}-\mathbf{v}_r$. By normalizing, small measurement values are scaled up, and have a larger impact on the reconstructed images. The baseline model uses a normalized difference data, while the variant model uses difference data (without normalization).

3. Conductivity background to model medium: *homogeneous* σ_r / lung σ_r

   TD-EIT assumes conductivity changes occur with respect to a reference conductivity, σ_r, which defines the sensitivity matrix, **J**. The most common choice for EIT algorithms is a homogeneous value for σ_r, which is a poor model for the thorax, in which the lungs are far less conductive than other tissues. For the landmine/tunnel application a homogeneous background is the appropriate medium model.

4. Model electrode movement: *static model* / elec. move.

   One key difficulty with thoracic EIT measurements is position uncertainty of the electrodes, in which the body surface moves during breathing and posture change. In the landmine/tunnel application the electrodes may be modelled as static.

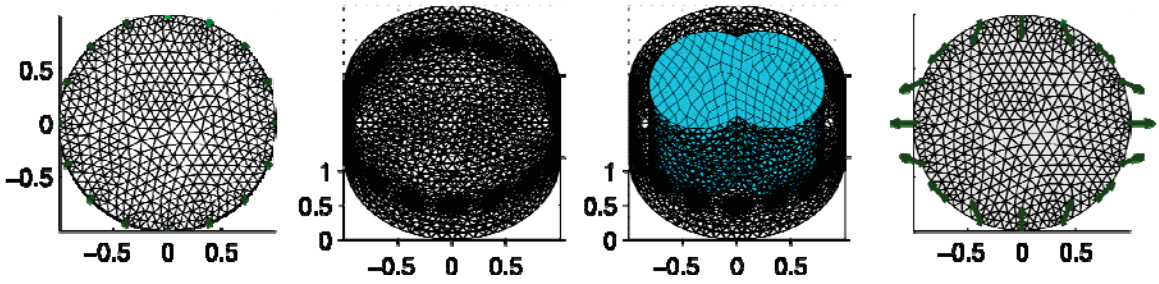

Figure 94. Finite element models used. Electrode nodes are indicated in green. A: 2D circular uniform FEM (R0) B: 3D cylindrical uniform FEM (R3D) C: 3D cylindrical FEM with lung regions (Rbkg) D: 2D circular uniform FEM with electrode movement (Rmv) (with arrows sh

C-4. Regularized EIT Reconstruction

The class of linear regularized EIT reconstruction algorithms seeks a solution $\hat{\mathbf{m}}$ which minimizes:

$$\hat{\mathbf{m}} = \underset{\mathbf{m}}{arg\,min} \left\| \mathbf{W}(\mathbf{d} - \mathbf{J}\mathbf{m}) \right\|_{n_d}^{n_d} + \left\| \lambda \mathbf{L}(\mathbf{m} - \mathbf{m}_0) \right\|_{n_m}^{n_m} \tag{3}$$

The first term, $|\mathbf{W}(\mathbf{d}-\mathbf{J}\mathbf{m})|_{n_d}^{n_d}$ is the data error term, the mismatch between the model and the measured data weighted by a matrix **W**, which models the measurement error on each data channel. The data error term has a norm $n_d \in [1,2]$. If a Gaussian model of data errors is used

(n_d=2), the data weighting matrix, **W**, is related to the channel noise covariance, Σ_n, by Σ_n^{-1}=$\mathbf{W}^t\mathbf{W}$. This formulation is also used to incorporate the structured noise due to electrode movement, Σ_n^* in (2). The second term, $|\mathbf{L}(\mathbf{m}-\mathbf{m}_0)|_{n_m}^{n_m}$ is a regularization term designed to address the ill-conditioning intrinsic to EIT; it serves as a penalty function which "discourages" unlikely (but otherwise feasible) solutions. It calculates the mismatch between the **m** and prior constraints on "likely" models. $\mathbf{m}_0$ is the prior mean and has always been set to zero for TD-EIT, since conductivity is as likely to increase as decrease. **L** implements a penalty for large changes or non-smooth conductivities. The model error term has a norm $n_m \in [1,2]$. λ controls the relative strength of data and model error terms, and is typically called the regularization hyperparameter. As λ increases, the solution matches more closely to the model, and becomes increasingly smooth. In order to adequately compare different algorithms, functionally equivalent values of λ are chosen. Many strategies to choose an appropriate value have been presented (see references of [graham06]). We choose the "Noise Figure" approach [adler96], in which λ is chosen such that the ratio in signal to noise ratio (SNR) from **d** to $\hat{\mathbf{m}}$ is required to be constant across algorithms. Since we have no control of the parameters of the SBP algorithm, all other algorithms are normalized to its value.

The most commonly studied case is for quadratic norms n_m=n_d=2, which has the advantage of modelling Gaussian error, and yielding a closed form, linear solution:

$$\hat{\mathbf{m}} = \left(\mathbf{J}^T\mathbf{W}^T\mathbf{W}\mathbf{J} + \lambda^2\mathbf{L}^T\mathbf{L}\right)^{-1}\mathbf{J}^T\mathbf{W}^T\mathbf{W}\mathbf{d} = \mathbf{R}\mathbf{y}, \qquad (4)$$

EIT algorithms of this form are known as one-step Gauss Newton solvers (GN) [cheney90]. One important advantage is that image reconstruction can be expressed as matrix multiplication by **R**; since **R** may be pre-calculated, reconstruction is rapid and may be implemented in real-time. If either n_m or n_d are not quadratic, image reconstruction must be formulated iteratively.

In general, regularized EIT imaging reconstruction techniques are popular due to their flexibility to represent arbitrary body geometry, measurement configurations, and mathematical models of the conductivity distribution. Many papers have used the basic regularized formulation, and have explored the choices of parameter values. In this paper, the baseline reconstruction algorithm, $\mathbf{R}_0$, follows an early widely used regularized approach, NOSER[cheney90], which makes the following parameter choices: it is quadratic, n_m=n_d=2, the data noise is identical on each channel **W=I**, and the regularization matrix, **L**, is diagonal such that, diag$\mathbf{L}^T\mathbf{L}$=diag$\mathbf{J}^T\mathbf{J}$, which implies the assumption that inter-element correlations are zero. The following section discusses various approaches to regularized image reconstruction (I), considering the *baseline* approach and its variants.

1. Data noise model (**W**): *uniform* / weighted.

   The most common approach is to "trust" all EIT data equally, and thus to model each channel with equal, uniform noise (**W=I**). It is not necessary to set the actual noise intensity, since the data to model noise trade-off is set by the hyperparameter, λ. In practice, however, EIT noise can vary considerably between data channels, most likely due to variability in electrode contact quality. Such variations in data quality can be addressed by decreasing **W** on channels with larger noise. One practical approach to setting an appropriate **W** is to calculate a reciprocity error[hartinger09] (the difference between data values that should be equal by reciprocity[plonsey63]) and to use this value

to scale **W**. Clearly, the value of modelling data noise depends on the measurement quality; we consider the EIT data in this study to be representative of relatively good measurements. The baseline model sets **W=I**, and the variant model sets **W** using the reciprocity error approach [hartinger09], where the parameter $\tau=10^{-5}$, such that the average data weighting was 0.66 (compared to 1.0 when no weighting is used).

2. Data norm (n_d): *Gaussian, n_d=2* / Robust, n_d=1.

   As mentioned, a Gaussian (n_d=n=m=2) model and data norms allows calculating of a linear matrix inverse. One disadvantage of this formulation is that it emphasizes larger errors (since the effect of an error is squared). One approach to address such errors is the use of a n_d=1 data norm. While this has been recently proposed in medical EIT[borsic09], it has been called “robust error norms" in the geophysical EIT literature. The baseline model uses a Gaussian data norm n_d=2, while the variant uses n_d=1 using the formulation of [borsic09].

3. Prior model (**W**): *diagonal* / smoothing.

   The regularization matrix, **L**, is chosen such that the term can penalize unlikely solutions. The NOSER regularization matrix is diagonal, and thus penalizes large image amplitudes. Several studies have suggested that a better prior model is a smooth, rather than simply low amplitude distribution [adle96, vauhkonen98, polydorides02]. To achieve such smoothing, **L** is designed to penalize non-smooth **m**, imposing a filter across nearby model elements. We choose a representative spatial smoothing **L** using the approach of [adler96] in which a high pass spatial Gaussian filter is calculated designed so spatial wavelengths below 10% of the medium diameter are penalized. One key difference between an amplitude and a smoothing filter is its behaviour as a function of model element density. As density increases, amplitude penalties tend to show a more “speckled” pattern of noise, since element penalties are independent. The baseline model sets **L** to penalize image amplitude [cheney90], and the variant model uses the spatial high pass filter[adler96].

4. Model norm (**W**): *Gaussian* / Total Variation.

   One disadvantage of a Gaussian (n_m=2) model norm is that it blurs edges in images, which is physiologically unrealistic, since organ boundaries are anatomically well-defined. This blurring can be addressed using the Total Variation (TV) formulation [borsic10], with n_m=1. While TV produces sharper images, it is still unknown whether it is robust in the context of EIT data errors. The baseline model uses a Gaussian model n_m=2, while the variant uses implements TV n_m=1 using the formulation of [borsic10, borsic09].

C-5. Optimization Based EIT Reconstruction (GREIT)

This algorithm was not implemented for this contract.

C-6. References

[adler09] A. Adler, J.H. Arnold, R. Bayford, A. Borsic, B.H. Brown, P. Dixon, T. J.C. Faes, I. Frerichs, H. Gagnon, Y. Gärber, B. Grychtol, G. Hahn, W.R.B. Lionheart, A. Malik, R.P. Patterson, J. Stocks, A. Tizzard, N. Weiler, G.K. Wolf “GREIT: a unified approach to 2D linear EIT reconstruction of lung images" Physiol. Meas., 30:S35–S55, 2009

[adler96b] A. Adler, R. Guardo, Y. Berthiaume “Impedance Imaging of Lung Ventilation: Do we need to account for Chest Expansion? " IEEE T. Biomed. Eng., 43:414–421, 1996.

[borsic10] A. Borsic, B.M. Graham, A. Adler, W.R. B. Lionheart, “Total Variation Regularization in Electrical Impedance Tomography", IEEE T Med Imag. 29:44–54 2010.

[borsic09] A. Borsic, A. Adler “A Primal Dual–Interior Point Framework for EIT Reconstruction and Regularization with 1-Norm and 2-Norm" Conf. EIT, Manchester, UK, 16-19 June 2009

[cheney90] M. Cheney, D. Isaacson, J.C. Newell, S. Simske, J. Goble, “NOSER: An algorithm for solving the inverse conductivity problem", Int. J. Imaging Systems and Technol, 2:66–-75, 1990.

[graham06] B. Graham, A. Adler “Objective selection of the hyperparameter for EIT", Physiol. Meas. 27:S65–S79, 2006

[hartinger09] A.E. Hartinger, R. Guardo, A. Adler, and H. Gagnon “Real-time management of faulty electrodes in electrical impedance tomography" IEEE T. Biomed. Eng. 56:369–377, 2009

[lionheart04] W.R.B. Lionheart, “EIT reconstruction algorithms: pitfalls, challenges and recent developments," Physiol Meas, vol. 25, pp. 125–42, Feb 2004.

[lionheart06] W.R.B. Lionheart, 2006

[polydorides02] N. Polydorides, W.R.B. Lionheart, “A Matlab toolkit for three-dimensional electrical impedance tomography: A contribution to the Electrical Impedance and Difuse Optical Reconstruction Software project", Meas. Sci. Technol., 13 1871–83, 2002.

[vauhkonen98] M. Vauhkonen, D. Vadàsz, P.A. Karjalainen, E. Somersalo, J.P. Kaipio , “Tikhonov Regularization and prior information in electrical impedance tomography", IEEE T. Med. Imaging 17 285–93, 1998.

ANNEX D Sensitivity Analysis

This appendix provides a theoretical development of sensitivity (i.e. distinguishability) analysis. It is excerpted from [4].

D-1. Distinguishability Measures

Figure 95 outlines our conceptual formulation of distinguishability measurement. Two configurations of the medium are possible, H_0 and H_1, with conductivity distributions σ_0 and σ_1, which differ by a change in conductivity $\Delta\sigma=\sigma_1-\sigma_0$ in a region of interest (ROI). Based on EIT measurements, we attempt to distinguish these configurations to test whether the configuration is H_0 or H_1. Clearly, a system with good distinguishability will make this determination accurately, while a system with poor distinguishability with perform this task with a higher probability of error. This formulation is based on previous models (Isaacson, 1986; Eyüboğlu and Pilkington, 1993; and Lionheart 2001)

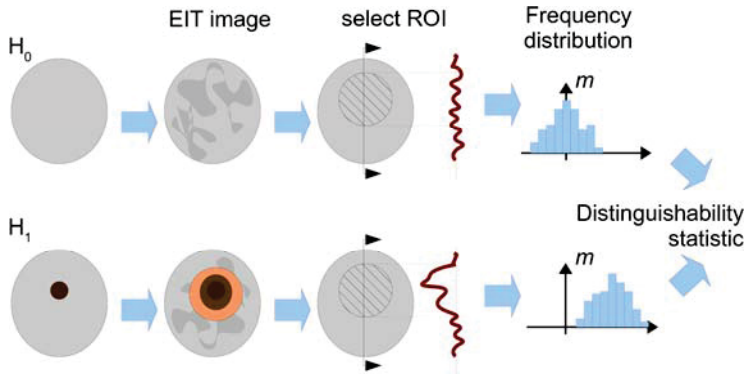

Figure 95. Conceptual diagram of distinguishability. Images H0 and H1 with conductivity distributions σ0 and σ1 are to be distinguished based on their EIT images. Over a large sequence of tests of each case, image are generated and the distribution of a measurement

We consider an EIT system which attaches N_e electrodes to the boundary, $\partial\Omega$ of an object Ω. During stimulation pattern k, a data set $\mathbf{d}^k$ is acquired by applying a current vector $\mathbf{c}^k$ to the electrodes, where each element j, $[\mathbf{c}^k]_j$, represents the phasor current amplitude into electrode j. By Kirchhoff's current law, $\sum [\mathbf{c}^k]_j=0$. A pair drive stimulation of current I at electrodes c_+, c_- will thus have $[\mathbf{c}^k]_{c_+}=+I$, $[\mathbf{c}^k]_{c_-}=-I$ and $[\mathbf{c}^k]=0$ elsewhere.

Such stimulation produces a distribution of voltage $\mathbf{v}^k=\mathbf{T}(\sigma)\mathbf{c}^k$ at the electrodes, where the voltage at electrode j is $[\mathbf{v}^k]_j$, and $\mathbf{T}(\sigma)$ is the transfer impedance matrix which depends on the (possibly complex) conductivity distribution σ in Ω. Most EIT systems do not directly measure voltage, but rather use differential instrumentation amplifiers to measure differences between electrode pairs. The measured data set, $\mathbf{d}^k$ is related to the electrode voltages by a

measurement protocol **M**. If the i^{th} measurement attaches the differential amplifier to electrodes m_+,m_-, then $[\mathbf{M}]_{i,m_+}=+G$, $[\mathbf{M}]_{i,m_-}=-G$ and the other values on row i are zero (G represents the channel gain). For systems which do not measure at stimulation electrodes, **M** is zero in columns c_+,c_-.

To the measured data, an EIT system adds a certain level of random noise $\mathbf{n}^k$, which we characterize as zero-mean and Gaussian with co-variance $\mathbf{\Sigma}_k$. This characterization is justified as follows: the noise has zero-mean because any average bias can be measured and incorporated into the EIT model. The assumption of Gaussian noise is designed to make the statistical computations easier; however, there is some evidence to indicate that EIT noise is not Gaussian (Hahn 2008), and specifically, large errors occur far more often than would be predicted by a Gaussian statistics. Noise samples may be correlated between measurements due to the design of amplifier and analog switch circuitry, giving non-zero off diagonal values in $\mathbf{\Sigma}_k$:

$$\mathbf{d}_k = \mathbf{M}_k\mathbf{T}(\mathbf{s})\mathbf{c}_k + \mathbf{n}_k. \qquad (1)$$

The scenarios to distinguish, H_0 and H_1 with conductivity distributions σ_0 and σ_1, yield EIT measurements which differ for the same $\mathbf{c}_k$,

$$\Delta\bar{\mathbf{d}}_k = \bar{\mathbf{d}}_k(\boldsymbol{\sigma}_1) - \bar{\mathbf{d}}_k(\boldsymbol{\sigma}_0) = \mathbf{M}_k(\mathbf{T}(\boldsymbol{\sigma}_1) - \mathbf{T}(\boldsymbol{\sigma}_0))\mathbf{c}_k = \mathbf{T}_\Delta\mathbf{c}_k \qquad (2)$$

where the change in transfer impedance, $\mathbf{T}_\Delta=\mathbf{T}(\sigma_1)-\mathbf{T}(\sigma_0)$, may be determined experimentally or calculated from finite element model (FEM) or analytic techniques.

D-2. Distinguishability

From the EIT images in Figure 95, we wish to distinguish H_1 from H_0 using a measurement m of the average EIT image in the ROI. The null hypothesis H_0 may be rejected with a probability given by the z-score

$$z = \frac{\Delta\bar{m}}{\sigma_m} \qquad (3)$$

where $\Delta\bar{m}=\bar{m}_1-\bar{m}_2$ is the difference between mean m in the scenarios and σ_m is the standard deviation. The use of normal statistics is appropriate, as the noise for a given EIT system can be well characterized and will be equal under both scenarios. As z increases, the probability of error decreases corresponding to the increased capability of EIT distinguish. Note that z may also be interpreted as SNR.

An EIT system measures a set or *frame* of data, **d**, by applying, in sequence, N_c current patterns and measuring the output, yielding a column concatenated data set $\mathbf{d}=[\mathbf{d}_1^t|\mathbf{d}_2^t|\cdots|\mathbf{d}_{N_c}^t]^t$. This EIT system is characterized by $F(\cdot)$ where

$$\mathbf{d} = F(\boldsymbol{\sigma}) + \mathbf{n} \qquad (4)$$

where noise, **n** has zero mean and a block diagonal covariance **Σ** with blocks $\mathbf{\Sigma}_k$, $1\le k\le N_c$.

We assume that the distinguishability problem consists of a small Δσ for which a linearized reconstruction is valid. Difference measurements $\Delta\mathbf{d}=\mathbf{d}-\mathbf{d}_0$ are made between the current (unknown) distribution and a reference distribution known to match H_0. We further assume that data $\mathbf{d}_0$ represent the average of an extended calibration measurement, so that the noise contribution is exclusively due to **d**. Linearizing around σ_0, we express

$$\Delta\mathbf{d} = \mathbf{J}\Delta\boldsymbol{\sigma} + \mathbf{n}, \tag{5}$$

where **J** is the Jacobian (sensitivity) defined as

$$[\mathbf{J}]_{i,j} = \left.\frac{\partial F_i(\boldsymbol{\sigma})}{\partial \sigma_j}\right|_{\boldsymbol{\sigma}=\boldsymbol{\sigma}_0} \tag{6}$$

This linearization is appropriate because the distinguishability limits for most EIT systems, correspond to relatively small changes in conductivity.

From measurements Δ**d**, an impedance change image estimate $\Delta\hat{\sigma}$ is reconstructed from a linearized difference EIT reconstruction algorithm as $\Delta\hat{\sigma}=\mathbf{R}\Delta\mathbf{d}$, defined from

$$\Delta\hat{\boldsymbol{\sigma}} = \underset{\Delta\boldsymbol{\sigma}}{arg\ min} \|\Delta\mathbf{d} - \mathbf{J}\Delta\boldsymbol{\sigma}\|_{\boldsymbol{\Sigma}^{-1}} + P(\mathbf{x}) \tag{7}$$

where *arg min*$_{\Delta\sigma}$ selects the value of the parameter (Δσ) which minimizes the expression which follows, and $P(\cdot)$ represents a penalty or regularization term. For quadratic $P(\cdot)$, image reconstruction may be represented as multiplication by a reconstruction matrix. Such linear reconstruction matrix can also describe the majority of difference EIT reconstruction algorithms, such as the Sheffield Backprojection (Barber and Seagar, 1987) and many regularization based schemes.

In general, we are interested in investigating the image output within a ROI of area A_R, defined by a vector τ_R, of size $N\times 1$ in which each element $[\mathbf{I}_R]_i$ is the area fraction of element in the ROI, and is zero outside the ROI. Based on the ROI, we define the measurement *m* as the area weighted average impedance change in the ROI ($\Delta\bar{\sigma}_R$):

$$m = \boldsymbol{\Theta}_R^t\Delta\hat{\boldsymbol{\sigma}} = \boldsymbol{\Theta}_R^t\mathbf{R}\Delta\mathbf{d} = \mathbf{R}_R\Delta\mathbf{d} = A_R\Delta\bar{\sigma}_R \tag{8}$$

where $\mathbf{R}_R=\tau_R^t\mathbf{R}$ is the reconstruction matrix of the scalar measurement *m*; this scalar reconstruction makes the problem not ill-posed and no regularization term $P(\cdot)$ is required, and the maximum likelihood solution matrix, $\mathbf{R}_R$, is given by:

$$\mathbf{R}_R = \left(\mathbf{J}_R^t\boldsymbol{\Sigma}^{-1}\mathbf{J}_R\right)^{-1}\mathbf{J}_R^t\boldsymbol{\Sigma}^{-1} \tag{9}$$

where $\mathbf{J}_R=\frac{1}{A_R}\mathbf{J}\tau_R$, since we require $\Delta\mathbf{d}=\mathbf{J}_R m$ for changes in the ROI.

This result shows that the distinguishability is a product of the target size and amplitude (*m*), the measurement strategy (**J**) and the inverse of the noise amplitude (**Σ**).

D-3. Distinguishability of Current Patterns

This formulation may be extended to clarify the effect of the choice of stimulation and measurement patterns on the SNR and *z*. Equation 14 may be separated into the components from each stimulation pattern *k*.

$$z^2 = \|\Delta \mathbf{d}\|^2_{\mathbf{\Sigma}_n^{-1}} = \sum_k \|\Delta \mathbf{d}_k\|^2_{\mathbf{\Sigma}_k^{-1}} = \sum_k \|\mathbf{M}_k \mathbf{T}_\Delta \mathbf{c}\|^2_{\mathbf{\Sigma}_k^{-1}} \quad (14)$$

As mentioned, most EIT systems have independent noise, which is often equal for all channels. Some systems vary the gain for each measurement to compensate for the large dynamic range (i.e. Sheffield Mk I, (Brown and Seagar, 1987)) or explicitly filter measurements (i.e. Hartinger, 2007). In general, a noise-normalized measurement sequence may be calculated as $\hat{\mathbf{M}}_k = \mathbf{S}_k^{-\frac{1}{2}} \mathbf{V}_k^t \mathbf{M}_k$ based on the SVD, $\mathbf{\Sigma}_k = \mathbf{V}_k \mathbf{S}_k \mathbf{V}_k^t$. Thus

$$z^2 = \sum_k \|\hat{\mathbf{M}}_k \mathbf{T}_\Delta \mathbf{c}_k\|^2 = \sum_k \sum_j (\hat{\mathbf{m}}_{k,j} \mathbf{T}_\Delta \mathbf{c}_k)^2 \quad (15)$$

where $\hat{\mathbf{m}}_{k,j}$ is the j^{th} row of $\hat{\mathbf{M}}_k$, which is measurement at the k^{th} of current pattern.

Equation 15 shows how measurements combine to produce the total system distinguishability. The signals with the highest SNR have the greatest impact, while noisier signals contribute little to the system performance. In most EIT systems, noise is independent and equal across channels, and $\hat{\mathbf{M}} = \sigma^{-1}\mathbf{M}$. It is also worth noting that, since $\mathbf{T}_\Delta$ is symmetric, measurements and current patterns play an equivalent role in calculation of distinguishability. This function may be regarded as a compliment to an analysis of the information content of EIT signals (Adler and Lionheart, 2008).

D-4. References

Adler A, Lionheart WR, Uses and abuses of EIDORS: An extensible software base for EIT, *Physiol. Meas.* 27:S25-S42, 2006.

Adler A, Youmaran R, Lionheart WRB, A measure of the information content of EIT data *Physiol Meas*, 29:S101–S109, 2008.

Barber D C and Seagar A D 1987 Fast reconstruction of resistance images, *Clin. Phys. Physiol. Meas.* 8 47.

Brown B H and Seagar A D 1987 The Sheffield data collection system, *Clin. Phys. Physiol. Meas*. 8, Suppl. A, 91-97.

Eyüboğlu BM and Pilkington T C 1993 Comment on distinguishability in electrical-impedance imaging *IEEE Trans. Biomed. Eng.* 40 1328–1330.

Hahn G, Just A, Dittmar J, Hellige G 2008 Systematic errors of EIT systems determined by easily-scalable resistive phantoms *Physiol. Meas.* 29 S163-72.

Hartinger AE, Gagnon H, Guardo R 2007 Accounting for Hardware Imperfections in EIT Image Reconstruction Algorithms *Physiol. Meas.* 28(7), p. S13-S27.

IEC 60601-1:2005, “Medical Electrical Equipment Part 1: General Requirements for Basic Safety and Essential Performance", *Brussels: International Electrotechnical Commission*, 2005.

Isaacson D 1986, Distinguishability of conductivities by electric current computed tomography *IEEE T Med Imaging* 5:91-95.

Lionheart WR, Kaipio J, McLeod CN 2001, Generalized optimal current patterns and electrical safety in EIT *Physiol. Meas.* 22 85-90.

ANNEX E Accurate Modelling of Electrode Contact

Preliminary work was done to produce more accurate models, in particular of electrode contact. This appendix provides an informal summary of the work performed.

The key result is the following image:

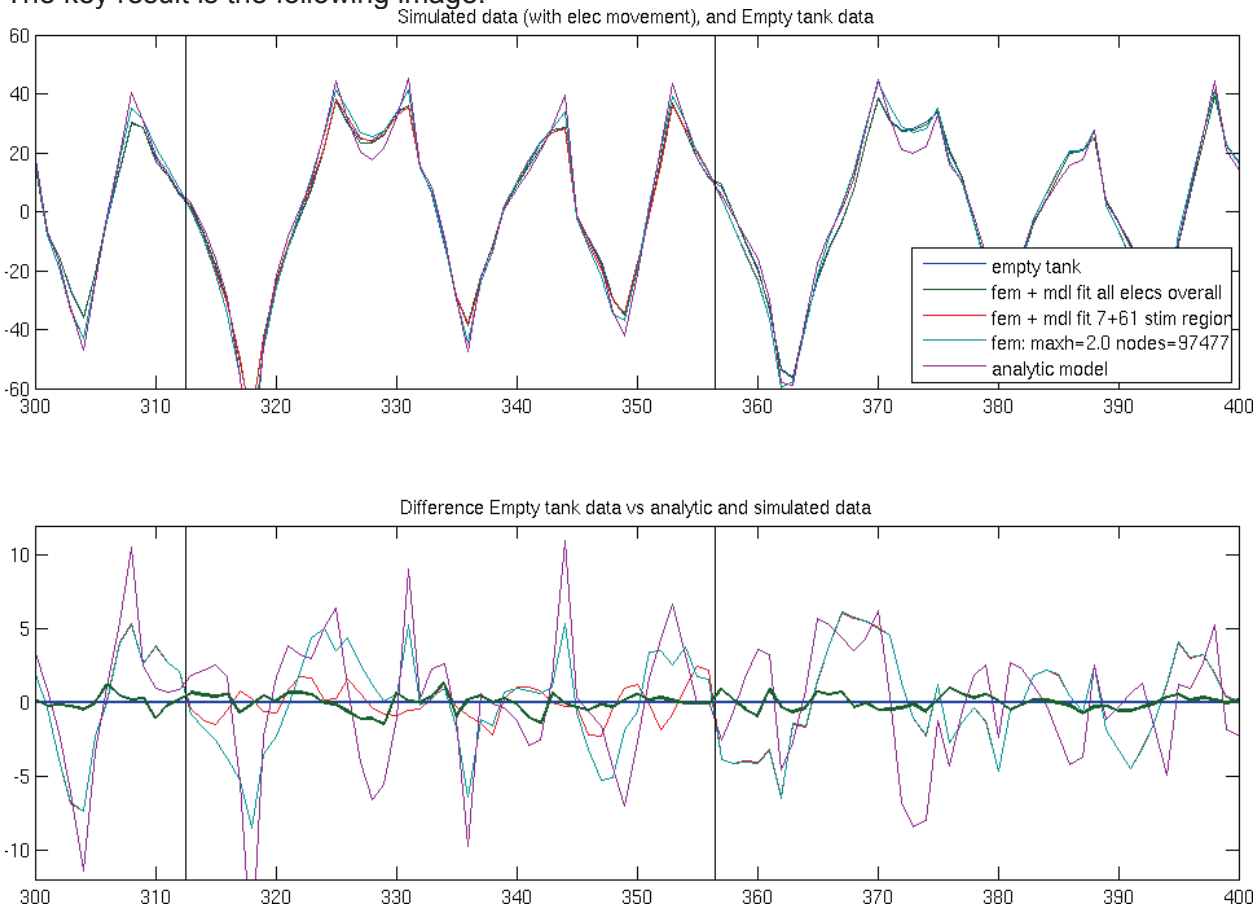

The top figure shows absolute measurement values from several sources, including one scan of an empty tank, the predicted measurements from the analytic model, and the predicted measurements from several versions of the Finite-Element Model (FEM). The bottom figure shows the same data with the empty tank data subtracted, so the closeness of each model to the empty tank can be seen. The best FEM result is shown in bold green and is substantially better than the original (analytic) model in magenta.

This shows the various stages of FEM modelling to try to improve the model of the data to the empty tank case. The idea is that by carefully modelling the electrodes and then making small displacements in each electrode (to fit it to the local conditions) we are able to dramatically improve the fit to the raw data.

The table shows that the overall fit (RMSd = RMS fit to the difference, AAVd = average abs value difference) doesn't improve much from analytic to FEM, but it does when you add electrode fitting.

empty tank: RMS=26.342 AAV=22.208 RMSd= 0.000 AAVd= 0.000
fem + mdl fit all elecs overall: RMS=26.295 AAV=22.145 RMSd= 0.511 AAVd= 0.409
fem: maxh=2.0 nodes=97477: RMS=26.590 AAV=22.266 RMSd= 3.621 AAVd= 3.005
analytic model: RMS=26.723 AAV=21.575 RMSd= 4.496 AAVd= 3.559

So we can conclude that this fit reduces model misfit by 4.496/0.511 = 8.7984 times

Overall misfit goes from [4.496, 0.511]/26.342 = 0.1707 0.0194 => 17% to 2%.

The first step in achieving this result was modelling of electrode shape, as summarized in the following images.

Show Electrode. Only on outside

Tank electrode shapes

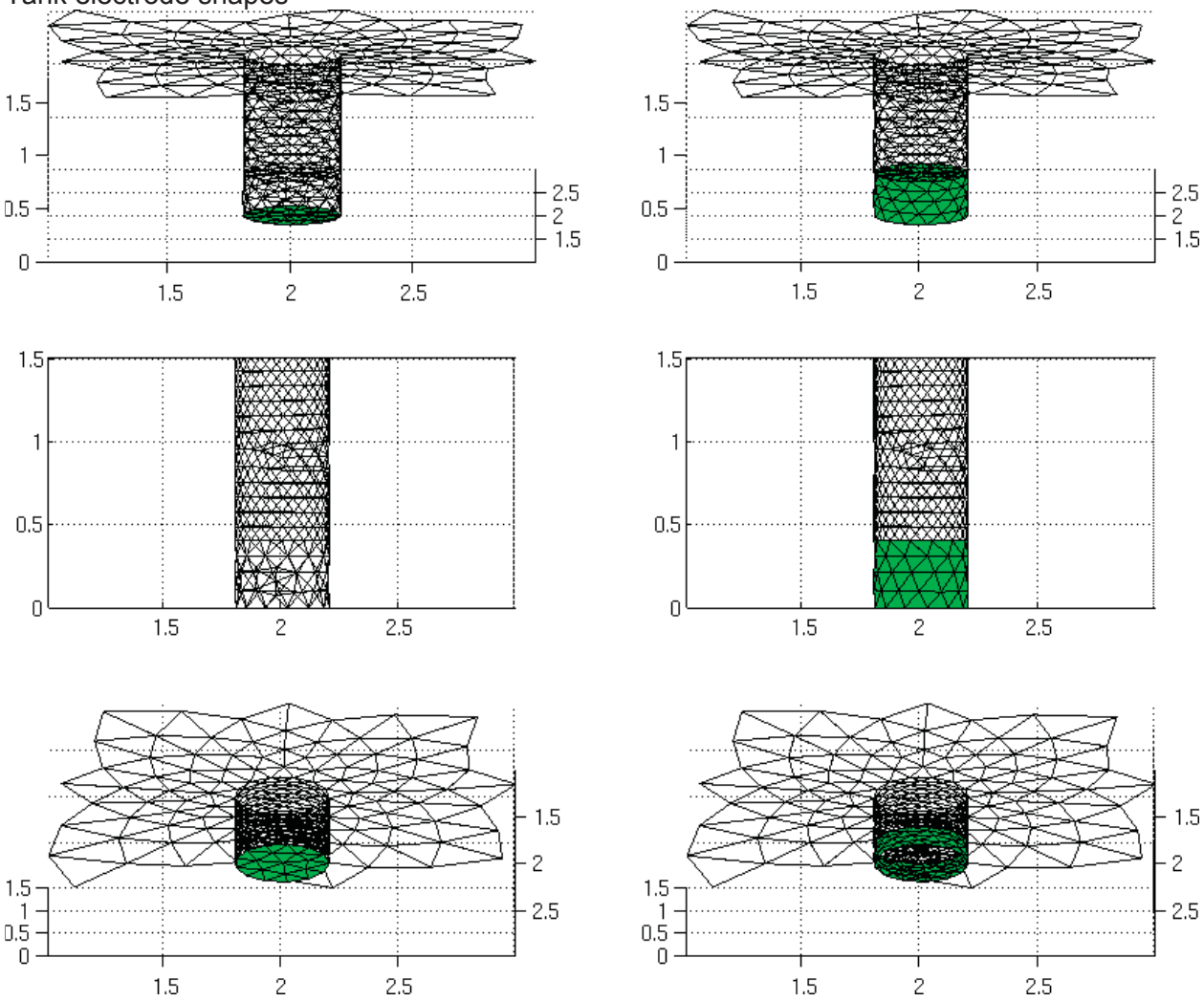

Next we need both the top and bottom of the electrode shape

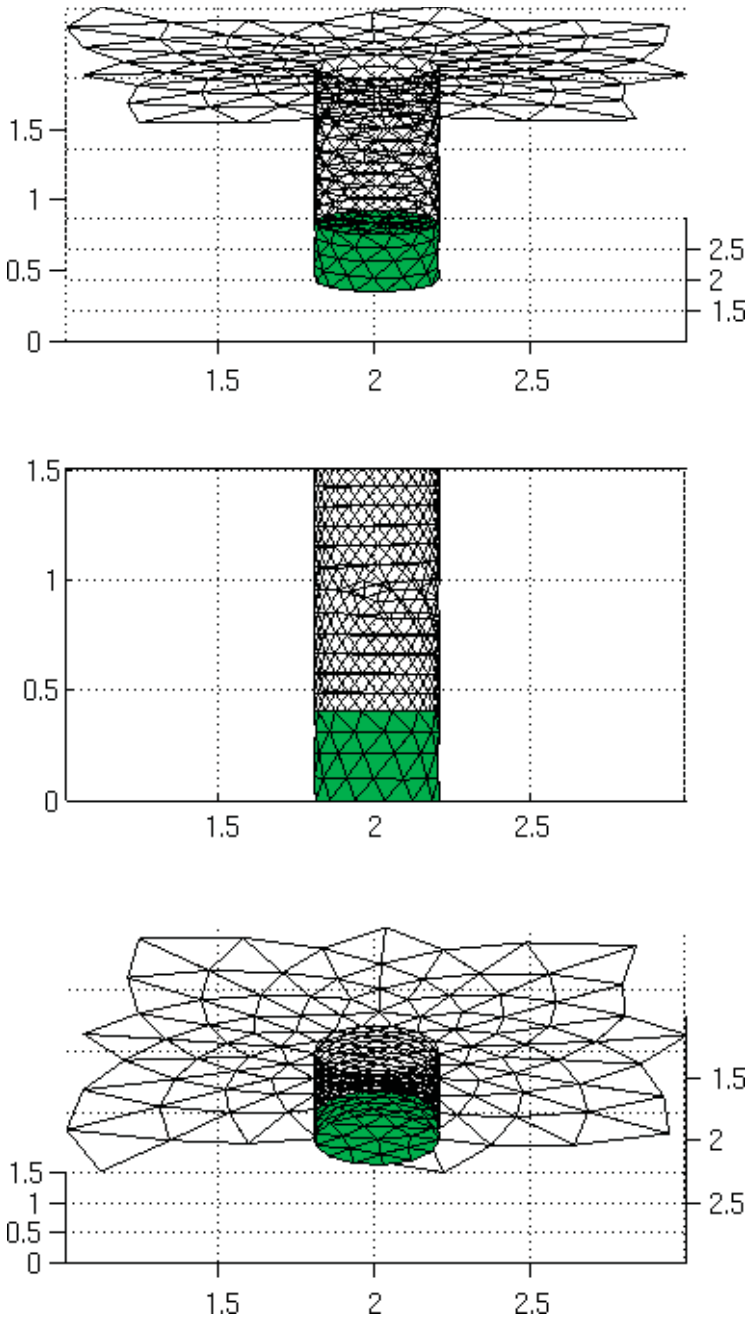

The following figures show measurements from the analytical model, the FEM, an empty tank scan (“may19”), and two scans with an object in the tank. They show the effects of model variations as compared to the effects of a signal.

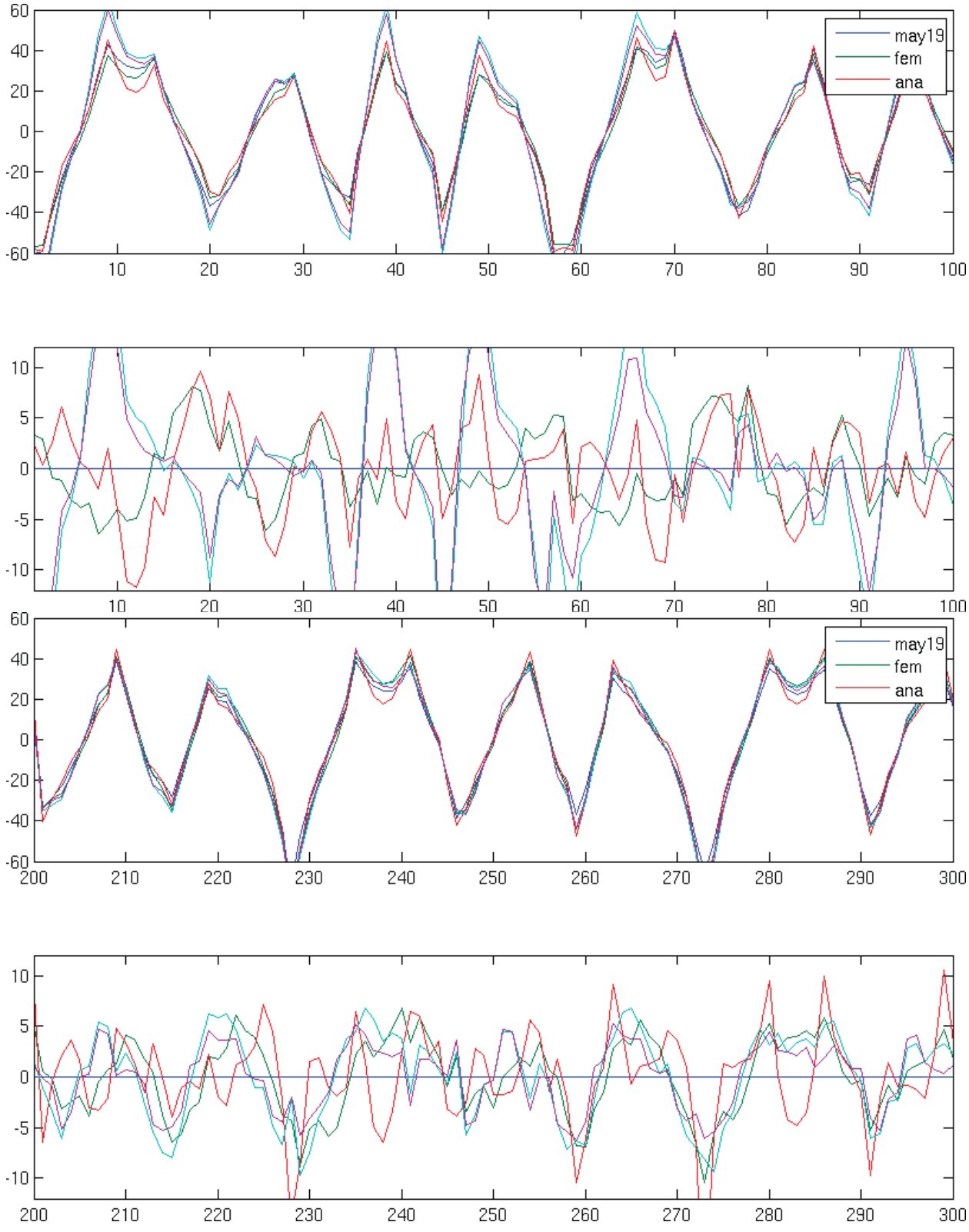
may19
fem
ana
may19
fem
ana

The next investigation was whether model accuracy depends on the density of the FEM. Higher density models are more detailed but require greater computation time in processing. It was found that density does not greatly affect model accuracy, as shown in the figures below.

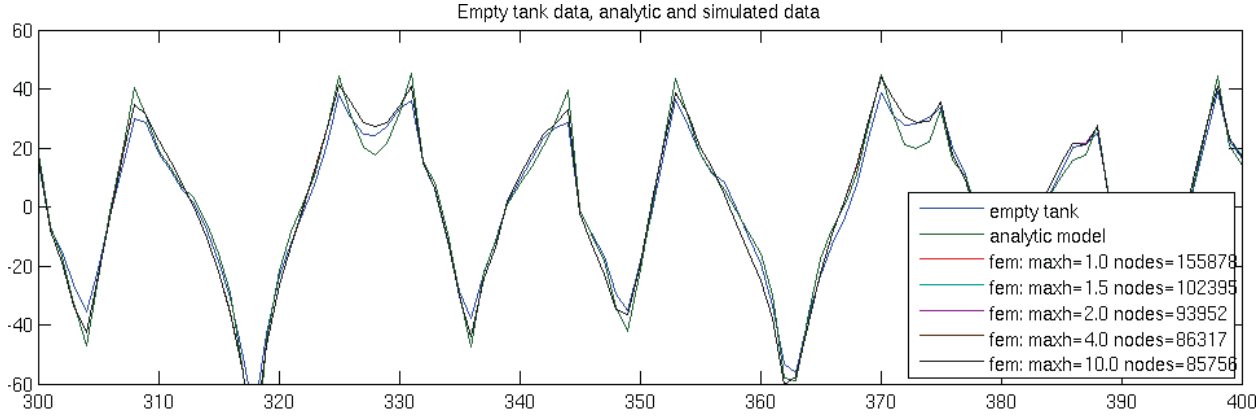

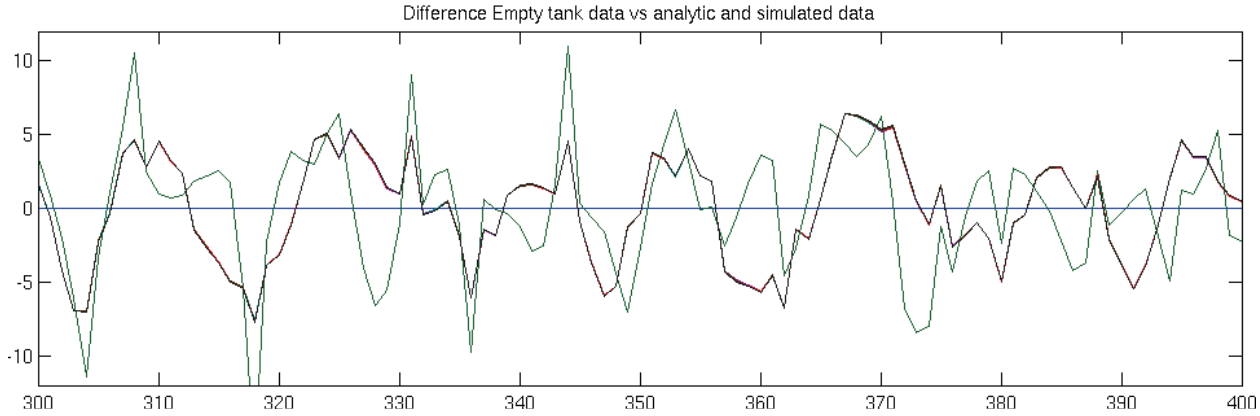

Next, the depth of the modelled tank was varied to determine effect on model accuracy. This model parameter does affect modelling accuracy substantially, with higher depth values giving more accurate models. See figures below.

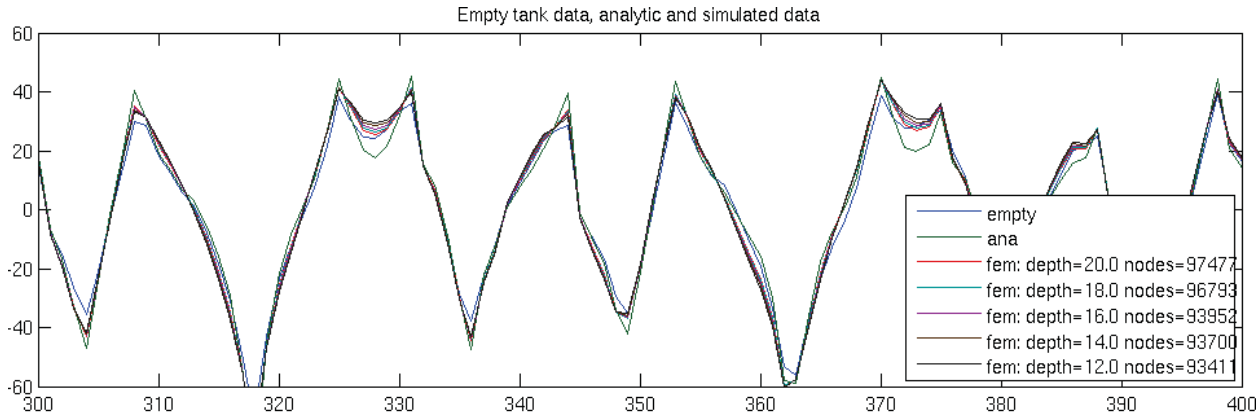

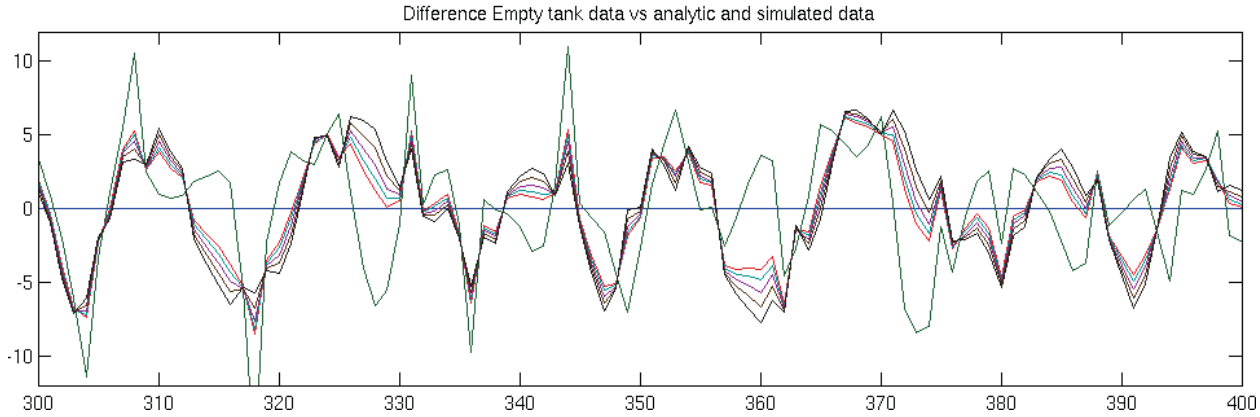

Finally the physical positions of the electrodes were varied in the model. This modelling exercise is not intended to model true imperfections in the physical instrument so much as to use modelled physical location to compensate for spatial variation in contact quality. Soil contact quality may be stronger on one side of an electrode, for example, because of the randomly placed air gaps and spaces within the soil. By “moving” the electrodes these asymmetries can be compensated for. The figures below show the effects of moving electrode 7 in x, y, and z.

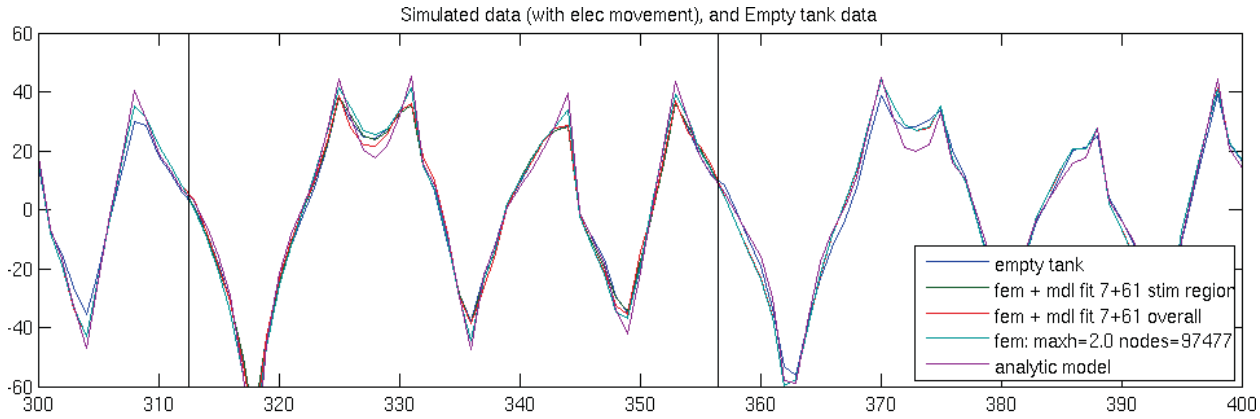

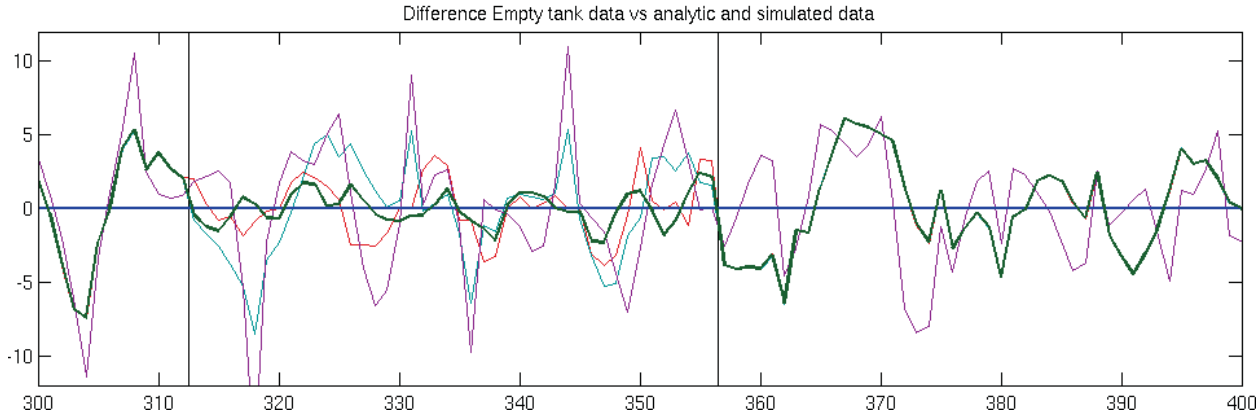

The end result of this preliminary study shows that these combined improvements greatly reduce the error between the model and the true empty-tank data, as shown below. The figures show the empty tank data compared to the analytic model and several variations on the FEM model. As shown in the bottom plot (with scan data subtracted so values close to zero are low-error), the analytic model (magenta) has much greater error than the best FEM model (bold green). This preliminary investigation suggests that model improvements may improve reconstruction.

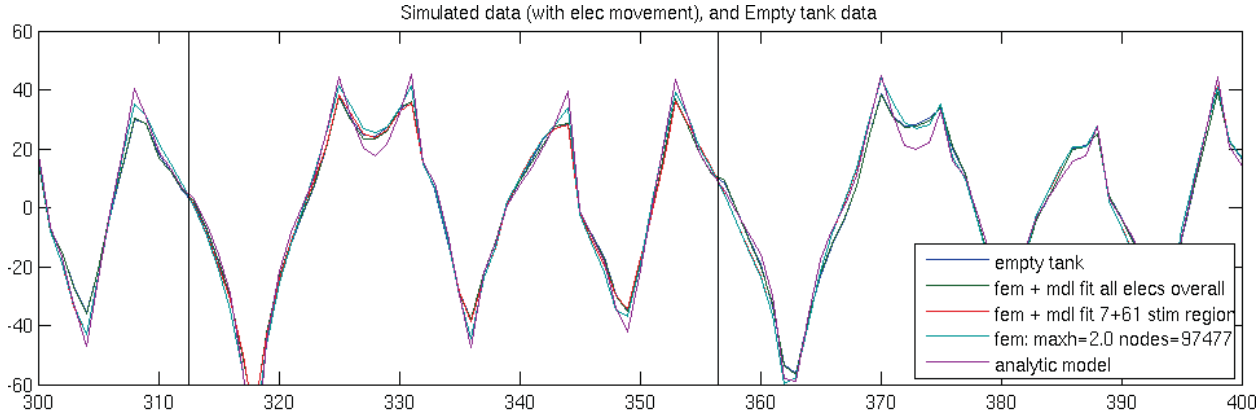
Simulated data (with elec movement), and Empty tank data
60
40
20
0
-20
-40
-60
300
310
320
330
340
350
360
370
380
390
400
empty tank
fem + mdl fit all elecs overall
fem + mdl fit 7+61 stim region
fem: maxh=2.0 nodes=97477
analytic model

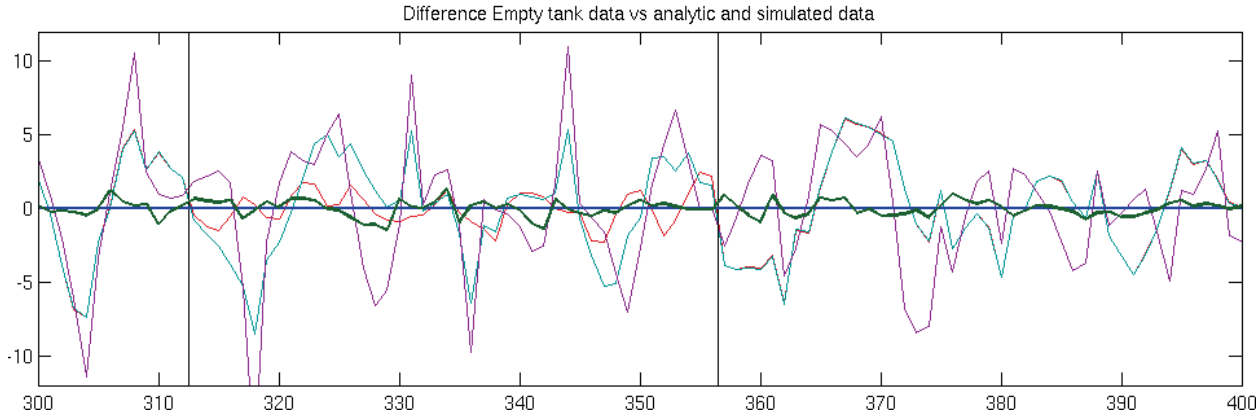
Difference Empty tank data vs analytic and simulated data
10
5
0
-5
-10
300
310
320
330
340
350
360
370
380
390
400

DOCUMENT CONTROL DATA

(Security classification of title, body of abstract and indexing annotation must be entered when the overall document is classified)

1. ORIGINATOR (the name and address of the organization preparing the document. Organizations for who the document was prepared, e.g. Establishment sponsoring a contractor's report, or tasking agency, are entered in Section 8.)

Neptec Design Group
320 Legget Drive
Kanata, ON K2K 1Y5

2. SECURITY CLASSIFICATION
(overall security classification of the document, including special warning terms if applicable)

UNCLASSIFIED
(NON-CONTROLLED GOODS)
DMC of A
REVIEWED: GCEC JUNE 2010

3. TITLE (the complete document title as indicated on the title page. Its classification should be indicated by the appropriate abbreviation (S, C or U) in parentheses after the title).

Electrical impedance imaging study; Final Report

4. AUTHORS (Last name, first name, middle initial. If military, show rank, e.g. Doe, Maj. John E.)

Bouchette, G.: Neptec Design Group

5. DATE OF PUBLICATION (month and year of publication of document)

March 2012

6a. NO. OF PAGES (total containing information, include Annexes, Appendices, etc) 118

6b. NO. OF REFS (total cited in document) 10

7. DESCRIPTIVE NOTES (the category of the document, e.g. technical report, technical note or memorandum. If appropriate, enter the type of report, e.g. interim, progress, summary, annual or final. Give the inclusive dates when a specific reporting period is covered.)

Contract Report

8. SPONSORING ACTIVITY (the name of the department project office or laboratory sponsoring the research and development. Include the address.)

Defence R&D Canada – Suffield, PO Box 4000, Station Main, Medicine Hat, AB T1A 8K6

9a. PROJECT OR GRANT NO. (If appropriate, the applicable research and development project or grant number under which the document was written. Please specify whether project or grant.)

Shield Thrust 12ru

9b. CONTRACT NO. (If appropriate, the applicable number under which the document was written.)

W7702-09-R241

10a. ORIGINATOR'S DOCUMENT NUMBER (the official document number by which the document is identified by the originating activity. This number must be unique to this document.)

DRDC Suffield CR 2012-122

10b. OTHER DOCUMENT NOs. (Any other numbers which may be assigned this document either by the originator or by the sponsor.)

Neptec NDG011406

11. DOCUMENT AVAILABILITY (any limitations on further dissemination of the document, other than those imposed by security classification)

(X) Unlimited distribution
( ) Distribution limited to defence departments and defence contractors; further distribution only as approved
( ) Distribution limited to defence department and Canadian defence contractors; further distribution only as approved
( ) Distribution limited to government departments and agencies; further distribution only as approved
( ) Distribution limited to defence departments; further distribution only as approved
( ) Other (please specify):

12. DOCUMENT ANNOUNCEMENT (any limitation to the bibliographic announcement of this document. This will normally corresponded to the Document Availability (11). However, where further distribution (beyond the audience specified in 11) is possible, a wider announcement audience may be selected).

UNLIMITED

13. ABSTRACT (a brief and factual summary of the document. It may also appear elsewhere in the body of the document itself. It is highly desirable that the abstract of classified documents be unclassified. Each paragraph of the abstract shall begin with an indication of the security classification of the information in the paragraph (unless the document itself is unclassified) represented as (S), (C) or (U). It is not necessary to include here abstracts in both official languages unless the text is bilingual).

This final report summarizes the findings obtained during the electrical impedance tomography study carried out during the period of July 2010 to March 2012 (Contract No: W7702-09 R241/001/EDM). The project was intended to evaluate the capability of detecting underground tunnels using EIT as well as to pursue various means of improving signal-to-error ratio through examination of random noise, modeling error and hardware imperfections. Phenomenology studies were conducted and the applications of tunnel detection and detection of munitions in culverts were examined.

Recommendations are made for a potential new instrument to be used for research and development purposes. Investigation into detection of ammunition rounds led to the conclusion that EIT is not an effective technology for this application.

Le présent rapport final résume les résultats obtenus au cours de l'étude de la tomographie par impédance électrique (TIE) réalisée de juillet 2010 à mars 2012 (no de contrat : W7702-09R241/001/EDM). Le projet visait à évaluer la capacité de détecter des tunnels souterrains au moyen de la TIE ainsi qu'à chercher divers moyens pour améliorer le rapport signal sur erreur, grâce à l'examen d'un bruit aléatoire, d'une erreur de modélisation et des imperfections du matériel. Des études phénoménologiques ont été réalisées, et des applications relatives à la détection de tunnels et de munitions dans les ponceaux ont été examinées.

Le rapport présente des recommandations relativement à un nouvel instrument potentiel à utiliser aux fins de recherche et développement. Les études sur la détection des munitions ont permis de conclure que la TIE n'est pas une technologie efficace pour cette application.

14. KEYWORDS, DESCRIPTORS or IDENTIFIERS (technically meaningful terms or short phrases that characterize a document and could be helpful in cataloguing the document. They should be selected so that no security classification is required. Identifies, such as equipment model designation, trade name, military project code name, geographic location may also be included. If possible keywords should be selected from a published thesaurus, e.g. Thesaurus of Engineering and Scientific Terms (TEST) and that thesaurus-identified. If it is not possible to select indexing terms which are Unclassified, the classification of each should be indicated as with the title.)

Landmine, unexploded ordnance; detection; underwater; electrical impedance tomography; conductivity imaging; electrical impedance imaging; one sided electrical impedance imaging.

Defence R&D Canada

Canada's Leader in Defence
and National Security
Science and Technology

R & D pour la défense Canada

Chef de file au Canada en matière
de science et de technologie pour
la défense et la sécurité nationale

www.drdc-rddc.gc.ca